The Dissertation Committee for Hakan Ertürk Certifies that this is the approved version of the following dissertation :

Inverse Design and Control of Thermal Systems

Committee:

John R. Howell, Supervisor

Ofodike A. Ezekoye

Kenneth S. Ball

Richard H. Crawford

Donald S. Fussell

Inverse Design and Control of Thermal Systems

by

Hakan Ertürk, B.S., M.S.

Dissertation

Presented to the Faculty of the Graduate School of

The University of Texas at Austin

in Partial Fulfillment

of the Requirements

for the Degree of

Doctor of Philosophy

The University of Texas at Austin

December, 2002

Dedication

To my family

Sevgi, Altan and Can Ertürk

Acknowledgements

The author of this dissertation wishes to express his deepest appreciation and gratitude to the supervisor of this study, Prof. John R. Howell, for his guidance, support, understanding, generosity, kindness and sense of humor. He was a great supervisor and a mentor. Our conversations especially when traveling for a conference was really enjoying and also mostly revealing. Without his enormous support and guidance this study would not be possible.

Prof. Ofodike A. Ezekoye's contributions are also sincerely appreciated. He constituted an excellent model for a young academician and his enthusiasm and excitement about everything going on around him including this study was really motivating. Moreover, his energy, dynamism and big laughter, together with Prof. Howell's sense of humor were making our research meetings not only a time to discuss, exchange ideas, and learn but also a time we really enjoyed.

Prof. Kenneth S. Ball's comments about the study and dissertation together with his support for gathering experimental data are very appreciated. He and his research group were really helpful. The other members of the dissertation committee, Prof. Richard H. Crawford and Donald S. Fussell are acknowledged for reviewing this dissertation and commenting about it during the whole study.

I would like to thank the National Science Foundation, for the support under the grant CTS-0070545.

The groundwork of this study started really long ago, during the time I was a graduate student in Middle East Technical University, Ankara, Turkey.

Therefore, it is a must to remember and acknowledge my supervisors then, Prof. Nevin Selçuk and Prof. Faruk Arınç, once more for equipping me with fundamental knowledge and mental motivation to be able to come here and do this study. Prof. Selçuk was extremely influential, teaching me how to do research, and feeling her support along with Prof. Arınç's was always very assuring. Their support while I was applying for universities for Ph.D. was really unforgettable for me.

During my time here, I spend most of my time in ETC 7.144. Our office did not have any window to let the sunlight in or to feel fresh air, but it was always full of nice people, fellow graduate students from all over the world. Among all these people, it is impossible to forget Francis França, and Charles Lan, and how helpful and friendly they were especially in my very first years here. Mirko Gamba's contributions must be acknowledged for the experimental data he provided and the time he spent in front of the computer. Besides them, I would also like to thank my other officemates and fellow graduate students for being around to share the good and the bad times all through these years; Erik Wassen, Kyle Daun, Cengiz Vural, Fabrizio Bisetti, John Dunn, Daijiao Wang, Sean Bulla, and Dong Mei Zhou.

Besides my friends in the department, my other friends that I have spent most my time here in Austin also deserve to be remembered. Özge Öztürk, Onur Sonuvar, Özgür Ekici and Umut Beşpınar-Ekici's friendship was very valuable for me. I must thank Ahmet Yakut for the orientation helping me land smoothly in US. Some of my friends whom I was in contact all these years, Alkim Özaygen, Altay

Özaygen, Altuğ Yavuz, Batur Avgan, Oytun Tuzcu and Kerem Pekkan, who once were my buddies in depth or on high altitude, knowing that you are there to share a breath of air or hang on to my belay no matter what, always felt secure.

At last, but definitely not the least, I want to thank to my family, Sevgi, Altan and Can Ertürk for nothing in particular but everything in general. Whatever is accomplished, they are the ones who really deserve to be commemorated. I won't be saying anything more, knowing that I am not that good with words to express my gratitude for them. Besides, I would like to thank my aunt and my cousin Meral and Özlem Yonar not only for visiting me a number of times but also for being there for me whenever I need all the time.

Realizing that I have been acknowledging for almost three pages, I might have given the impression to the reader that this study is a ground shaking one or a breakthrough in our field. Of course this is not true. But sitting down to write an acknowledgement for this dissertation makes me feel that this might be good chance to remember people that add something to my life during this period.

Inverse Design and Control of Thermal Systems

Publication No._____

Hakan Ertürk, Ph. D.

The University of Texas at Austin, 2002

Supervisor: John R. Howell

This study considers the design of thermal processing systems where the goal is to design a system with the correct geometry and materials, so that together with the necessary energy input from the engineering devices, it would satisfy the needs of the process to be carried out. In some systems, conditions at a specified steady state are of interest, while in some others the goal is to follow a specific thermal history. Some of the common applications for such systems include rapid thermal processing of semiconductor wafers, curing, annealing, chemical vapor deposition applications, industrial baking or certain biomedical applications.

Solution of a coupled boundary condition estimation problem together with geometry and property estimation problems is necessary. This study focuses on boundary condition design so that the challenges of the problem can be

investigated and tackled in isolation from the other two problems. The traditional method of solution for such a problem is by trial-and-error methods, which consider the solution through a series of forward problems, where the effects are calculated for prescribed causes. Trial-and-error solution methods are computationally very expensive and it is often hard to achieve reasonable solutions.

An alternative approach, inverse design, is based on formulating the design problem as an inverse problem and it is used here so that a direct solution is possible. Here the cause for a certain effect is sought directly. However, the use of an inverse formulation leads to an ill-posed problem where solutions become unstable and even unphysical. Therefore, the use of regularization techniques is essential to achieve reasonable and accurate solutions.

Generic design methodologies are developed and presented to solve steady and transient boundary condition design problems making use of an inverse formulation and regularization. The developed solution techniques are experimentally validated and their applications are demonstrated through solution of sample thermal design problems in radiating enclosures. Moreover, control algorithms based on artificial neural networks are developed for control of distributed transient systems.

Table of Contents

List of Tables

List of Figures

Nomenclature

A	area, m^2
A	coefficient matrix for a system of equations
b	right hand side vector for a system of equations
c	speed of sound, 2.998×10^8 m/s
c_p	specific heat, J/ kg K
E	emissive power, W/m^2
$f(t)$	unknown function in the Fredholm integral equation of the first kind
F_{i-j}	configuration factor between elements i and j
$\widetilde{F}_{i-j}$	exchange factor between elements i and j
$F(\mathbf{x})$	objective function to be minimized by the conjugate gradient method and the Tikhonov regularization
g	asymmetry constant for Henyey-Greenstein scattering phase function
$g(s)$	known function in the Fredholm integral equation of the first kind
h	convective heat transfer coefficient, W/m^2 K
h	exact solution for a linear system of equations
I	intensity, W/m^2 sr
$K(s,t)$	kernel of the Fredholm integral equation
k	thermal conductivity, W/ m K
$\mathbf{L}_i$	discrete i-th order differentiation operator
M	number of equations
Ma	Mach number
n	normal to the surface

$\mathbf{n}$	unit normal vector of a surface
N	number of unknowns
N_S	number of surface elements
N_V	number of volume elements
P	pressure, Pa
P	probability density function
$\mathbf{p}$	A-conjugate vectors
Q	external power addition or energy generation, W
q	heat transfer, W
$r(s)$	residual function of the analytical form of Fredholm integral equation
$\mathbf{r}$	residual vector for a system of equations
R	cumulative distribution function
R	random number
$\mathbf{s}$	direction of incident intensity or photon bundle
S	pathlength, m
$\mathbf{S}$	diagonal matrix of singular values
$\mathbf{S'}$	diagonal matrix of multiplicative inverses of singular values
T	temperature, K
t	time, seconds
$\mathbf{t_1}$	unit tangential vector of a surface
$\mathbf{t_2}$	unit tangential vector of a surface
$u_i(s)$	singular function of the kernel
$\mathbf{U}$	orthogonal matrix

$\mathbf{U}$ velocity vector, m/s

$v_i(t)$ singular function of the kernel

V volume, m^3

$\mathbf{V}$ orthogonal matrix

w energy per bundle, W

$\mathbf{x}$ unknown vector for a system of equations

$\mathbf{x_e}$ coordinate of emission point

x x coordinate

x_j j coordinate, m

$\mathbf{x_p}$ coordinates of an arbitrary point on the surface

y y coordinate

z z coordinate

$\%Err$ absolute percentage error

Symbols

α absorptivity

α^k coefficient of conjugate vectors to modify the solutions for the k-th step for the conjugate gradient method

α_i i-th order regularization parameter for Tikhonov regularization

β expansion coefficient, K^{-1}

β extinction coefficient, m^{-1}

β^k coefficient to calculate the new conjugate direction from the old ones for the k-th step for the conjugate gradient method

δ the surface thickness, m

Φ scattering phase function

$\mathbf{\Phi_d}$ viscous dissipation term

ε emissivity

γ standard deviation

φ azimuthal angle, radians

κ absorption coefficient, m^{-1}

λ wavelength, μm

μ_i the singular values of the kernel or the coefficient matrix

μ_o cosine of scattering angle

θ polar angle, radians

ρ density, kg/m^3

ρ reflectivity

σ Stefan-Boltzmann number, $5.67x10^{-8}$ W/m^2K^4

σ_s scattering coefficient, m^{-1}

τ optical thickness

ϖ solid angle, sr

ω scattering albedo

∇ gradient

Subscripts

b blackbody

cd due to conduction

cv due to convection

d design object

g	gas
i	incident
i	of element i
in	in
o	reference value
out	out
p	Planck mean value
r	radiative
r	reflected
∞	ambient property
λ	wavelength dependent

Superscripts

k	k-th step of conjugate gradient method
n	n-th time step
q	based on heat flux
T	based on absolute temperature
$''$	per area, m^{-2}
$'''$	per volume, m^{-3}

CHAPTER 1

Introduction

1.1 MOTIVATION

Engineering is a profession devoted to solving problems using applicable scientific knowledge and, in the absence of that, simply intuition. Engineers have long been facing and solving problems to satisfy basic needs like accommodation, transportation, conditioning, protection, nourishment, exploration and health. The way engineers tackle these problems is by designing and manufacturing the appropriate tools. Therefore, major professional activities of engineers include research, development, design, construction, and sales.

This study focuses on design, particularly the design of thermal processing systems that can be used for a wide variety of purposes. The immediate result of the design procedure is often a report that includes a set of calculations and/or a drawing that are abstractions of the designed equipment or system; the subject being a process, an element or a component of a larger assembly or an entire system. The design procedure is followed by construction of the equipment or application to the system where control is an important issue.

Design of thermal processing systems involves satisfying desired conditions in the part of the system where the thermal processing takes place. This part of the system is named the “design environment”. The conditions desired in the design environment are dependent on the process for which the

thermal system is built. For example, a semiconductor wafer is to be heated in a given series of temperature steps while holding the wafer spatially isothermal. The design conditions can be reached by controlling the conditions in other parts of the system through heaters, burners or coolers. The ultimate goal in a thermal design problem is to build the required system with the correct geometry and materials, so that together with the necessary input from the engineering devices for the system, it would satisfy the needs of the process to be carried out in the design environment. Therefore, the design problem is a coupled problem of geometry, material and boundary condition or source estimation problems. Generally, the whole design process is very complex, highly nonlinear and involves a number of design iterations of prototype building and testing. Reducing the total number of design iterations by one or two will result in significant savings. This can often be achieved through the use of available simplified models and numerical simulation techniques.

This study focuses on one part of the design problem: The design of a system, for which the design environment, geometry and the materials are specified and the required boundary conditions are to be calculated. The developed methodology can then be used as a tool for the complete design problem.

For a process furnace, such as the ones used for rapid thermal processing (RTP), chemical vapor deposition (CVD), drying, curing of paint, food processing, annealing, or curing of powder coated materials, the thermal problem is to heat the design object with a prescribed distribution of temperature and net

radiant energy input. These known distributions are usually spatially uniform, as uniform temperatures prevent thermal stresses, non-uniform chemical deposition, and uneven drying or cooking due to temperature gradients. As each object has a finite heat capacitance, no steady state is available instantly. In some of the processes, the final steady state is of interest; in many other problems it is the temperature path that is important. In order to reach a steady state, the design object must be heated from an initial state while the object follows a particular heating history, during which the design environment is to be kept at the desired spatial distribution at all times.

This study involves the design of thermal systems where high temperatures are present. The dominant mode of heat transfer is thermal radiation as the exchange of thermal radiation depends on the fourth power of temperature. The physical problem considered here is often very complex, with wavelength, direction and temperature dependent properties, involving non-linearity due to multimode heat transfer and the transient nature of the problem. Furthermore, the geometry of the systems can include other levels of complexities like blockage effects.

The traditional way to solve a design problem is to guess an input for the energy supply devices used in the system and then to check through mathematical models whether the desired conditions in the design environment are satisfied or not. This involves the solution of the "forward problem", where the input or the cause is given and the output or the effect is estimated. The guessed value is modified based on the preceding results until the desired conditions are reached.

Such trial-and-error methods are computationally expensive; moreover, it can be difficult to obtain accurate, smooth, physically reasonable or feasible solutions.

So called “inverse design”, on the other hand, involves the solution of the design problem by using all available information prescribed for the design environment at once to provide a direct solution for the necessary input. As the required input or the cause for the system is determined from the output or the effect, this kind of formulation is called the “inverse formulation” and the method of design is called “inverse design”. As a direct solution is considered, the computational expense of the inverse methods is considerably lower than trial-and-error methods, but the drawback is that the inverse problem is defined in terms of a set of Fredholm equations of the first kind, which is known to be ill-posed.

The next section underlines the literature on the inverse heat transfer problems and previous studies applying inverse formulation as a design tool.

1.2 LITERATURE REVIEW

Hadamard (1923) defines a well-posed problem as one with a solution that is unique and stable under small perturbations in the input data. By not satisfying these characteristics, many believed that even though ill-posed problems are solvable, the solution would be useless. Moreover, these problems were considered as artificial and not reflecting real physical systems. However, inverse problems are known to be ill-posed and real.

Inverse problems started attracting attention in the late 1950’s, when the emerging space programs brought the advancement in computational techniques

required and the necessity to tackle inverse problems. One of the first inverse problems proposed was related with re-entry of space vehicles. During re-entry, the temperature of the heat shields of space vehicles become so high that direct measurement of thermal conditions and thermo-physical properties with known techniques is impossible. The only alternative is setting the problem as an inverse problem by placing the sensors elsewhere, and estimating the thermal conditions and thermo-physical properties of the shield from its effect at the location the sensor is placed. It was apparent that the way to solve the inverse problem was stabilization or regularization; i.e., re-formulating the ill-posed problem, so that the information causing the ill-posedness is ignored and a well-posed system is obtained.

Before proceeding with investigating the literature in inverse heat transfer problems, it is reasonable to classify the inverse problems. Inverse problems can be classified as follows:

1. Inverse initial condition estimation problem
2. Inverse property estimation problem
3. Inverse geometry estimation problem
4. Inverse boundary condition or load estimation problem

In all these problem types, the inverse formulation of the problem is based on cause-effect relations, where the cause is calculated from information about the effect and the physical system. In the problem types listed, the cause is the initial condition, certain properties of the materials on the boundary or the medium, the geometry, the boundary condition or the load in the medium, respectively. The

effects are desired conditions in the design environment for the design problem or measured values in the case of measurement problem.

The literature includes many studies that consider inverse problems in thermal systems. Among these, it will be reasonable to concentrate on the pioneering studies that laid the basis for following studies, the studies that present a review of state-of-art of inverse problem solution, and studies that constitute the basis for the current study.

1.2.1 The Pioneering Studies and Reviews

Tikhonov and his co-workers Ivanov and Lavrentiev are attributed with the pioneering work in the area of developing regularization methods for inverse problems. Tikhonov carried out a considerable amount of research on ill-posed problems and published the results in the 1960's. Tikhonov et al. (1995) introduce solution techniques based on regularization, named after him, to solve linear and non-linear ill-posed problems. He also combined his ideas with his computing skills to implement computer algorithms to solve ill-posed problems computationally (Tikhonov et al., 1995).

In the area of inverse thermal problems, Alifanov's and Beck's group are credited for the majority of the initial work, both concentrating on inverse conduction problems.

Alifanov focused on the use of iterative regularization techniques. The idea of using iterative techniques, like gradient-based methods, was first introduced by Lavrentiev as these methods are resistant to the errors in the input data (Alifanov et al., 1995). With these methods, the iteration number can be

used as the regularization parameter, and the error decreases as the iteration number increases. The use of iterative regularization methods is explained in detail in Alifanov et al. (1995). Alifanov (1994) presents a more comprehensive discussion focusing on the definition of the inverse problem, iterative regularization techniques and the variational principle of regularization. Moreover, numerical aspects, the existence, uniqueness and stability characteristics of the solutions for the inverse problems are also investigated. In both references, the proposed solution techniques are applied to a number of inverse conduction problems. The problems are transient boundary condition and load estimation problems with fixed and moving boundaries. The application area of the problems of interest in both studies is measurement rather than design.

Similarly, Beck et al. (1985) investigated inverse heat conduction problems and the solution techniques, including exact solutions, the single future time step method, function specification techniques, regularization methods, the trial function method, use of filters and optimization for parameter estimation. The problems they focus on are boundary condition and property estimation problems; estimation of single and multi heat flux on the boundary and estimation of the heat transfer coefficient. This study also discusses the inverse problems with an emphasis on its use as a measurement technique.

More recently, Özışık and Orlande (2000) presented a more comprehensive investigation of inverse heat transfer problems, covering most of the possible problem configurations including, steady-state and transient, property, boundary condition, load, and initial condition estimation problems.

Moreover, besides inverse conduction problems, they covered inverse convection and radiation problems. They explained and used the Levenberg-Marquardt method, conjugate gradient method (CGM), CGM with adjoint problem for parameter estimation and CGM with adjoint problem for function estimation.

1.2.2 Initial Value and Property Problems

There are many studies in the literature involving property estimation in radiating systems. These studies mainly focus on estimating the surface properties, emissivity, absorptivity, reflectivity or medium properties, the extinction coefficient, scattering albedo or the scattering phase function.

Mengüç and Manickavasagam (1993) determined the profiles of extinction coefficient and the single-scattering albedo in an absorbing and scattering cylindrical media, where the radiative properties in the medium vary radially. They used the angular radiosity distribution obtained from the solution of the forward problem as an input to the inverse analysis. For an anisotropically scattering medium, the asymmetry factor is also recovered.

Wu and Wu (1998) developed a technique based on a successive approximation method to solve direct and inverse problems of radiative exchange among surfaces. They formulated the radiative exchange by an expression in terms of some integrals independent of surface reflectivity. The integrals can be obtained by only one calculating procedure provided that the geometry is fixed. The inverse problem of estimating the surface reflectivity is then solved without solving the associated direct problem repetitively.

The literature on initial value problems is relatively limited. One of the significant studies is presented by Silva Neto and Özışık (1994). They used CGM with an adjoint equation to estimate the initial condition of a one-dimensional transient heat conduction problem. Making use of the available data of measured temperatures at numerous locations along the slab at a certain time, they were able to recover the initial temperature distribution along the slab.

1.2.3 Geometry Design

None of the studies listed above are focused on design. The first studies that make use of inverse design are in the field of diffuser or airfoil design (Hokenson, 1979; Volpe and Melnik, 1984). One of the first studies addressing the applicability of inverse formulation for thermal design is Kennon and Dulikravich (1985), where the internal cooling of turbine blades is considered. The same problem with additional inverse conduction problems involving shape design and unsteady boundary condition problems are explained in detail in Dulikravich and Martin (1997).

Howell (1999) presented one of the first studies that considers inverse design of geometry for radiating enclosure problems. The problem considered is to satisfy the design conditions by using the appropriate geometric configuration of the heater surfaces. Simulated annealing, a well known stochastic technique for global optimization, is used to find the optimal geometry configuration.

More recently, Daun et al. (2001) solved the problem using a more deterministic approach utilizing the sensitivity coefficients. The geometry is defined using Non-Uniform Rational B-Splines (NURBS), which is a common

way to parametrically define two and three dimensional surfaces, and the configuration factors for radiation transfer are calculated by infinitesimal area analysis. As the geometry is defined in terms of parametric curves, the sensitivity coefficients can analytically be calculated and using non-linear programming techniques, the optimal geometry can then be evaluated.

1.2.4 Inverse Boundary Condition or Load Design

The use of inverse formulation as a design tool in radiating systems was first introduced by Howell's group in the mid-nineties. One of the initial works was presented by Harutunian et al. (1995), which solved the inverse problem of radiative exchange within evacuated two-dimensional rectangular enclosures composed of diffuse-gray surfaces. The goal was to predict the required temperature distribution at the heater surfaces. They used modified truncated singular value decomposition (MTSVD) to regularize the resulting ill-posed system of equations and were able to recover the unknown emissive power distributions to an acceptable level of accuracy.

Howell et al. (2000) presented the design of two-dimensional rectangular enclosures with absorbing-emitting medium and three-dimensional evacuated enclosures. They used the conjugate gradient method (CGM), truncated singular value decomposition (TSVD), Tikhonov regularization (TR) and MTSVD to solve the resulting ill-conditioned system of equations and compared the results from the different methods.

Kudo et al. (1995) investigated the inverse source estimation problem in a radiating enclosure containing absorbing-emitting medium. They solved for the

optimal locations for the specified power input in the medium to satisfy design conditions on the boundaries of the two-dimensional rectangular enclosure. They have employed TSVD to produce stable and accurate solutions.

França et al. (1999) solved a similar problem to the one presented by Kudo et al. (1995), but they have fixed the locations of the burners and estimated the required source input. Moreover, they have also included the diffusive effects in their analysis leading to a non-linear combined conduction-radiation solution. As a regularized solver, they used TSVD iteratively in order to cope with the non-linearity of the problem.

The inverse boundary condition estimation problem is also investigated by França et al. (2001). They presented a heater design of a dryer system. The required input for the heaters located on one surface of a plane parallel channel, where an absorbing-emitting gas flows through, is estimated so as to satisfy desired design conditions over the surface to be dried. The problem requires a solution of combined conduction-convection-radiation, which is highly non-linear, in addition to the ill posedness due to the governing inverse formulation. They tackled the problem using TSVD iteratively, and calculated the optimal heater length and required power input.

França et al. (2002) presented a comprehensive review of the inverse design concept in thermal systems dominated by thermal radiation. Besides the solution techniques and the characteristics of the problem, their review also included sample applications of purely radiating or multi-mode design problems.

However, the geometries considered in these studies are simple rectangular or plane parallel enclosures, and no transient effects are considered.

Park and Jung (2001) presented a system to control RTP systems, where they measure the temperature over the design object making use of a number of sensors, then making use of inverse analysis estimating the temperature distribution over the design object. Once the temperature distribution is known, estimating the required heater configuration constitutes another inverse problem. They have used Kalman filters together with the Karhaunen-Loève Galerkin procedure to tackle the inverse conduction problem. The inverse radiation problem is solved by least squares minimization technique.

1.3 OBJECTIVE

Considering the previous work done, there seems to be enough background to expand the application areas of inverse design concept from the simplified academic problems to relatively more complex problems industry is facing. The academic problems in radiating systems that have been solved usually involve pure absorbing-emitting media in simple rectangular enclosures, with diffusely reflecting surfaces. However, industry faces problems with further complexities such as irregular geometries with blocking or shading effects that create severe discontinuities in the distributions, mirror-like reflecting surfaces, and anisotropically scattering media. One of the goals of this study is to expand the limits of the current state-of-art of inverse design concept to tackle problems with such complexities.

In the area of inverse heat transfer problems, transient effects have been considered in problems that involve conduction and convection. In many systems like the ones involving RTP, transient effects are important together with the dominance of thermal radiation. The required power input for the heaters is to be estimated as they heat an object that must follow a specified temperature history. This is a challenging problem because attaining a certain level of accuracy might be impossible based on the system selected. But nevertheless, the intent is to develop a design technique that will be able to solve a variety of problems that involve transient effects, as long as a solution exists.

Another aspect of the problem is to develop some means of control. No matter how complex the numerical model is, it is very common that there will be discrepancies between the predictions of the numerical model and the response of the physical model. In order to reduce these discrepancies to more acceptable levels, a control system is required. Our objective is to design such a control system.

1.4 THE ORGANIZATION OF THE DISSERTATION

This dissertation is divided into eight chapters. Chapter 2 presents the required background for thermal system analysis, including the thermal energy equation, and the radiative transfer equation. It also includes the numerical discretization of the governing equations and the numerical solution techniques employed in this study. The mathematical and physical aspects of inverse problems and the available solution techniques are presented in Chapter 3. The design of steady thermal systems constitutes Chapter 4. Transient thermal system

design is investigated in Chapter 5. Chapter 6 includes the application of the control algorithm. The application of the inverse design predictions compared to the experimental results is presented in Chapter 7. The last four chapters mentioned include the results presented in Ertürk et al. (2000, 2001a, 2001b, 2002a, 2002b, 2002c, 2002d), Daun et al.(2002) and Gamba et al. (2002). The conclusions and the recommendations for future work are included in Chapter 8.

CHAPTER 2

Mathematical Model of The Physical System

2.1. INTRODUCTION

This chapter presents the basic information required for carrying out thermal analysis. Thermal analysis of a system requires satisfying three basic laws, representing the conservation of mass, momentum and energy. Some of the systems considered in this study are evacuated so the flow inside is negligible. Therefore, the solution of the momentum and continuity equations is unnecessary in such systems, leaving only the energy equation. Moreover, high temperatures are present in the systems considered in this study; consequently thermal radiation is the dominating mode of heat transfer and special attention will be paid to the equation defining radiation transport.

The derivation of the energy equation is presented in many references such as Incopera and De Witt (2002) or Mills (1992). Therefore, it will be appropriate to start with the general form of the energy equations for enclosure geometries. From the general form of the relations presented, these equations can then be simplified for the particular cases considered in this study.

Numerical solution techniques are employed throughout this study; control volume approach is used for spatial discretization of the energy equation and the Monte Carlo method (MCM) is used for modeling the transport of thermal

radiation. The details of the numerical discretization schemes employed and the MCM are also presented in this chapter.

2.2 THE ENERGY EQUATION

The laws of thermodynamics are the fundamental laws that describe the thermal nature of every system. Thermal analysis usually involves the application of these laws together with the available information to estimate the unknown states, properties, or characteristics. The mathematical expression that represents the first law of thermodynamics, also known as the conservation of energy, is the energy equation. The energy equation in its general form is

$$\rho c_p \frac{DT}{Dt} = \beta T \frac{DP}{Dt} + \nabla \cdot \left(k \nabla T - \mathbf{q}_r'' \right) + Q''' + \Phi_d \tag{2.1}$$

where the *D/Dt* terms are the substantial derivatives that include the local rate of change with time combined with convective effects as

$$\frac{D}{Dt} = \frac{\partial}{\partial t} + \mathbf{U} \cdot \nabla \tag{2.2}$$

The term on the left hand side and the first term on the right hand side of the energy equation, Eq. (2.1), represent the rate of change in the energy and the compression work, respectively. The second and third terms on the right hand side are the divergence of heat flux, diffusive and radiative, respectively, and the energy generation, such as due to a combustion or another chemical reaction. The final term represents the dissipated energy due to viscous effects.

The velocity appearing in the convective terms of the substantial derivatives demands information about the flow-field, which necessitates the solution of momentum and continuity equations. For an incompressible flow (Ma

< 0.3), the energy equation is uncoupled from the other two and can be solved separately. Otherwise, energy, continuity and momentum equations are coupled and must be solved simultaneously.

In order to carry out a thermal analysis of an enclosure, both the medium and the conditions at the boundaries must be considered.

2.2.1 The Energy Equation for the Medium

The energy equation for the medium inside an enclosure is identical to Eq. (2.1), but in many situations some of the terms can be negligible. For enclosure problems where the flow is negligible, the convective terms, the compression work and the viscous dissipation terms are negligible leading to

$$\rho c_p \frac{\partial T}{\partial t} = \nabla \cdot \left(k \nabla T - q_r'' \right) + Q''' \tag{2.3}$$

where the divergence of radiative flux is defined by the radiation transfer equation. In such a situation the solution of momentum and continuity equations is not required.

Thermal radiation is directly proportional to the fourth power of the absolute temperature. Therefore, in systems where high temperatures are present, the radiative terms become dominant to the diffusive terms. For a steady system with negligible diffusive terms, the energy equation becomes

$$\nabla \cdot \mathbf{q}_r'' = Q''' \tag{2.4}$$

A special case of Eq. (2.4) where Q'''=0, is termed radiative equilibrium.

2.2.2 The Energy Equation for the Boundaries

In order to complete the thermal analysis of an enclosure, the conditions at the boundaries must also be considered. The boundary conditions can be a specified state as in the case of a Dirichlet condition or in terms of energy equations with certain conditions on these locations as in the case of Neumann or Robin conditions. A generalized relation that includes the radiation on the bounding surface can then be written as

$$q_r'' + h\left(T_g - T\right) = k\left.\frac{\partial T}{\partial n}\right|_{wall} \tag{2.5}$$

where convection is defined in terms of a heat transfer coefficient and the derivative ∂/∂n denotes the gradient normal to the surface. This is the required boundary condition for the general energy equation for a differential element in the solid wall

$$Q''' + \nabla \cdot \left(k \nabla T\right) = \rho c_p \frac{\partial T}{\partial t} \tag{2.6}$$

Then Eqs. (2.6) and (2.5) should be solved coupled with corresponding equations for medium.

Consider the enclosure geometry represented in Fig. (2.1). In such an enclosure, the thicknesses of the surfaces are usually small enough to neglect diffusion across the surface thickness. The energy equation for an enclosure boundary, considering the surfaces as lumped across its thickness, δ, can be written as

$$q_r'' + Q'''\delta + \nabla \cdot \left(k \nabla T\right)\delta + h_{in}\left(T_g - T\right) + h_{out}\left(T_\infty - T\right) = \rho c_p \delta \frac{\partial T}{\partial t} \tag{2.7}$$

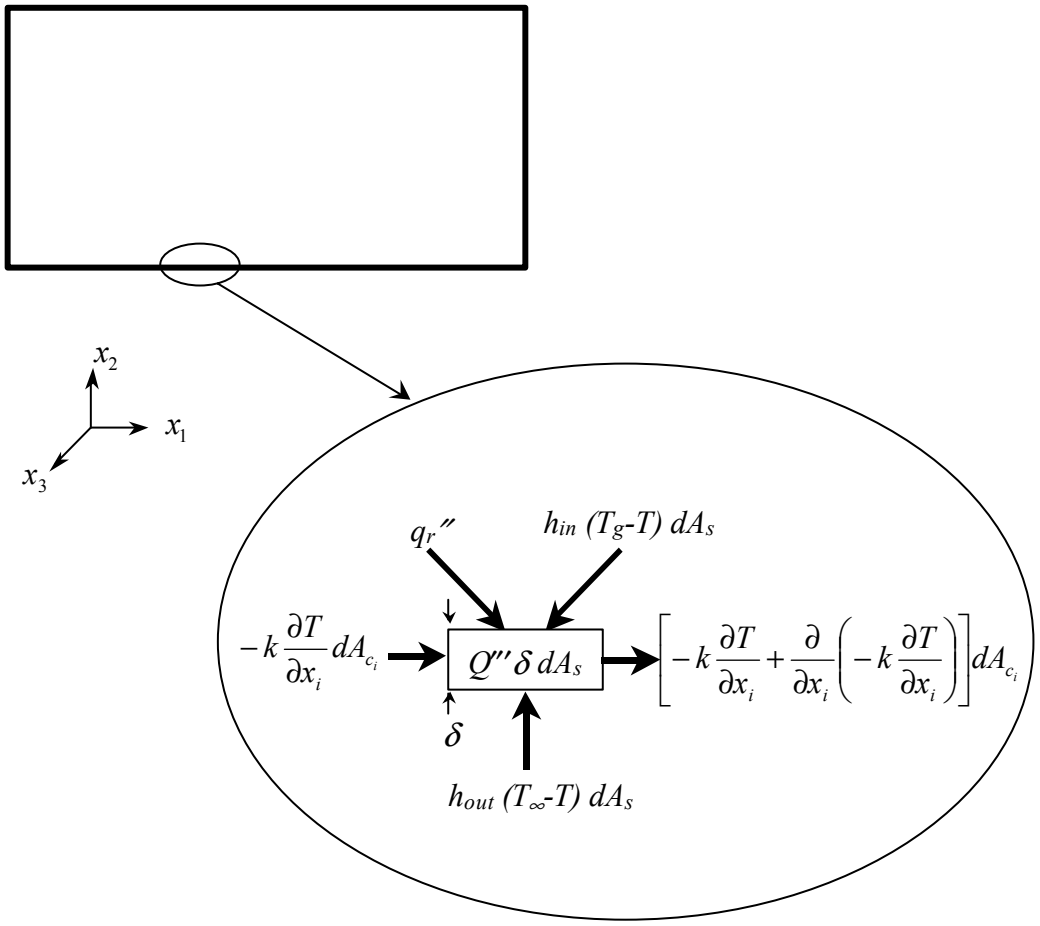

Figure 2.1: The energy balance over a differential element on the boundary of an enclosure

It should be noted that Eq. (2.7) is given for a control volume on the boundary of an enclosure, for which the surface does not move. If the surface moves with a constant velocity U along the coordinate x_1, the energy entering and leaving the control volume as the energy of the moving surface should also be taken into account. This can be achieved by using a substantial derivative of time

rather than a partial derivative that only includes the local rate of change with time.

$$q_r'' + Q''' \delta + \nabla \cdot (k \nabla T) \delta + h_{in} (T_g - T) + h_{out} (T_\infty - T) = \rho c_p \delta \frac{DT}{Dt} \qquad (2.8)$$

The equation can be simplified for special cases. In case of no external power input, the $Q''' \delta = Q'' = 0$ as in the case of all surfaces but heaters. It is a common practice to approximate separate isothermal elements as heaters, for which case the conduction term is ignored. If the surface is well insulated on the outside so that there is no heat loss to the environment at T_∞, the corresponding convection term can be neglected by setting $h_{out} = 0$. The similar case holds when there is negligible free or forced flow inside the enclosure, $h_{in} = 0$. Moreover, for a steady problem where heat diffusion along the plate is negligible when compared with radiation the energy equation for the enclosure surfaces simply reduce to a pure radiation problem, where

$$Q''' = \frac{-q_r''}{\delta} \qquad (2.9)$$

for the heater elements, and

$$q_r'' = h_{out} (T - T_\infty) \qquad (2.10)$$

for the other elements losing heat to the outside.

For all the systems where the radiative effects are present, the radiative heat flux, q_r'', or the divergence of radiative flux, $\nabla \cdot q_r''$, must be calculated using the radiative transfer equation.

2.3 THERMAL RADIATION

The energy transferred by electromagnetic waves or photons is referred to as thermal radiation. Thermal radiation becomes important in the presence of high temperatures, as it is directly proportional to the fourth power of the absolute temperature, and in vacuum systems because a medium is not required to transfer energy through radiation. For the purposes of this study, the understanding of thermal radiation is essential as the systems under consideration are high temperature systems where thermal radiation dominates.

Rather than explaining the phenomenon extensively, brief information including the basic equations is presented here while further information about the topic can be found in literature such as Siegel and Howell (2002) and Modest (1993).

It is practical to present the topic in two sub-titles: thermal radiation between surfaces that focuses on the exchange between surfaces in the presence of a transparent gas or vacuum and thermal radiation in a participating medium, which considers the exchange in the presence of a participating gas.

2.3.1 Thermal Radiation Between Surfaces

The most common radiation problem is the exchange among numerous surfaces. For enclosure geometries with diffuse-gray surfaces such as the one shown in Fig. 2.2-a, the relation defining the radiation exchange can be written as

$$q_r''(x_j) = \varepsilon(x_j)\sum_{k=1}^{N}\int_{A_k}\left[\frac{1-\varepsilon(x_k)}{\varepsilon(x_k)}q_r''(x_k) + \frac{1}{\varepsilon(x_k)}E(x_k)\right]dF_{dA_j-dA_k} - E(x_j) \qquad (2.11)$$

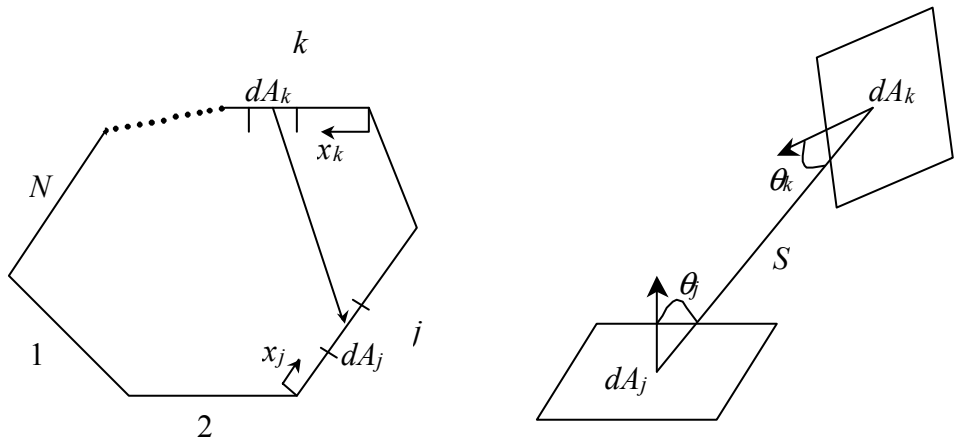

(a) (b)

Figure 2.2: (a) The enclosure with transparent medium and diffuse-gray walls, (b) the two differential areas

in terms of the emissivities, configuration factors, emissive power and the radiative heat flux distributions. The configuration factor between two infinitesimal elements dA_j and dA_k, such as in Fig 2.2-b is

$$dF_{dA_j - dA_k} = \frac{\cos\theta_j \cos\theta_k}{\pi S^2} dA_k \tag{2.12}$$

and it represents the ratio of the solid angle that the surface element dA_j sees as subtended by surface element dA_k directly, to all the hemisphere over the element.

The evaluation of the configuration factors constitutes an important part of the solution of the enclosure problems. While in simple geometries, configuration factors can be calculated through direct integration, or other simple methods such as the Hottel's crossed string method, for complex geometries that might include blockage effects, advanced techniques are required.

For enclosure problems with specularly reflecting surfaces, the configuration factor formulation becomes inadequate. An alternative to configuration factor formulation is the exchange factor formulation, which can be given as

$$q_r''(x_j) = \sum_{k=1}^{N} \int_{A_k} E(x_k)\, d\widetilde{F}_{dA_j - dA_k} - E(x_j) \tag{2.13}$$

where the exchange factor, $\widetilde{F}_{dA_j - dA_k}$ between the differential elements dA_j and dA_k is defined as the net rate of radiative heat emitted from dA_j that is absorbed by dA_k by all means including all intermediate reflections or scattering. Although, the exchange factor formulation of the enclosure problem is much simpler than configuration factor formulation, it is usually a more difficult task to calculate the exchange factors. Nevertheless, the resulting equation with the exchange factor formulation is an explicit relation, whereas the resulting relation with configuration factor relation is an implicit one and usually more difficult to solve. For an enclosure with black walls, the exchange factors and the configuration factors are identical.

2.3.2 Thermal Radiation in Participating Media

The equation that defines the rate of radiative transfer inside a medium that emits, absorbs and scatters is called the radiative transfer equation. The derivation of the equation is available in Siegel and Howell (2002) and Modest (1993) and its generalized form for an incident beam directed in the direction $\mathbf{s}_i$ at a location s is

$$\frac{1}{c}\frac{\partial I_\lambda}{\partial t} + \mathbf{s}\cdot\nabla I_\lambda = \kappa_\lambda I_{b\lambda} - (\kappa_\lambda + \sigma_{s\lambda}) I_\lambda + \frac{\sigma_{s\lambda}}{4\pi}\int_{4\pi} I_\lambda(\mathbf{s}_i)\Phi_\lambda(\mathbf{s}_i,\mathbf{s})d\varpi_i \quad (2.14)$$

where the first term on the left hand side is the transient term and is negligible unless time scales in the order of picoseconds or very small length scales are considered. The terms on the right hand side represent the emission, the attenuation by absorption and scattering and the augmentation by scattering into the intensity of the beam at point *s* by the element of size *ds*, respectively as shown in Fig. 2.3.

In order to calculate the net radiative energy deposited within or withdrawn from a differential volume element, the radiative transfer equation should be integrated over all directions. The resulting equation is

$$\int_{4\pi}\mathbf{s}\cdot\nabla I_\lambda(\mathbf{s})d\varpi = \int_{4\pi}\kappa_\lambda I_{b\lambda}(\mathbf{s})\,d\varpi - \int_{4\pi}\beta_\lambda I_\lambda(\mathbf{s})\,d\varpi + \frac{\sigma_{s\lambda}}{4\pi}\int_{4\pi} I_\lambda(\mathbf{s}_i)\left[\int_{4\pi}\Phi_\lambda(\mathbf{s}_i,\mathbf{s})d\varpi\right]d\varpi_i \quad (2.15)$$

which can also be integrated over the whole spectrum to yield

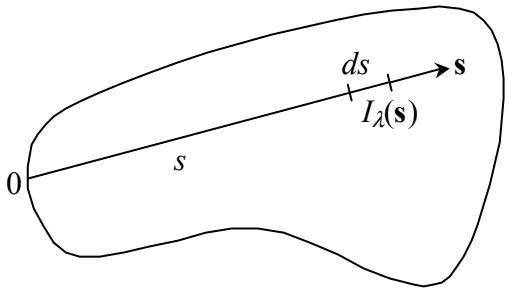

Figure 2.3: The incident intensity traveling through the participating medium

$$\nabla \cdot q_r'' = 4\kappa_p E_b - \int_0^\infty \left[4\pi\beta_\lambda \bar{I}_\lambda + \sigma_{s\lambda} \int_{4\pi} I_\lambda(\mathbf{s}_i) \overline{\Phi}_\lambda(\mathbf{s}_i) d\varpi_i \right] d\lambda \qquad (2.16)$$

where κ_p is the Planck mean absorption coefficient and the overbar indicates the mean value over the hemisphere such as

$$\bar{I}_\lambda = \frac{1}{4\pi} \int_{4\pi} I_\lambda d\varpi \qquad (2.17)$$

Equation (2.16) should be solved coupled with Eq. (2.1), the energy equation, using the boundary conditions as given in Eqs. (2.5-8). The solution of the multi-mode heat transfer problem is a difficult task due to its high degree of non-linearity and demands iterative solution. Even the pure radiation problem, in the absence of the transient, convective and diffusive terms, is quite complicated with absorbing, emitting and anisotropically scattering medium with wavelength and direction dependent properties.

There are many different solution techniques specially developed for solving thermal radiation problems. Some of these techniques are based on transforming the transfer equation into a number of partial differential equations, as in the case of method of spherical harmonics (P-N approximation), the discrete ordinates method (S-N approximation) and the flux methods. The traditional zonal method is based on defining the radiative exchange in terms of direct exchange areas between discrete surface and volume elements. The Monte Carlo method is a statistical solution technique based on simulating a finite number of photon bundles to statistically simulate the physical event. The discrete transfer method is similar to the Monte Carlo method, but rather than being statistical it follows a deterministic approach. Solution is also possible with more

conventional numerical methods like finite volume, finite element or spectral methods.

In this study the Monte Carlo method is preferred to model the radiative transfer for its versatility over the other methods. The details of the method are presented in the upcoming section.

2.4 THE MONTE CARLO METHOD

The Monte Carlo method (MCM) is a very generalized technique to statistically simulate a wide variety of events in terms of a Markov chain. A Markov chain represents a sequence of events, of which the probability of each succeeding event is independent of the prior events. The MCM can be applied to different problems in a wide variety of fields such as demographics, economics and engineering. In the area of thermal problems, it has been applied to simulation of thermal radiation problems, heat diffusion problems (Haji-Sheikh and Sparrow, 1967) or the simulation of rarified gas flow (Bird, 1976).

Howell and Perlmutter (1964) used the method for the first time for solution of a thermal radiation problem. Since then, the method has become one of the most basic solution techniques for thermal radiation problems often used to produce benchmark solutions such as in Hsu and Farmer (1997). There is a broad literature on the use and applications of the MCM in thermal radiation problems, of which the highlights can be listed as Howell (1998, 1968), Siegel and Howell (2002), Farmer and Howell (1997), Modest (1993) and Yang et al. (1995).

The method is based on simulating a finite number of photon bundles that carry a finite amount of radiative energy. The physical events such as emission,

reflection, absorption and scattering that happen in the "life" of a photon bundle are all decided using the probability density functions derived from the physical laws and random numbers. Therefore, once a large enough number of samples is used, the method can produce solutions within the statistical accuracy limits no matter how complex the problem is, which makes it the most versatile solution technique for the radiation problems. On the other hand, this also brings the main drawback for the MCM, which has always been the required high computational expense.

The usual tendency is that the method requires a considerable amount of computation even for a simple surface exchange problem, but adding further complexities does not require a significant amount of additional computation. Therefore, the method is extremely advantageous over the others for problems with many complex phenomena like wavelength and direction dependent properties, geometries with shading or blockage effects. The method gained even more popularity in recent years with the increase in the computational power and introduction of the parallel processing.

2.4.1 Random Numbers

It would be reasonable here to define what is meant by a random number. A random number can be defined as a number chosen from a large set of numbers of equal intervals without a sequence. The simplest way to "generate" random numbers might be writing down a series of numbers of equal intervals on small pieces of paper, putting all the papers in a bag and after mixing them up, picking a number at a time. While carrying out a computational simulation, applying this

method of generating random numbers is impractical. One possible way might be generating a finite number of random numbers and storing them for future use. This will of course require a very large memory if a large number of random numbers is required or otherwise the random numbers would start repeating themselves and their randomness would be questionable.

The standard way to generate a random number that is to be used during a computation is through the use of a piece of code that is developed to perform the task. It might sound quite unacceptable to expect a computer, arguably the most precise and deterministic machine produced by mankind, to generate a true random number, therefore random numbers generated as such are usually referred as pseudo-random numbers.

The topic of generating pseudo-random numbers is a broad area and it is beyond the interests of this study. Further information about the topic is available at Press et al. (1992), Hammersley and Handscomb (1964) and Taussky and Todd (1956). It is important that, while simulating a physical event using the random numbers such as in the case of using a MCM, one should be aware that the pseudo-random numbers generated should have the correct distribution, which is a uniform distribution in our case, and they should not be repeating themselves throughout the whole simulation.

2.4.2 Simulating Physical Events using Random Numbers

Suppose the goal is to statistically simulate a physical event, such as to calculate the wavelength of emission from a surface. The probability of a surface to emit at a specific wavelength λ can be defined as

$$P_\lambda(\lambda) = \frac{E_\lambda}{\int_0^\infty E_\lambda(\lambda')d\lambda'} \tag{2.18}$$

where the function $P_\lambda(\lambda)$ is called the probability density function (PDF) and it is the ratio of radiation emitted at the particular wavelength λ to the total emitted radiation. Therefore, the PDF always has a value smaller than unity and moreover, the sum of all the probabilities, the area under the PDF curve should be equal to unity.

In order to simulate the wavelength of emission, two random numbers, R_1 and R_2, are required. Using these random numbers two wavelength values, λ_1 and λ_2, should be estimated; one from the relation $P_\lambda(\lambda_1) = R_1$ and the other from $\lambda_2 = (\lambda_{max} - \lambda_{min})\, R_2 + \lambda_{min}$. If λ_2 is smaller than λ_1, the wavelength λ_2 is accepted as the wavelength of emission. Otherwise, the two random numbers are rejected and another two are generated to estimate λ_1 and λ_2 until the condition is satisfied.

The process of simulating physical events using a PDF and two random numbers as explained is an expensive one as depending on the PDF a large amount of random numbers generated could be rejected until the appropriate pair is found. An alternative approach necessitates the definition of a cumulative distribution function (CDF) as

$$R_\lambda(\lambda) = \int_0^\lambda P_\lambda(\lambda')d\lambda' \tag{2.19}$$

which denotes the probability of selecting a wavelength in the range 0 to λ. The value of the CDF monotonically increases from 0 to 1 as λ increases from λ_{min} to λ_{max} or 0 to ∞, for the particular case. Therefore, once a relation is developed for

CDF, $R_\lambda(\lambda)$, it can be inverted for $\lambda(R_\lambda)$, R_λ being a pseudo-random number. The relation $\lambda(R_\lambda)$ is referred to as the random number relation (RNR).

If N random numbers are generated and by using the RNR, N wavelength values are calculated, $N_{\Delta\lambda}$ being in each $\Delta\lambda$ increment, it can be related that

$$\frac{N_{\Delta\lambda}/N}{\Delta\lambda} = \frac{\Delta R_\lambda}{\Delta\lambda} \tag{2.20}$$

When a small $\Delta\lambda$ or a large enough N is used, the quantity $\Delta R_\lambda/\Delta\lambda$ approaches $dR_\lambda/d\lambda$, which is simply the PDF or $P_\lambda(\lambda)$. Therefore, if the number of samples used is large enough, the event can be simulated satisfying the PDF that describes the event.

The same approach can be applied for physical events that could be described by multiple independent variables. Consider the PDF for direction of emission from a gray surface

$$\begin{aligned} P_{\theta\varphi}(\theta,\varphi)d\theta\,d\varphi &= \frac{I\cos\theta\sin\theta\,d\theta\,d\varphi\,dA}{\int_0^{2\pi}\int_0^{\pi} I\cos\theta'\sin\theta'\,d\theta'\,d\varphi'\,dA} \\ &= \frac{I\cos\theta\sin\theta\,d\theta\,d\varphi\,dA}{\varepsilon E_b dA} \end{aligned} \tag{2.21}$$

For a diffuse surface the PDF can be separated into two separate PDFs, one for the polar angle another for the azimuthal angle as $P_{\theta\varphi}(\theta,\varphi)=P_\theta(\theta)\,P_\varphi(\varphi)$ where

$$P_\theta(\theta)d\theta = 2\cos\theta\sin\theta\,d\theta \tag{2.22}$$

and

$$P_{\varphi}(\varphi)d\varphi = \frac{(\varepsilon E_b/2\pi)\,d\varphi\,dA}{\varepsilon E_b dA} \tag{2.23}$$

Then the CDFs for the polar and azimuthal angle can be derived as

$$R_{\theta}(\theta) = \int_0^{\theta} 2\cos\theta'\sin\theta'\,d\theta' = \sin^2\theta \tag{2.24}$$

and

$$R_{\varphi}(\varphi) = \int_0^{\varphi} \frac{d\varphi'}{2\pi} = \frac{\varphi}{2\pi} \tag{2.25}$$

both of which can be inverted easily for the corresponding RNR.

There might be cases where the PDF considered is defined in terms of two independent variables but it is not possible to expand it as a multiplication of two separate PDFs. To illustrate this, consider the PDF that defines the location of emission from a rectangular sub-element of a diffuse-gray surface that has a blackbody emissive power distribution $E_b(x,y)$.

$$P_{xy}(x,y) = \frac{\varepsilon E_b(x,y)}{\int_{x_{\min}}^{x_{\max}}\int_{y_{\min}}^{y_{\max}} \varepsilon E_b(x',y')\,dy'\,dx'} \tag{2.26}$$

then the CDFs can be derived as

$$R_x(x) = \frac{\int_{x_{\min}}^{x}\int_{y_{\min}}^{y_{\max}} \varepsilon E_b(x',y')\,dy'\,dx'}{\int_{x_{\min}}^{x_{\max}}\int_{y_{\min}}^{y_{\max}} \varepsilon E_b(x',y')\,dy'\,dx'} \tag{2.27}$$

and

$$R_y(R_x, y) = \frac{\int_{y_{\min}}^{y} \varepsilon E_b[x(R_x), y']dy'}{\int_{y_{\min}}^{y_{\max}} \varepsilon E_b[x(R_x), y']dy'} \tag{2.28}$$

which can be inverted for the RNRs, $x(R_x)$ and $y(R_x, R_y)$, respectively.

It can be observed that the x coordinate of the point of emission is only dependent on a random number, while the y coordinate depends on both random numbers. The Eqs. (2.27) and (2.28) are often termed as the marginal and conditional distributions of the PDF.

2.4.3 Different Monte Carlo Approaches

One of the major advantages of the MCM is its flexibility. For the solution of the same problem a number of different approaches can be implemented in terms of the ray tracing, book keeping procedure, calculating the mean values for the sub-elements. Dependent on the nature of the problem, one could be advantageous over the others.

Literature about the application of the MCM in thermal radiation problems contains a wide variety of different approaches. The most comprehensive study that covers and compares the majority of the possible approaches is by Farmer and Howell (1998) who presented two major approaches for the ray tracing procedure, which is the heart and soul of a MCM simulation. They named the first of these approaches as "the collision-based method", where a photon bundle is assumed to move undisturbed from its emission until it collides with a molecule or a particle and is absorbed or scattered. In this approach the bundle is completely absorbed in a gas element, completely reflected from or absorbed by a surface. The second approach they presented was named "the pathlength-based method", where the energy of the bundle is distributed to the medium as it moves through the absorbing medium or to the surfaces as it is reflected. They have

compared the performances of both methods in a number of different problems and shown that both approaches have similar performances in most of the problems, while the pathlength-based method is slightly advantageous in some.

Another alternative approach, originally proposed by Walters and Buckius (1992), was the "reverse approach" where the photon bundles are simulated from their points of absorption to their points of emission unlike the case of more traditional forward approaches. This approach is especially advantageous when only a certain part of a system is of interest.

2.4.4 Ray Tracing

In this study, a forward, collision-based method is employed for its simplicity and versatility. This section presents ray tracing using the collision-based method in detail. Besides the collision-based method, the outline of ray tracing using the pathlength-based method is also presented to complete the discussion.

Ray Tracing with the Collision-Based Method

As mentioned in the preceding section, in the collision-based method, a photon bundle is assumed to travel undisturbed between its emission and collisions, where it is absorbed or scattered. This simply means that the energy of the photon bundle is not split as the photon bundle moves through the absorbing medium or as it reflects from a surface.

The emission point and direction of emission are calculated using the CDF's developed earlier, given by Eqs. (2.24), (2.25), (2.27) and (2.28). It should be noted that the CDF's for direction of emission differ slightly when the bundles

are emitted from the medium. The CDF for the polar angle of emission from the medium is given as

$$R_\theta(\theta) = \int_0^\theta \frac{\sin\theta'}{2}\, d\theta' = \frac{1-\cos\theta}{2} \tag{2.29}$$

After the emission angles of the photon bundle are calculated, with the available geometric information its direction vector can be calculated as

$$\mathbf{s} = \cos\theta\, \mathbf{n} + \sin\theta(\cos\varphi\, \mathbf{t_1} + \sin\varphi\, \mathbf{t_2}) \tag{2.30}$$

where $\mathbf{n}$ is the unit normal, $\mathbf{t_1}$ and $\mathbf{t_2}$ are the tangential vectors of the surface that are normal to each other so that they satisfy $\mathbf{n} = \mathbf{t_1} \times \mathbf{t_2}$. For the case of medium emission, $\mathbf{t_1}$, $\mathbf{t_2}$ and $\mathbf{n}$ are equivalent to x_1, x_2, x_3 coordinates, as shown in Fig. 2.1.

Once the direction vector and the emission point are known, the next step is to find out what next happens to the bundle in the event history. Two different approaches can be employed at this point.

In the first of these approaches, a random number, R_e, is generated to decide on how far the bundle will travel before it is absorbed or scattered. The bundle is allowed to travel through the medium as long as

$$\int_0^{S_e} \beta(S')dS' < -\ln R_e \tag{2.31}$$

The photon bundle is traced until it is absorbed by an enclosure surface or medium. If the bundle is absorbed or scattered by the medium before it is absorbed by a surface, a new random number, R_ω, is generated to decide if the bundle is absorbed or scattered. If the random number is greater than the scattering albedo, $R_\omega > \omega$, the bundle is absorbed by the gas at that point, otherwise it is scattered and the geometric ray tracing continues.

In the second approach, two random numbers are generated to decide on where the bundle is absorbed or scattered in the medium. The pathlength required for the bundle to get absorbed or scattered by the medium can be calculated simply from

$$\int_0^{S_a} \kappa(S')dS' = -\ln R_a \tag{2.32}$$

and

$$\int_0^{S_s} \sigma_s(S')dS' = -\ln R_s \tag{2.33}$$

respectively. Once these path lengths, together with the pathlength the bundle should travel to hit the surface it is directed towards, are calculated, all three can be compared and the event with the shortest pathlength happens first.

The second approach can be advantageous whenever the medium properties are homogeneous or the geometry is complex. It is also the approach used whenever there is no participating medium inside the enclosure.

It should be noted that the geometric ray tracing that is required to calculate the pathlength the bundle should travel before hitting a surface, is a very critical operation in terms of accuracy and efficiency of the simulation as it is repeated many times. There are many different approaches for geometric ray tracing, and lots of ways to increase the efficiency. In order to complete the discussion it is required to highlight some of them here, and the rest can be referred to Glassner (1989), which presents a very thorough discussion of the topic.

The basic condition for a photon bundle to strike a surface is that the bundle should be directed towards the front of the surface. This can be checked by making use of the dot product of the direction vector of the photon bundle, **s**, and the normal vector of surface, $\mathbf{n}_s$, the bundle might hit**.** If the bundle is directed to the surface the dot product should have a negative value ($\mathbf{n}_s \cdot \mathbf{s} < 0$).

The parametric equation for the photon bundle in terms of the distance traveled is given as, $\mathbf{x} = \mathbf{x_e} + S\ \mathbf{s}$, where $\mathbf{x_e}$ is the coordinate of the point of emission and S denotes the pathlength. The implicit relation defining a surface is, $\mathbf{n}_s \cdot (\mathbf{x}-\mathbf{x_p}) = 0$, where $\mathbf{x_p}$ is the coordinate of an arbitrary point on the surface and $\mathbf{n_s}$ is the surface normal. Then the distance the bundle should travel before it strikes the surface, S, can be calculated by solving the equation for the bundle together with the surface equation as $S = (\mathbf{x_p}-\mathbf{x_e})\mathbf{n_s} / \mathbf{n_s} \cdot \mathbf{s}$.

The rest is identical in both approaches. If the bundle strikes a non-black surface before it is absorbed in the medium, another random number, R_α, is generated to decide if the bundle is absorbed, transmitted or reflected. If the random number is greater than the sum of absorbtivity and transmissivity, $R_\alpha > \alpha+\tau$, the bundle is reflected. If it is smaller than or equal to absorbtivity, $R_\alpha \leq \alpha$, the bundle is absorbed by the surface otherwise, $\alpha < R_\alpha \leq \alpha+\tau$, the bundle is transmitted through the surface. If the bundle is reflected, based on the surface properties the reflected bundle's direction and the reflection point is calculated. If the surface is a diffuse reflector the reflected directions is independent from the incident direction and Eqs. (2.24) and (2.25) are used to calculate the reflected

direction. If the surface is specularly reflecting, the bundle is reflected so that it satisfies $\theta_r = \theta_i$, and $\varphi_r = \varphi_i + \pi$.

If the bundle is scattered by the medium, the point of scattering and the new direction that the bundle is scattered to must be calculated. The probability of a bundle traveling in the direction **s** being scattered in a new direction **s′** is

$$P_{\varpi}(\mathbf{s}')d\varpi = \Phi(\mathbf{s},\mathbf{s}')d\varpi \tag{2.34}$$

leading to the CDFs for polar and azimuthal angles that can be derived from

$$R_{\varphi}(\varphi) = \frac{\int_0^{\varphi}\int_0^{\pi} \Phi(\mathbf{s},\mathbf{s}')\sin\theta'\, d\theta' d\varphi'}{\int_0^{2\pi}\int_0^{\pi} \Phi(\mathbf{s},\mathbf{s}')\sin\theta'\, d\theta' d\varphi'} \tag{2.35}$$

and

$$R_{\theta}(\theta) = \frac{\int_0^{\theta} \Phi(\mathbf{s},\mathbf{s}')\sin\theta'\, d\theta'}{\int_0^{\pi} \Phi(\mathbf{s},\mathbf{s}')\sin\theta'\, d\theta'} \tag{2.36}$$

As the bundles are emitted and absorbed, the exchange factors or the configuration factors for the system can be calculated directly. If all the temperature distributions in the system are known the heat transfer can also be simulated directly.

Ray Tracing with the Pathlength-Based Method

The pathlength-based method is a more realistic approach for simulating the physical event from a macroscopic point of view. The main difference of the pathlength-based method from the collision-based method is that as the bundles move through the absorbing medium the energy carried by the bundle is

distributed to the medium according to Beer's law. If the energy the bundle carries is w as it enters a medium element, and travels the distance S through the element before it leaves, it will leave the element with the energy $we^{-\kappa S}$ leaving $w(1-e^{-\kappa S})$ in the element.

The scattering can be treated similar to the collision-based method, the distance the bundle travels before it is scattered should be calculated from Eq. (2.33) and the new direction of the bundle should be calculated using Eqs. (2.35) and (2.36).

The way to treat reflection also slightly differs from the collision-based method. When a bundle with energy w strikes a non-black surface, it reflects from the surface with the energy in the amount of $w(1-\alpha)$ leaving $w\alpha$ of its energy with the surface. The direction of the reflected bundle is calculated as in the case of collision-based method.

The bundle is traced until the energy level decreases below a previously specified cut-off level. The selection of cut-off level is critical in achieving a certain uncertainty level.

When enough sample photon histories are used, both methods yield close results with a similar level of statistical uncertainty. The collision-based method simulates the physical event from a more microscopic point-of-view, while the pathlength-based method simulates the physical event from a macroscopic perspective. As a result, the collision-based method usually requires more samples than the other. However, this does not necessarily mean that more CPU time is required for all problems. It would be appropriate to conclude stating that

there is no ultimately best Monte Carlo approach, but it is certain that some approaches are better than the others based on the particular problem under consideration.

2.4.5 Error Estimation

One of the most powerful aspects of MCM is that it is a statistical simulation technique, and the error can be estimated in terms of statistical uncertainty. In most other methods defining such a confidence level is not possible.

The most practical way of estimating the error in the value is to subdivide the calculation of the mean into a group of submeans. The central limit theorem, which states that the statistical distribution of the submeans should be distributed in a Gaussian distribution about the overall mean, is then applicable. For a Gaussian distribution the measure of the fluctuations in the means is called the variance. Therefore, instead of making a single Monte Carlo simulation that uses N sample photon histories, M simulations, using N/M samples each, should be carried out to calculate a property, P. If P is distributed based on the Gaussian around the overall mean, $\overline{P}$, an estimate of the error can be made in terms of variance. The variance, γ^2, is

$$\gamma^2 = \frac{1}{M-1}\sum_{i=1}^{M}(P_i - \overline{P})^2 = \frac{1}{M-1}\left[\sum_{i=1}^{M}P_i^2 - \frac{1}{M}\left(\sum_{i=1}^{M}P_i\right)^2\right] \qquad (2.37)$$

The variance, the square of the standard deviation, is an estimate of the mean square deviation of the sample mean $\overline{P}$ from the true mean assuming the true mean could have been calculated using an infinite number of samples. From

the statistical theory, the probability of the sample mean lying within $\pm\gamma$ of the true mean is 68%, $\pm 2\gamma$ of the true mean is 95%, and $\pm 3\gamma$ of the true mean is 99.7% for a Gaussian distribution.

From Eq. (2.37), it can be observed that to reduce the standard deviation by half, the number of simulations, *M*, and at the same time the number of samples, *N*, should be quadrupled. Usually this will result in quadrupling the CPU time.

2.5 NUMERICAL DISCRITIZATION

In order to be able to produce a numerical solution of the mathematical model of the physical system considered, the governing equations should be discretized. The most common methods of discritization in heat transfer and fluid flow problems are the finite difference, finite element, finite volume or spectral schemes. The discritization based on a finite difference scheme represents the flux-based partial differential equations using the finite difference equivalents of the differentials. A finite volume scheme considers the integration of the partial differential equations over the sub-elements considered. The spectral scheme transforms the equations from the physical space to the coefficient space by using transformation techniques like Fourier or Chebychev transformations.

As a coupled solution is sought the selection of the numerical discritization scheme is very dependent on the radiation solver employed. The MCM is selected for the solution of radiative transfer equation. As MCM employs a control volume approach for calculating the heat fluxes at discrete

locations it will be reasonable to discretize the energy equation using a control volume approach.

When the energy equation for the medium element, Eq. (2.3) is discretized for the volume element i with a control volume approach

$$\rho_i c_{p_i} V_i \frac{\partial T_i}{\partial t} = q_{cd,i} + q_{r,i} + Q_i \tag{2.38}$$

will be the resulting equation where $Q_i = Q_i''' V_i$,

$$q_{r,i} = \sum_{j=1}^{N_V} E_j' V_j \widetilde{F}_{j-i} + \sum_{j=1}^{N_S} E_j A_j \widetilde{F}_{j-i} - E_i' V_i \tag{2.39}$$

and

$$q_{cd,i} = k V_i \nabla_{3d}^2 T_i \tag{2.40}$$

The emissive power per volume term in Eq. (2.39) is $E_i' = 4\kappa\sigma T_i^4$, the emissive power per area $E_i = \varepsilon_i \sigma T_i^4$, and the $\widetilde{F}_{j-i}$ denotes the exchange factor from the surface or volume element j to the volume element i that represents the rate of radiative energy emitted from element j, which is absorbed by the medium element i by all means. The exchange factors include the effects of intermediate reflected or scattered energy and can be calculated using any method. The ∇_{3d}^2 term in Eq. (2.40) denotes the finite difference equivalent of the three-dimensional Laplacian operator as

$$\nabla_{3d}^2 T_i = \sum_{j=1}^{3} \frac{T_{i+1}{}^{j} + T_{i-1}{}^{j} - 2T_i}{\Delta x_j{}^2} \tag{2.41}$$

where $T_{i+1}{}^{j}$ and $T_{i-1}{}^{j}$ are the neighboring elements of T_i with respect to the x_j coordinate.

For a steady problem, the term on the left hand side of Eq. (2.38) vanishes, while for a transient problem the equation should be discretized along time. The simplest discretization scheme in time is the first order Euler discretization. There are two different alternative Euler schemes; the implicit scheme considers all the terms but one in the time derivative in the future time step, when the variables are calculated, while the explicit scheme does the opposite.

As the name implies, the implicit scheme results in an implicit set of equations for which a simultaneous solution is required for the whole domain. On the other hand, in the explicit scheme the variables can usually be calculated one at a time. The down side of explicit schemes is the possibility of stability problems and the step sizes become an important issue, whereas the implicit formulations are known to be very stable.

While using the explicit scheme, one should always be aware of the fact that the stability is a big problem. Unlike an implicit scheme, very small time steps must often be used to achieve stable solutions. The equations presented here are highly nonlinear with the absolute temperature to the power four terms inside the integrals, partial second derivatives of temperature to the first power along spatial coordinates and partial derivative along time of absolute temperature. Consequently, it is not possible to derive a direct relation between the appropriate time step and the spatial resolution to achieve a stable solution. Therefore, whenever a transient problem is handled, the solution needs to be tested for stability using different time steps.

Using an explicit Euler discretization scheme the Eq. (2.38) becomes

$$\rho_i c_{p_i} V_i \frac{T_i^{n+1} - T_i^n}{\Delta t} = q_{cd,i}^{\ n} + q_{r,i}^{\ n} + Q_i^n \tag{2.42}$$

where all the conductive and radiative heat transfer terms are evaluated at the n-th time step or at time, $t = n\Delta t$.

Similarly, Eq. (2.7) can be discretized as

$$q_{r,i} + Q_i + q_{cd,i} + h_{in} A_i \left(T_g - T_i\right) + h_{out} A_i \left(T_\infty - T_i\right) = \rho c_p \delta A_i \frac{\partial T_i}{\partial t} \tag{2.43}$$

where $Q_i = Q_i''' \delta A_i = Q_i'' A_i$, the radiative and conductive heat transfer terms are

$$q_{r,i} = \sum_{j=1}^{N_V} E_j^{'} V_j \widetilde{F}_{j-i} + \sum_{j=1}^{N_S} E_j A_j \widetilde{F}_{j-i} - E_i A_i \tag{2.44}$$

and

$$q_{cd,i} = k \delta A_i \nabla_{2d}^2 T_i \tag{2.45}$$

The ∇_{2d}^2 term in Eq. (2.45) denotes the finite difference equivalent of the two-dimensional Laplacian operator defined by Eq. (2.41).

When discretized along time using an explicit Euler scheme, the Eq. (2.43) becomes

$$\begin{aligned} q_{r,i}^{\ n} + Q_i^n + q_{cd,i}^{\ n} + h_{in} A_i \left(T_g^{\ n} - T_i^n\right) \\ + h_{out} A_i \left(T_\infty^{\ n} - T_i^n\right) = \rho c_p \delta A_i \frac{T_i^{n+1} - T_i^n}{\Delta t} \end{aligned} \tag{2.46}$$

As in the case of Eq. (2.3), the radiative, conductive and convective heat transfer terms are evaluated in the n-th time step or at a time, $t = n\Delta t$.

2.5 CODE VERIFICATION USING BENCHMARK PROBLEMS

In order to be able to carry out a design, some tools are required. Whenever these tools are available in terms of commercial codes or codes

presented in literature, they are used; otherwise, the required tools are developed. One of the required tools for this study is a radiation model that is versatile enough and capable of modeling radiation problems that involve complex geometries, and absorbing-emitting and anisotropically scattering media. Therefore, the model is developed using the MCM, and it is then used as a design tool coupled with regularization techniques to tackle inverse design problems.

Before these numerical models are used it would be reasonable to make sure that they are capable of accurately modeling the systems under consideration. This process is often called verification. Moreover, the validity of the mathematical model should also be confirmed by comparing the verified solutions with the response of real physical systems. This process is called validation.

The verification requires comparisons of the numerical solutions produced by the developed codes with analytical solutions wherever they are possible or the benchmark solutions available in the literature. As a part of verification, studies of grid refinement, stability, and statistical convergence should also be considered. In order to be able to carry out these studies, verification of the codes should be carried out using well-posed problems.

For highly radiating systems, validation is a more challenging problem than verification as a complete set of data is very rare and in the cases when it is available it contains coupled effects like chemical reactions due to combustion or other modes of heat transfer. As Howell et al. (2001) indicates, the literature does not contain the required complete experimental data sets to validate a radiation

model isolated from other effects like fluid flow, other modes of heat transfer or chemical reactions when systems with participating media is of interest.

Before using the radiation model developed here, it has been tested against a number of benchmark problems. This section briefly presents the comparisons of the numerical solutions developed with these benchmark solutions.

One of major reasons of the selection of the MCM as a radiation solver is to tackle irregularly shaped enclosure problems. Although the literature includes many studies of axisymmetric or rectangular enclosures, there are not many studies that involve irregular geometries or geometries with blocking effects. One of the few studies involving irregular geometries is Parthasarathy et al. (1995) where three different enclosures containing absorbing-emitting and anisotropically scattering media are considered.

For the verification of the Monte Carlo model used, the first three enclosure problems from Parthasarathy et al. (1995) are solved. The first problem is the quadrilateral enclosure with hot bottom wall, as illustrated in Fig. 2.3. The second and third problems consider the rhombus with hot medium emission and hot bottom wall, respectively. For all three problems, all other media or surfaces except the hot surface or media indicated are cold. The media are absorbing-emitting and isotropically scattering with an extinction coefficient of $\beta = 1\ m^{-1}$ with various scattering albedos, while all surfaces are black. The non-dimensional temperature for the hot surface in the first and third problem and the homogeneous medium in the second problem is given as unity.

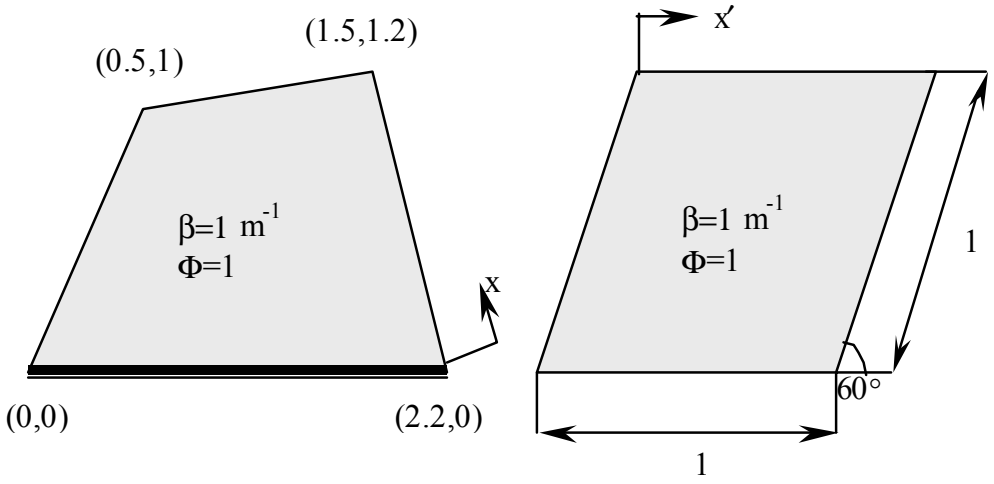

Figure 2.3: The geometries of the quadrilateral and rhombus shaped enclosures, from Parthasarathy et al. (1995)

Figures 2.4 and 2.5 display the non-dimensional radiative heat fluxes on the right wall of the quadrilateral and top wall of the rhombus, for the surface emission problems for different scattering albedos. Figures 2.4 and 2.5 compare well with the distributions for isothermal scattering in Figs. 3 and 5 of Parthasarathy et al. (1995), but due to the lack of tabulated data it is not possible to calculate the relative error. The author of this dissertation contacted the authors of Parthasathy et al. (1995) and requested the tabulated data from that study, but the authors no longer had the original tabulated results. Figure 2.6 presents the heat fluxes for different scattering albedos on the top wall of the rhombus compared to those presented in Parthasarathy et al. (1995). The average of the absolute percentage errors for the quadrilateral enclosure problem with medium emission was evaluated by using scanned data for the pure scattering case, $\omega=1$, and its value is 0.7 %. Therefore, comparisons between the solutions produced by

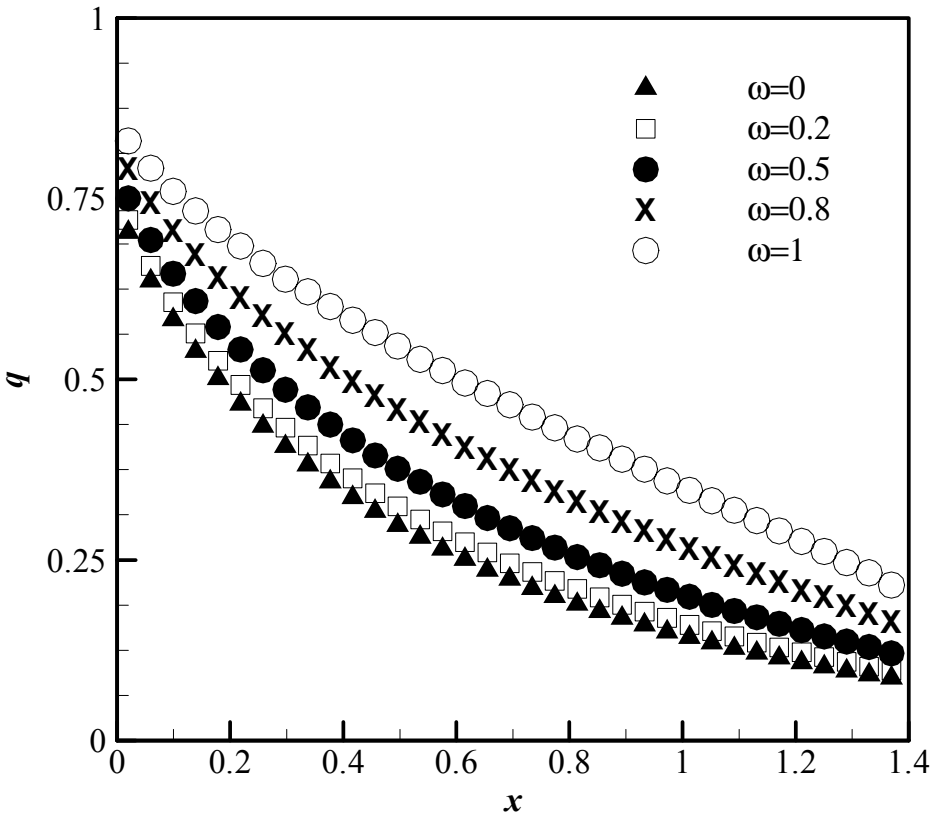

Figure 2.4: Heat flux on the right wall of the quadrilateral

the code developed for this study and the ones presented in Parthasarathy et al. (1995) for the three problems verify the solutions.

Although these problems involve irregular geometries, the thermal conditions are simple with an isothermal hot medium or a hot wall whereas everything else in the system is cold. The Monte Carlo method used in this study has also been tested using another problem with varying temperature distribution in the absorbing emitting medium enclosed in a three-dimensional box-shaped

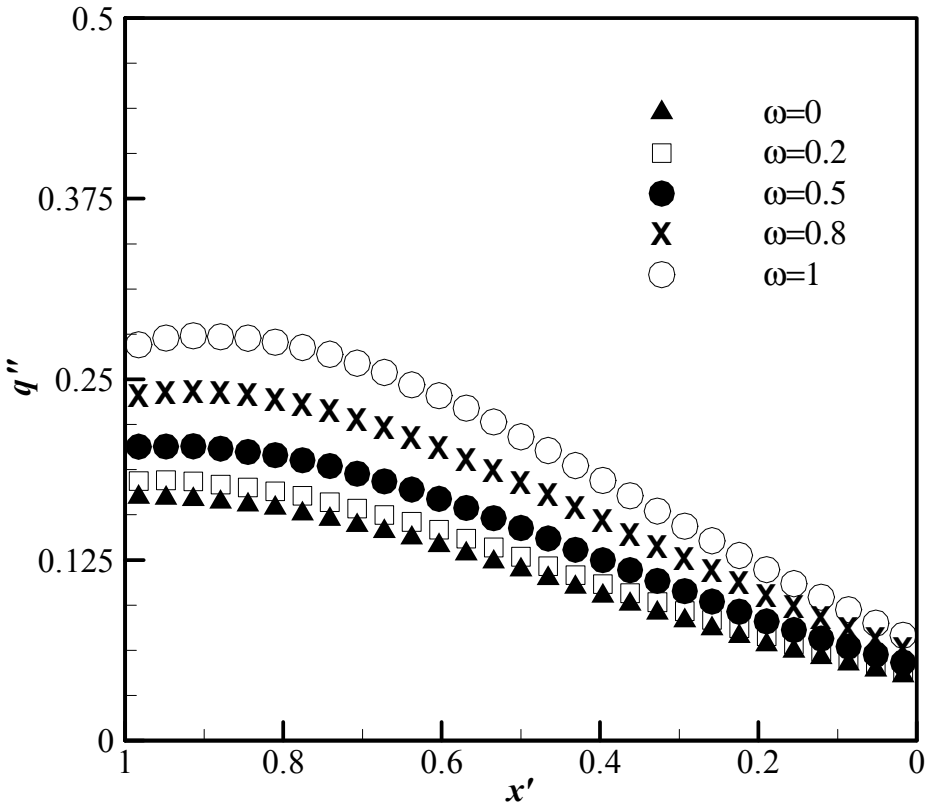

Figure 2.5: Heat flux on the top wall of the rhombus for surface emission problem

furnace. Selçuk (1985) presented the benchmark problem and the exact numerical solution.

The Monte Carlo method used in this study was verified using this problem carrying out a detailed analysis. The details about the verification have been presented in Ertürk et al. (1997) and Ertürk (1997) and will not be repeated here.

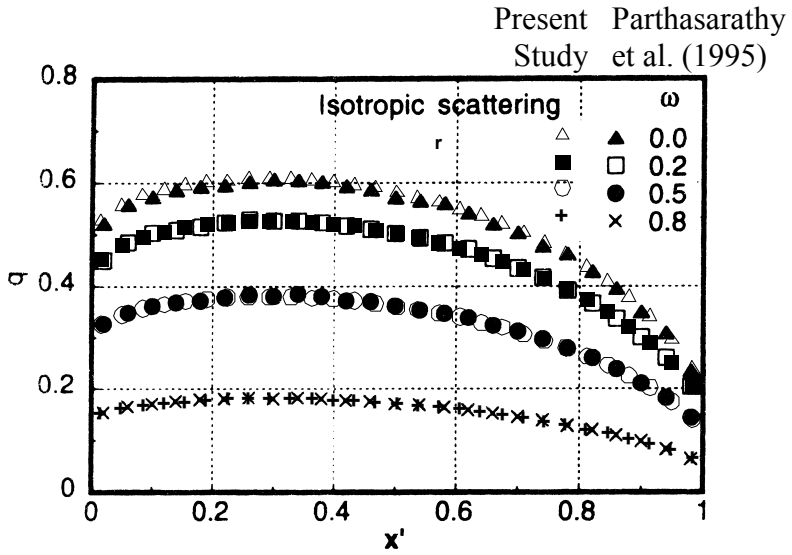

Figure 2.6 Heat flux on the top wall of the rhombus for isothermal medium emission (Parthasarathy et al., 1995)

CHAPTER 3

Inverse Problems and Solution of Ill-Conditioned Systems

3.1 INTRODUCTION

It was stated in the previous chapters that the goal of this study is to develop design methodologies to various problems using the inverse formulation. This simply means that the design problem is considered as an inverse problem where the desired effect is known from the design objective and the necessary cause is sought. It is a well-known fact that the inverse problems result in ill-posed systems, where the solutions become unstable. Most of the conventional solution techniques like Gauss-elimination, LU decomposition or Gauss-Seidel methods suffer from instability, necessitating the use of special solution techniques.

This chapter presents the general aspects of the inverse problems; explaining the ill-posed character and behavior making use of some examples and comparisons with forward problems. In addition, three of the solution techniques that can be used to produce stable solutions for inverse problems, truncated singular value decomposition, the conjugate gradient method and Tikhonov regularization that are used in this study are also presented in detail.

3.2 ILL-POSED AND INVERSE PROBLEMS

Hadamard (1923) is credited with defining the terms well and ill-posed for the first time. He stated that a problem is ill-posed if it does not have a unique

solution or the solution is not a continuous function of the data. This means that the solution is not stable and any small perturbation in the data results in significant changes in the solution. He thought ill-posed problems were artificial and did not describe real physical systems. Nevertheless, it is known that ill-posed problems are encountered in various inverse problems of science and engineering.

In general, inverse problems arise whenever the required input is to be estimated to achieve a desired output in a physical system, or a characteristic of the system is to be predicted from an observed or measured behavior. The former of these problems resembles the design problem that this study deals with and the latter is the measurement problem, which is quite similar to the design problem in most senses. Hansen (1998) defines a linear inverse problem as

$$\int_{\Psi} Input \times System \, d\Psi = Output \tag{3.1}$$

where the output is the available information and the input is desired for a given system. The situation is opposite in a forward problem that considers estimating the output for a given input for the particular system. The same expression can be defined mathematically as

$$\int_0^1 K(s,t)\, f(t)\, dt = g(s) \tag{3.2}$$

for $0 \le s \le 1$, where the $g(s)$ is the known function representing the output of the system that is defined by the $K(s,t)$, the kernel of the integral equation and $f(s)$ is the unknown function. The integral equation presented by the Eq. (3.2) is known as the Fredholm equation of the first kind.

From the given form, it is quite intuitive to expect a Fredholm equation of the first kind to be ill-posed since there might be a number of different solutions that might satisfy the particular output for a given system. However, in order to be able to analyze the Fredholm equation of the first kind and the source of the ill-posedness, the use of singular value expansion (SVE) is essential. The singular value expansion is defined for systems with square integrable kernels, for which the norm defined as

$$\|K\|^2 = \int_0^1 \int_0^1 K(s,t)\, ds\, dt \tag{3.3}$$

is bounded. The SVE of a square integrable kernel is an infinite series

$$K(s,t) = \sum_{i=1}^{\infty} \mu_i u_i(s) v_i(t) \tag{3.4}$$

where the coefficients μ_i are the singular values of the kernel that are non-negative and can be ordered so that $\mu_1 \geq \mu_2 \geq \mu_3 \cdots \geq 0$. The functions $u_i(s)$ and $v_i(t)$ are the singular functions for the kernel and they are orthonormal with respect to the inner product, which is defined by

$$(u_i, u_j) = \int_0^1 u_i(s) u_j(s)\, ds, \tag{3.6}$$

so that

$$(u_i, u_j) = (v_i, v_j) = \begin{cases} 1 & if \quad i = j \\ 0 & if \quad i \neq j \end{cases} \tag{3.7}$$

The singular functions and singular values are the characteristics of a kernel; hence they are unique. The solution for $f(t)$ can then be defined in terms of singular values and functions as

$$f(t) = \sum_{i=1}^{\infty} \frac{(u_i, g)}{\mu_i} v_i(t) \tag{3.8}$$

In order to achieve a square integrable solution the Picard condition should be satisfied (Hansen, 1998). The Picard condition is defined as

$$\sum_{i=1}^{\infty} \left(\frac{(u_i, g)}{\mu_i} \right)^2 < \infty \tag{3.9}$$

which demands that (u_i, g) decay faster than μ_i. This condition is identical to the function g being in the range of the kernel. If this condition is not satisfied or if g is subject to any perturbation so that the resulting right hand side is outside the range of the kernel, the function must be replaced by g_k, which is an approximation achieved by truncating the SVE of the original function g so that it is in the rank of the kernel

$$g_k = \sum_{i=1}^{k} (u_i, g)\, u_i(s) \tag{3.10}$$

Then the approximate solution is given by

$$f_k(t) = \sum_{i=1}^{k} \frac{(u_i, g)}{\mu_i} v_i(t) \tag{3.11}$$

constituting the basic idea behind regularization.

If the solution given by Eq. (3.8) is considered as a spectral expansion of the function f with spectral coefficients $\mu_i^{-1}(u_i, g)$, the inverse problem is nothing but an inverse transformation of the coefficients to construct the function. Then any perturbation in g is amplified with a factor of μ_i^{-1}. This amplification becomes significant especially in the high frequency terms explaining the source of the ill-posedness in a system governed by a Fredholm equation of the first kind.

In order to achieve a smooth solution the system should be regularized. At this point, the residual $r(s)$ is defined as a measure of the solution accuracy for a system defined by Eq. (3.2).

$$r(s) = g(s) - \int_0^1 f(t) K(t,s)\, dt \tag{3.12}$$

The regularization is usually performed following one of four different schemes.

1. Minimize the norm of the residual subject to the constraint that the solution belongs to a specified subset.
2. Minimize the norm of the residual subject to the constraint that a measure of the "size" of the solution is less than some specified upper bound.
3. Minimize the norm of the residual so that it is smaller than some specified convergence criteria.
4. Minimize a linear combination of the norm of the residual and the measure of the "size" of the solution.

All of these schemes require the use of a minimization technique such as least square minimization, steepest descent, Newton's method or the conjugate gradient method. The details about some of these minimization techniques will not be included in this study and are available in the related literature such as Bertsekas (1999).

3.3 LINEAR SYSTEMS OF EQUATIONS

Most problems of science and engineering require solutions of discretized forms of mathematical relations that represent the physical laws. When a set of

Fredholm equation of the first kind is discretized for a number of discrete points in the solution domain, a linear system of equations result. The system can generically be defined as

$$\mathbf{A}\,\mathbf{x} = \mathbf{b} \tag{3.13}$$

where **A** is the coefficient matrix, the discretized kernel that defines the system, **x** is the unknown vector, the values of $f(t)$ at discrete points and **b** is the right hand side vector, or the values of $g(s)$ at discrete points.

Like the analytical form of the Fredholm equation of the first kind, a linear system of equations that is formed by a number of discretized Fredholm equations of the first kind is ill-conditioned. This nature can be investigated using the singular value decomposition (SVD) in discrete systems analogous to SVE in analytical systems. If **A** is an arbitrary MxN matrix, the SVD of **A** is defined as

$$\mathbf{A} = \mathbf{U}\mathbf{S}\mathbf{V}^{\mathrm{T}} \tag{3.14}$$

where **U** is a MxN orthogonal matrix, **S** is a diagonal matrix of N positive or zero singular values $\mu_i = S_{i,i}$ sorted in descending order so that $\mu_1 \geq \mu_2 \geq \ldots \geq 0$, and **V** is an NxN orthogonal matrix. Once SVD is performed, the inverse of **A** can be defined as

$$\mathbf{A}^{-1} = \mathbf{V}\mathbf{S}'\mathbf{U}^{\mathrm{T}} \tag{3.15}$$

where **S′** is a diagonal matrix of N elements where the elements are multiplicative reciprocals of the singular values ($S_{i,i}'=1/\mu_i$).

A characteristic of a discrete ill-posed system is that the singular values decay gradually to zero. As the condition number, the ratio of the greatest

singular value to the smallest one (μ_1/μ_N), approaches infinity the system can be termed as singular and ill-conditioned.

The source of the ill-conditioning for the system can also be explained as follows: A system of linear equations can be interpreted as the linear mapping of the vector space **x** to the vector space **b** defined by the matrix **A**. If **A** is singular there exists a subspace of **x** called the null-space, which is mapped to zero rather than **b**. If the vector **b** is in the range of such an **A** (the sub-space of **b** that can be mapped by **A**), the system will have a number of solutions of linear combinations of the null-space.

In order to be able to solve a linear system that consists of discretized Fredholm equations of the first kind, the system should be regularized in a way similar to the analytical systems. Some minimization techniques can be employed to minimize an objective function based on any four of the regularization approaches. Nevertheless, for the problems with complexities such as absorbing, emitting and anisotropically scattering medium, or non-linearities due to transient effects or multi-mode heat transfer in our applications, the calculation of the sensitivity coefficients that are required for many minimization techniques might not be feasible for a discrete system. For these types of problems, it is common to use direct techniques that iteratively find the solution that minimizes the residual or various decomposition techniques that gets rid of the source of ill-conditioning in the system.

These techniques can be used to produce a set of solutions at different levels of regularization. Then the "optimal" solution that has acceptable accuracy

and smoothness can be selected. In order to make this decision, the use of the so-called "L-curve" is essential. The L-curve can be constructed by plotting the variation of the norm of the residual with the norm of the solution for every alternative solution available in the set. The residual is defined as

$$\mathbf{r} = \mathbf{b} - \mathbf{A}\,\mathbf{x} \tag{3.16}$$

For a discrete system, the norm is referred to as an L_2 norm. The decrease in the norm of the residual represents the increase in the accuracy of the solution. Usually as the norm of the solution increases, which represents the loss of smoothness of the solution, the norm of the residual decreases. The optimal solution can then be selected as one with small norm of the residual and norm of the solution at the same time.

A typical L-curve for a discrete ill-posed system is presented in Fig. 3.1. The typical trend can be explained as follows: As the regularization level or the filtering is increased corresponding to movement from left to right along the horizantal axis for log ($\|\mathbf{r}\|$), a slight ascent in the norm of residual with a sharp drop in the solution norm is observed while this trend slows down quite suddenly after a certain regularization level is reached. The L-curve has a corner at this point and further regularization greatly increases the norm of the residual with a slight decrease in the solution norm. The optimal solution usually lies around the corner of the L-shape where the solution norm is reduced slightly with a small decrease in the norm of the residual. .

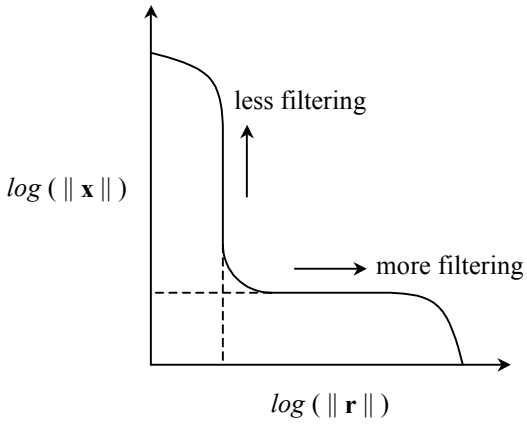

Figure 3.1: L-curve for a discrete ill-posed system

3.4 REGULARIZED SOLUTION TECHNIQUES

Some of the most commonly used regularized solution techniques are the truncated singular value decomposition (TSVD), the conjugate gradient method (CGM) and the Tikhonov regularization (TR). Of these TR follows the fourth scheme while TSVD is a decomposition technique that minimizes the residual. The conjugate gradient method is more flexible and can be coupled with either one of the schemes outlined.

3.4.1 Truncated Singular Value Decomposition

Truncated singular value decomposition is a direct solution technique based on SVD explained in the previous section.

For a system characterized by an ill-conditioned coefficient matrix, the direct use of the inverse of a matrix that has a high condition number yields a

solution that is dominated by high amplitude fluctuations caused by inversion of very small singular values. This usually results in a loss of physical meaning in a problem. Therefore, the part of the system that causes this amplification should be filtered.

This can be carried out by setting the elements in **S′** to zero corresponding to the zero valued elements in **S**. Moreover, in practice not only the elements corresponding to zero singular values but also the ones corresponding to other small singular values must be truncated from the system to eliminate round off errors in a numerical solution. Then using the truncated **S′** and the resulting pseudo-inverse of matrix **A**, a solution can be obtained as

$$x_n = \sum_{k=1}^{p} V_{n,k} \frac{b_m U_{m,k}}{S_{k,k}} \qquad n = 1, 2, \ldots, N \tag{3.17}$$

where p has a value smaller than the rank of **A** and denotes the number of singular values used to construct the pseudo-inverse of matrix **A**.

In a numerical solution of an inverse design problem, retaining different numbers of singular values that yield a number of alternative solutions to the system that is within acceptable differences from the desired design condition at different regularization levels is essential, as having alternatives is advantageous from the designer's point of view. Then the most suitable solution for the designer's needs can be selected by the help of an L-curve as explained before.

It is shown in Hansen (1992, 1998) and Press et al. (1992) that the solution given in Eq. (3.17) is equivalent to a least squares solution that minimizes the residual of the system.

3.4.2 The Conjugate Gradient Method

The conjugate gradient method is a general iterative minimization technique. The solution is defined as a linear combination of search directions, which are selected as conjugate vectors, **p**'s, that provide the maximum available information about the system. Each step introduces the generation and addition of a new conjugate vector to the solution of the previous step, providing a monotonic convergence of the objective function to a minimum.

In order to be able to solve a linear system of equations using the CGM, the algorithm presented by Beckman (1960) can be used. The algorithm provides the exact solution **h** to a linear system, such as Eq. (3.13), in *N*-steps, where *N* is the number of unknowns. For a system defined by a symmetric and positive-definite coefficient matrix, **A**, the objective is minimizing the functional,

$$F(\mathbf{x}) = [\mathbf{A}\,(\mathbf{h}-\mathbf{x})]\cdot(\mathbf{h}-\mathbf{x}), \tag{3.18}$$

which becomes zero at its minimum when $\mathbf{x}=\mathbf{h}$. In order to minimize the functional the gradient that is equivalent to the negative of twice the residual should reach zero ($\nabla F(\mathbf{x})=-2\mathbf{r}=0$). The CGM algorithm presented can be generalized for any arbitrary *M*x*N* system by modifying the system through multiplication of both sides of the equation by $\mathbf{A}^T$.

In the CGM presented here, the Gram-Schmidt orthogonalization technique is used for calculating the conjugate vectors at each step and the derivation of the method is presented by Beckman (1960) in detail and is not repeated here. The generalized algorithm that can be applied to solve an arbitrary linear system of equations is presented in Figure 3.2.

1. $\mathbf{x}^1=0$
2. $\mathbf{r}^1 = \mathbf{b} - \mathbf{A}\mathbf{x}^1 = \mathbf{b}$
3. $\mathbf{p}^1 = \mathbf{A}^{\mathrm{T}}\mathbf{r}^1$
4. $k = 1..N$
   - i. $\alpha^k = \dfrac{\left|\mathbf{A}^{\mathrm{T}}\mathbf{r}^k\right|^2}{\left|\mathbf{A}\mathbf{p}^k\right|^2}$
   - ii. $\mathbf{x}^{k+1} = \mathbf{x}^k + \alpha^k\mathbf{p}^k$
   - iii. $\mathbf{r}^{k+1} = \mathbf{r}^k - \alpha^k\mathbf{A}\mathbf{p}^k$
   - iv. $\beta^k = \dfrac{\left|\mathbf{A}^{\mathrm{T}}\mathbf{r}^{k+1}\right|^2}{\left|\mathbf{A}^{\mathrm{T}}\mathbf{r}^k\right|^2}$
   - v. $\mathbf{p}^{k+1} = \mathbf{A}^T\mathbf{r}^{k+1} - \beta^k\mathbf{p}^k$

Figure 3.2: The conjugate gradient algorithm

As an *N*-step solution technique, for inverse problems the solutions achieved at the end of every step can be considered as a unique, alternative solution with different accuracy and smoothness characteristics. The N different solutions can then be used to construct an L-curve in order to select the optimal solution.

The method presented is a very simple and elegant one that only makes use of simple matrix-vector multiplications. The requirement of small memory for storing intermediate results and parameters, and computation economy makes it the method of choice for large systems. It has robust convergence characteristics in that the approximation at each step is superior when compared

with the results of previous ones. In addition, the original matrix is stored and used as is.

It should be noted that the CGM algorithm presented and TSVD are very similar methods based on the same objective and the differences in the solutions are due to the different methodologies they follow.

3.4.3 Tikhonov Regularization

Tikhonov was the pioneering researcher in stabilizing ill-posed systems in the 1960's and proposed a method for regularization of ill-posed systems that is named after himself. Tikhonov's regularization scheme follows the fourth approach listed earlier, which is minimizing a linear combination of the norm of the residual and a measure of the "size" of the solution. The objective function to be minimized is

$$F(\mathbf{x}) = \left[\left\| \mathbf{A}\mathbf{x} - \mathbf{b} \right\| \right]^2 + \sum_{i=1}^{p} \alpha_i^2 \left[\left\| \mathbf{L}_i (\mathbf{x} - \mathbf{x_0}) \right\| \right]^2 \tag{3.19}$$

For a p-th order scheme, $\mathbf{L}_i$ approximates the discretized i-th derivative operator and α_i is the i-th order regularization parameter. In the given form, using a small regularization parameter will result in an accurate solution putting the emphasis on minimizing the norm of the residual, while using a large regularization parameter will result in a solution with improved smoothness characteristics rather than accuracy. In order to minimize the function, the following condition must be satisfied

$$\frac{dF}{d\mathbf{x}} = 0 = 2\mathbf{A}^{\mathrm{T}}(\mathbf{A}\mathbf{x} - \mathbf{b}) + 2\sum_{i=1}^{p} \alpha_i^2 \mathbf{L}_i^{\mathrm{T}} \mathbf{L}_i (\mathbf{x} - \mathbf{x_0}) \tag{3.20}$$

For the standard or zeroth order Tikhonov regularization scheme, p=0 and $\mathbf{L}_i$ becomes the identity matrix $\mathbf{I}$, leading to the modified set of linear equations

$$(\mathbf{A}^{\mathrm{T}}\mathbf{A} + \alpha_0^{\,2}\mathbf{I})\mathbf{x} = \mathbf{A}^{\mathrm{T}}\mathbf{b} + \alpha_0^{\,2}\mathbf{I}\,\mathbf{x_0} \tag{3.21}$$

Similarly for a second order regularization for which, p = 2, $\alpha_0 = \alpha_1 = 0$ the linear system modifies to

$$(\mathbf{A}^{\mathrm{T}}\mathbf{A} + \alpha_2^{\,2}\mathbf{L}_2^{\,\mathrm{T}}\mathbf{L}_2)\mathbf{x} = \mathbf{A}^{\mathrm{T}}\mathbf{b} + \alpha_2^{\,2}\mathbf{L}_2^{\,\mathrm{T}}\mathbf{L}_2\mathbf{x_0} \tag{3.22}$$

As in the cases of other regularization techniques using the correct regularization parameter is very important to achieve an optimal solution that is smooth and accurate enough for the designer's needs. A number of solutions with different regularization levels can be used to construct an L-curve, and the required regularization parameter can be selected accordingly.

However, the construction of such a L-curve solving Eq. (3.21) or Eq. (3.22) can be computationally expensive. Here, it is worthwhile to present the analogy between the zeroth order Tikhonov regularization scheme and the TSVD. The TSVD solution for an ill-conditioned system of equation was presented by Eq. (3.17). The solution of Eq. (3.21) analogous to the TSVD solution is

$$x_n = \sum_{k=1}^{N} V_{n,k} \frac{S_{k,k}}{S_{k,k}^{\,2} + \alpha_0^{\,2}} b_m U_{m,k} \qquad n = 1, 2, \ldots, N \tag{3.23}$$

where the Tikhonov filtering function replaces the TSVD filtering function (Vogel, 2002).

3.5 APPLICATION OF REGULARIZATION TECHNIQUES

In order to demonstrate the nature of an inverse problem together with the application of the regularization techniques a simple design problem is solved. Consider the two black parallel plates as shown in Fig. 3.3.

In the regular forward problem, a condition at each boundary is defined and the conditions other than the ones specified are estimated. Then, an equation is written for each lumped sub-element *i* as

$$\frac{1}{\varepsilon_i} q_i + \sum_{j=1}^{N} \left(1 - \frac{1}{\varepsilon_j} \right) q_j F_{j-i} = \sum_{j=1}^{N} \frac{1}{\varepsilon_j} E_j A_j F_{j-i} - \frac{1}{\varepsilon_i} E_i A_i \tag{3.24}$$

As long as one of the conditions is specified, E or q, for every sub-element, Eq. (3.24) is a discretized Fredholm equation of the second kind, which is known to be well-posed and the system of equations can then be solved using any solver capable of producing solutions to linear systems such as LU-decomposition, Gauss-Seidel method or Gauss elimination.

However, design problems can be different than the forward problem in many occasions. Consider the case where the bottom surface is to be heated to satisfy certain thermal conditions by the heaters located on the top or measurements from the bottom surface are used to estimate the conditions along the top plate. In both cases, the bottom surface can be referred as the design surface, where both temperature and heat flux distributions are defined. The top surface is the heater or the unknown surface for which the temperature and the required power distributions are to be estimated.

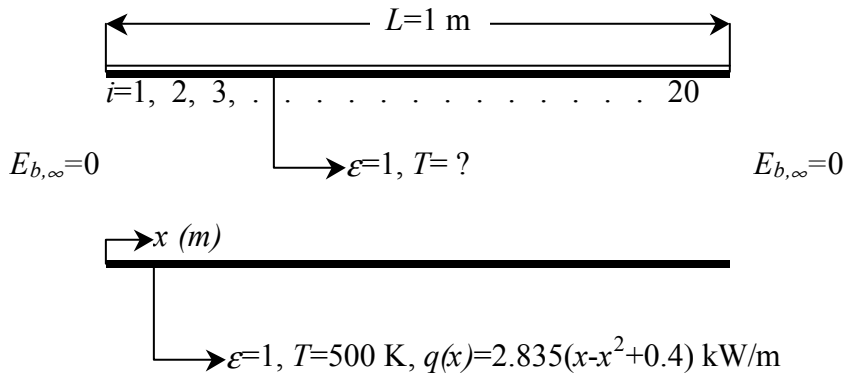

Figure 3.3: The geometry of the sample problem

For a problem with black surfaces as in the case of the system displayed in Fig. 3.3, the equation that is to be satisfied for the design surface elements is

$$\sum_{j=1}^{N_{top}} E_{b,j}\, A_j\, F_{j-i} = q_i + E_{b,i}\, A_i \tag{3.25}$$

The set of equations with unknown emissive powers inside the summation terms constitute a set of discretized Fredholm equations of the first kind, which is known to be ill-conditioned.

For 40 grid points, the configuration factors can be calculated simply by Hottel's cross-strings method, and the corresponding solution through matrix inversion yields the distribution in Fig. 3.4. The solution presented is very accurate with a norm of the residual of $3.5\text{x}10^{-6}$, the resulting maximum and average absolute percentage error based on the flux achieved on the bottom surface is $2.1\text{x}10^{-4}$ and $1.1\text{x}10^{-4}$ percent, respectively. The error in the solution presented is due to the round off error.

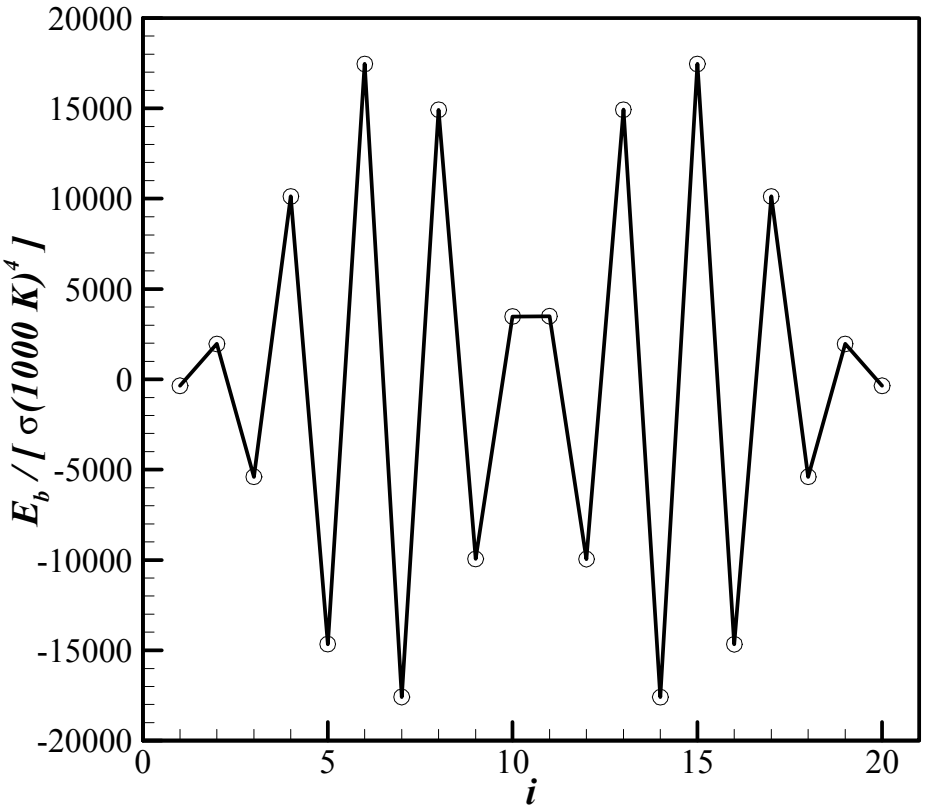

Figure 3.4: The exact solution to the problem of Fig. 3.3 by direct inversion of the coefficient matrix

Although the solution is very accurate, it is not acceptable for two reasons. First negative values of emissive power ($E_{b,i}=\sigma T_i^4$) imply imaginary absolute temperatures on surface 1. Second, the magnitude and fluctuations of emissive power along the unknown elements are impossible to realize in practice.

The reason for the fluctuations in the solution can be explained using the SVD. The singular values for the system are presented in Fig. 3.5. They decay

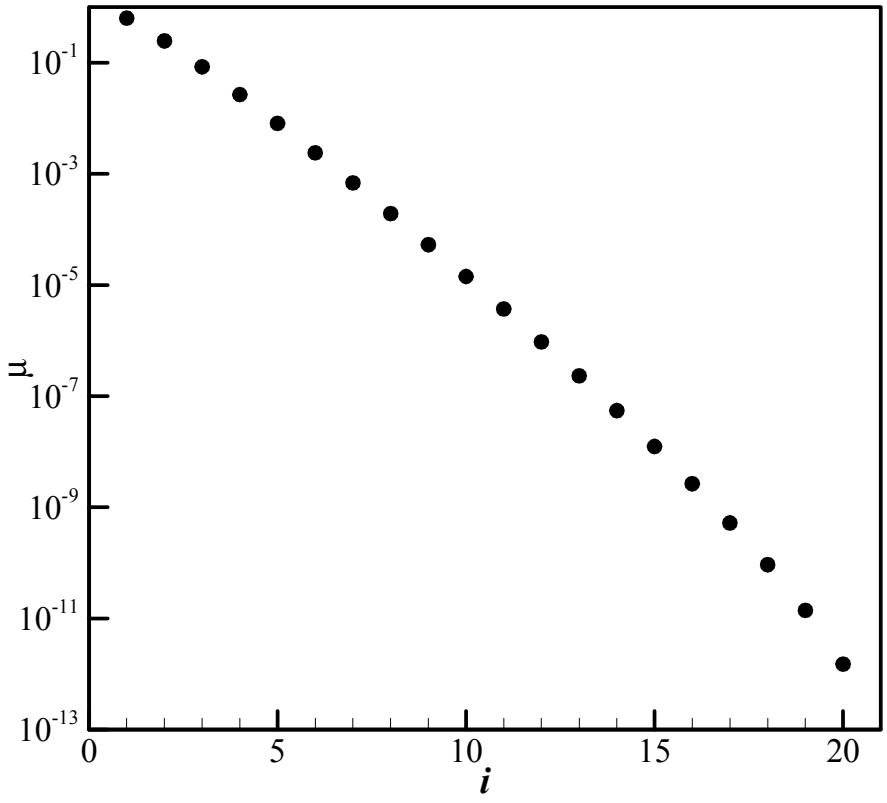

Figure 3.5: The singular values for the system presented in Fig. 3.3

continuously satisfying the characteristic of a discrete ill-posed problem (Hansen, 1998). The condition number, which is the ratio of the greatest singular value to the smallest singular value, for the system is 4.2×10^{11}. Therefore, the system can be recognized as an ill-conditioned system with high condition number. For such a system, regularization or filtering is required to achieve a reasonable solution. Here solutions with three different regularization methods, the TSVD, the CGM and the TR, are presented.

3.5.1 Solution with TSVD

The solution by TSVD can be achieved by back substituting the singular values presented as explained by Eq. (3.16). Some solutions that use different numbers of singular values are presented in Fig. 3.6 and the L-curve displaying the change in the norm of the residual vector with the norm of the solution vector for alternative solutions are presented in Fig. 3.7. In theory, for a system with N of these solutions are unique due to symmetry. As the number of singular values

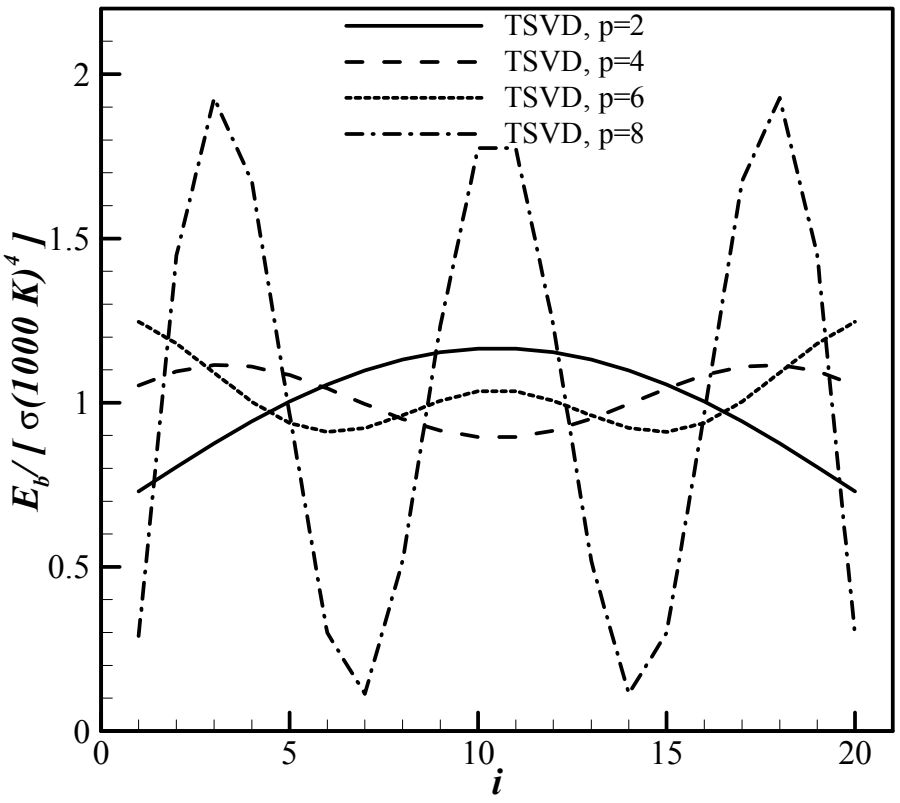

Figure 3.6: Alternative solutions achieved with TSVD

used increases, the solution becomes more accurate, while the fluctuations enlarge. The resulting maximum and average absolute percentage error based on the flux achieved on the bottom surface compared with specified desired value is presented in Table 3.1 together with the errors from the other solutions. From the L-curve, it can be observed that a solution with p=5 or 6 constitute the corner point, providing a smooth and accurate solution.

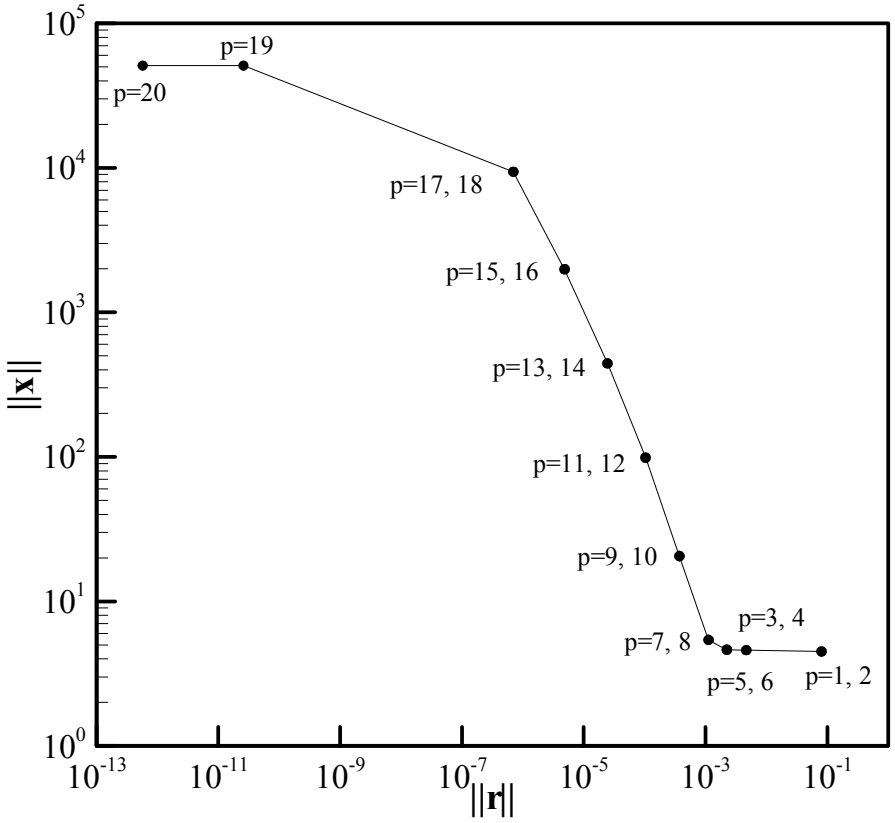

Figure 3.7: The L-curve for the TSVD solutions

3.5.2 Solution with CGM

Another method providing regularized solutions is the CGM, a very robust and economic alternative. The algorithm presented in Fig. 3.2 is applied to achieve the solutions displayed in Fig. 3.8. The profiles in Fig. 3.8 are very similar to the ones in Fig. 3.6, proving that the CGM used and TSVD are very similar in terms of minimizing the residual.

The L-curve for the CGM solutions is presented in Fig. 3.9 and it can be

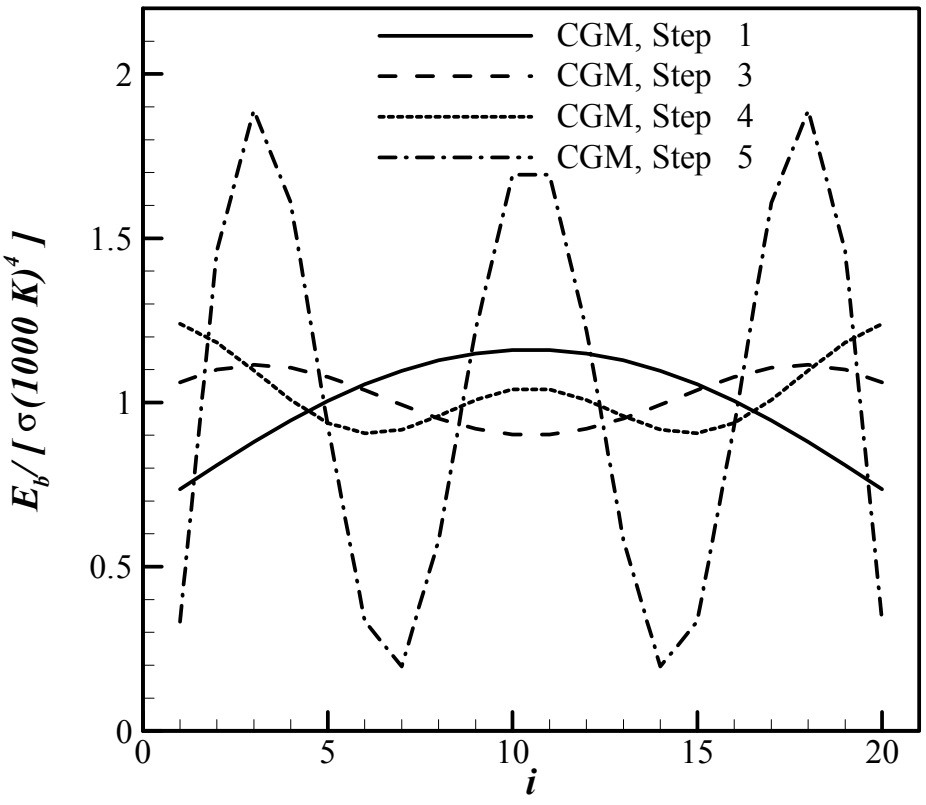

Figure 3.8: Alternative solutions achieved with CGM

observed that the range of the norm of the solutions and the corresponding norm of their residuals are smaller than it is for the solutions by TSVD. The number of unique solutions is identical for both. The L-curve suggests that the optimal solution is the one produced by fourth CG-step as this point is the one closest to the corner.

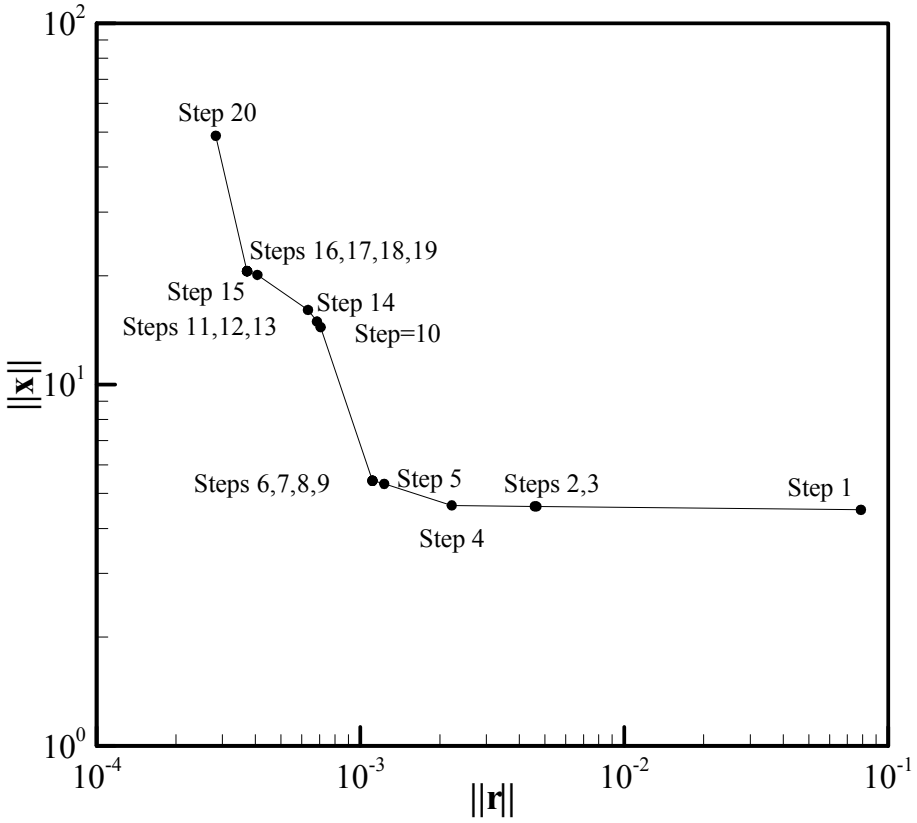

Figure 3.9: The L-curve for the CGM solutions

3.5.3 Solutions with TR

Solutions produced with TR at different orders and regularization levels are presented in Fig. 3.10. Three different orders are used and in order to show the effect of each order solely, the regularization parameters for the smaller orders are set to zero (for a first order regularization $\alpha_0=0$ and for a second order regularization $\alpha_0=\alpha_1=0$). Utilizing the regularization parameters presented in Fig. 3.10, the corresponding solutions yield to various levels of accuracy and solution shapes. Although some of the solutions have shapes similar to the TSVD or CGM solutions, some of the solutions have unique shapes, which is preferential from the designer's point of view.

It should be noted that the solutions produced with TR has a component in the numerical null-space of the coefficient matrix of the system. This is not the case with TSVD or the CGM applied. The requirement is due to the fact that not only minimizing the residual is desired, as in the case of TSVD and CGM, but also a constraint related to the shape is imposed on the system.

The comparison of solution accuracies for all methods employed is presented in Table 3.1. The error values presented are calculated based on the heat flux distribution recovered on the bottom surface with the distribution given in Fig. 3.3. The percentage errors are calculated from

$$\%Err_i = 100\frac{|q_i - q(x_i)|}{q(x_i)} \tag{3.26}$$

where q_i denotes the heat flux based on the calculated emissive power distribution.

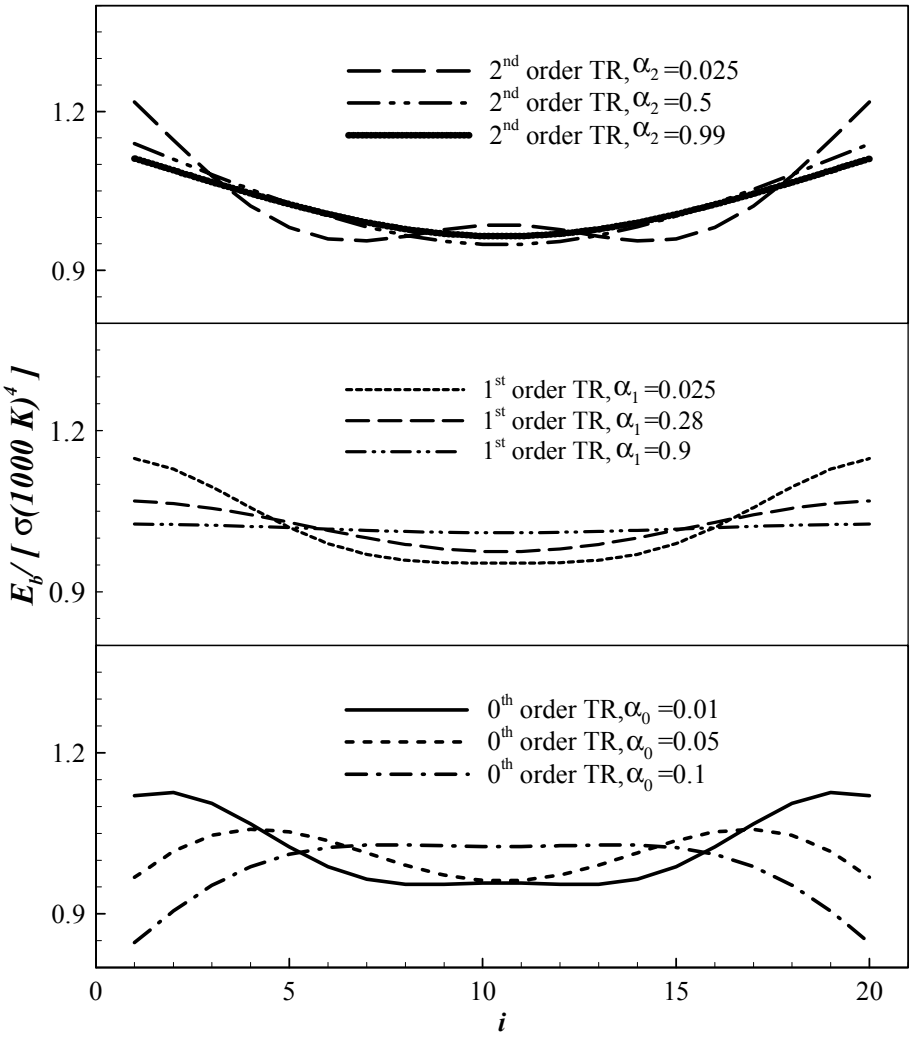

Figure 3.10: The alternative solutions achieved with three different orders of Tikhonov regularization.

When the resulting errors and the shapes of the consequent solutions are considered, it can be observed that smooth and accurate solutions are calculated using very small regularization parameters for all three orders.

One last comment should be addressed regarding computation economy. Although there is no significant difference in computation time between the methods presented for a simple problem like the one presented, for larger systems the computation economy can be a major criterion for selection of the method to use. Further discussion is presented in the next chapter.

Table 3.1: The solution accuracies for different methods at different regularization levels

Method	Figure	Regularization Level	Maximum(%Err)	Average(%Err)
Exact	Fig. 3.4		2.1×10^{-4}	1.1×10^{-4}
TSVD	Fig. 3.6	p=2	6.5	3.0
		p=4	0.29	0.17
		p=6	0.23	0.082
		p=8	0.10	0.04
CGM	Fig. 3.8	Step 1	6.4	3.0
		Step 3	0.27	0.16
		Step 4	0.23	0.081
		Step 5	0.12	0.043
TR	Fig. 3.10	0^{th} order α_0=0.01	0.24	0.11
		0^{th} order α_0=0.05	1.1	0.53
		0^{th} order α_0=0.1	6.5	3.2
		1^{st} order α_1=0.025	0.24	0.11
		1^{st} order α_1=0.28	1.1	0.53
		1^{st} order α_1=0.9	1.9	0.9
		2^{nd} order α_2=0.025	0.18	0.09
		2^{nd} order α_2=0.5	0.4	0.15
		2^{nd} order α_2=0.99	0.75	0.33

CHAPTER 4

Boundary Condition Design of Steady Thermal Systems

4.1 INTRODUCTION

Consider a thermal processing system with specific geometry and properties. If the goal is to satisfy specified conditions according to the needs of the process, the only way to achieve this goal will be arranging the power input for the heaters or the burners in the system. The problem of calculating the required input for heaters (or burners) in such a system is referred as boundary condition (or load) estimation problem. In Chapter 3, using a simple example problem, it has been demonstrated that this type of problem is an inverse problem and the governing system is ill-posed.

A generalized formulation and solutions for boundary condition estimation problems are presented in this chapter. These are more complex problems than the one presented in the previous chapter. The problems considered here are steady-state problems with pure radiation (with no other modes of heat transfer) that include certain levels of complexities such as blockage in the geometry, anisotropically scattering medium or mirror-like reflecting surfaces. Through the solutions of these problems, besides the ill-posed behavior and the characteristics of the solution, the physical aspects of design in such systems can also be investigated.

Two problems are considered: The first problem considers a two-dimensional irregularly shaped geometry. The heater input is calculated for a number of different medium conditions and heater configurations. The boundary conditions of a three-dimensional enclosure enclosing absorbing-emitting and anisotropically scattering medium are designed next using a number of different solution techniques. The solution techniques used are then compared in terms of their performance and accuracy.

It is adequate to start with the underlying characteristics and main aspects of the problem together with the governing equations and possible solution methodologies.

4.2 BOUNDARY CONDITION DESIGN AND INVERSE FORMULATION

A simple thermal processing system can be represented by the use of an enclosure such as the one presented in Fig. 4.1. For such an enclosure, for the forward problem, one condition (either T or q) is specified on every boundary and the medium and the unknowns are calculated from the available information (Fig. 4.1 a). The problem is analogous to observing the system's response to a known cause.

In a design problem, both and T and q are specified for some of the elements, while only either T or q is defined for others and no information is available for still others (Fig. 4.1 b). The first group is usually referred to as the design elements, while the second group is named the temperature or flux specified elements. The group where no information is available is the unknown

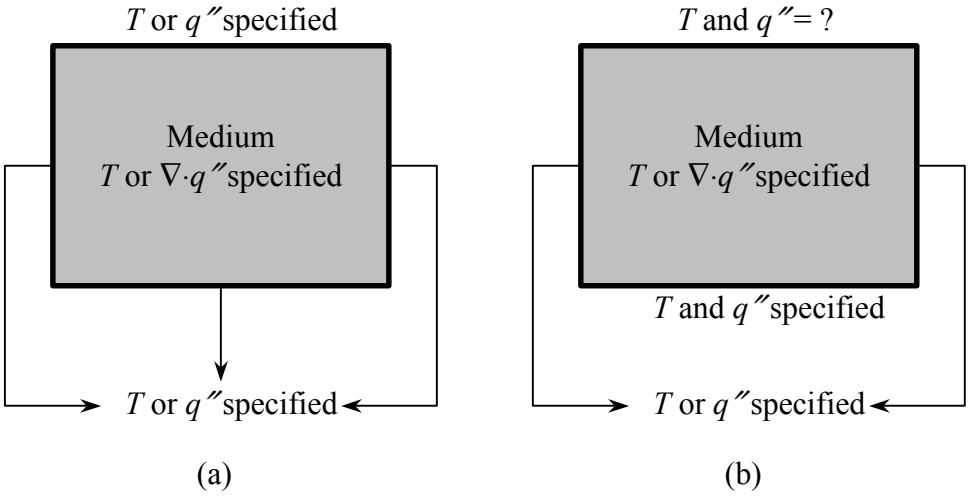

Figure 4.1: (a) Enclosure with the conditions of the forward problem, (b) Enclosure with the conditions of an inverse problem

elements. In a thermal processing system, the unknown elements represent the burners or heaters while the design elements represent the object processed.

Although, the design problem is an inverse problem, forward formulation together with iterative techniques (trial-and-error or optimization) can be employed for the solution. The inverse formulation, on the other hand, results in a direct solution as long as the problem is linear.

For a system at steady state with no flow inside, the discretized energy equation for surface and medium elements are

$$\sum_{j=1}^{N_V} E_j' V_j \widetilde{F}_{j-i} + \sum_{j=1}^{N_S} E_j A_j \widetilde{F}_{j-i} - E_i A_i + Q_i + k\delta A_i \nabla_{2d}^2 T_i + h_{out} A_i \left(T_\infty - T_i\right) = 0 \tag{4.1}$$

$$\sum_{j=1}^{N_V} E_j' V_j \widetilde{F}_{j-i} + \sum_{j=1}^{N_S} E_j A_j \widetilde{F}_{j-i} - E_i' V_i + Q_i + kV_i \nabla_{3d}^2 T_i = 0 \qquad (4.2)$$

from Eqs. (2.43-45) and (2.38-40), respectively. Both equations are non-linear with T^4 appearing in radiative terms and T appearing in diffusive and convective terms.

In a forward problem an equation is written for each element in the solution domain and the system can be solved simultaneously. The equations reorganized for a temperature specified surface are

$$\left[\sum_{j=1}^{N_V} E_j' V_j \widetilde{F}_{j-i} + \sum_{j=1}^{N_S} E_j A_j \widetilde{F}_{j-i}\right]_{T \text{ unknown}} + Q_i = E_i A_i - k\delta A_i \nabla_{2d}^2 T_i - h_{out} A_i (T_\infty - T_i) - \left[\sum_{j=1}^{N_V} E_j' V_j \widetilde{F}_{j-i} + \sum_{j=1}^{N_S} E_j A_j \widetilde{F}_{j-i}\right]_{T \text{ specified}} \qquad (4.3\text{-a})$$

The summations inside $[\ ]_{T \text{ specified}}$ are over the elements where the temperature is specified and inside $[\ ]_{T \text{ unknown}}$ are over the elements where temperature is unknown (heaters or burners and flux specified elements). Similarly, for a heat flux specified surface

$$\left[\sum_{j=1}^{N_V} E_j' V_j \widetilde{F}_{j-i} + \sum_{j=1}^{N_S} E_j A_j \widetilde{F}_{j-i}\right]_{T \text{ unknown}} + k\delta A_i \nabla_{2d}^2 T_i + h_{out} A_i (T_\infty - T_i) - E_i A_i = -\left[\sum_{j=1}^{N_V} E_j' V_j \widetilde{F}_{j-i} + \sum_{j=1}^{N_S} E_j A_j \widetilde{F}_{j-i}\right]_{T \text{ specified}} - Q_i \qquad (4.3\text{-b})$$

For the medium elements,

$$\left[\sum_{j=1}^{N_V} E_j^{'} V_j \widetilde{F}_{j-i} + \sum_{j=1}^{N_S} E_j A_j \widetilde{F}_{j-i}\right]_{T\ \text{unknown}} + Q_i = E_i^{'} V_i - \left[\sum_{j=1}^{N_V} E_j^{'} V_j \widetilde{F}_{j-i} + \sum_{j=1}^{N_S} E_j A_j \widetilde{F}_{j-i}\right]_{T\ \text{specified}} - kV_i \nabla_{3d}^2 T_i \tag{4.4-a}$$

for a temperature specified volume element and

$$\left[\sum_{j=1}^{N_V} E_j^{'} V_j \widetilde{F}_{j-i} + \sum_{j=1}^{N_S} E_j A_j \widetilde{F}_{j-i}\right]_{T\ \text{unknown}} + kV_i \nabla_{3d}^2 T_i - E_i^{'} V_i = -Q_i - \left[\sum_{j=1}^{N_V} E_j^{'} V_j \widetilde{F}_{j-i} + \sum_{j=1}^{N_S} E_j A_j \widetilde{F}_{j-i}\right]_{T\ \text{specified}} \tag{4.4-b}$$

for a source specified volume element.

In the given form, the non-linearity in the equations necessitates an iterative solution. A detailed discussion about solving non-linear multi-mode heat transfer problems is presented elsewhere (Siegel and Howell, 2002) and is not repeated here.

This study focuses on a special case of the physical conditions presented; radiation dominating the heat transfer, where the other means of heat transfer can be neglected. In this case, the equations describing the system become linear. As equations written for every point in the solution domain are discretized Fredholm equations of the second kind, the resulting system is stable and well posed. Consequently, any linear solver can be used to calculate unknown variables.

However, solution of a design problem using a forward formulation is not straightforward and requires more attention. As there is no information provided for some parts of the system (heaters or burners), an initial guess is required. Then the system can be solved using one of the boundary conditions specified in

the design surface and the other boundary condition over the design surface is estimated. Then, comparing the estimated value with the one specified, the guessed values must be modified. The procedure is repeated until the estimated condition and the specified condition over the design surface converges.

The most important part of the solution is the way the condition in the heaters or burners is modified between iterations. If the values are modified in an unorganized way then the solution technique is called a trial-and-error method. The method is referred to as optimization if a certain algorithm that minimizes the difference between the estimated and the specified condition over the design surface is employed. Solutions of boundary condition design using optimization techniques are discussed in Özışık and Orlande (2000), Daun et al. (2001) and Hussaini Sarvari et al. (2002).

On the other hand, the solution with inverse formulation requires no assumptions, consequently no iteration and is straightforward as long as the problem is linear. The equations for the design surface for the generalized case can be written as

$$\left[\sum_{j=1}^{N_V} E_j' V_j \widetilde{F}_{j-i} + \sum_{j=1}^{N_S} E_j A_j \widetilde{F}_{j-i}\right]_{T\,\text{unknown}} = E_i A_i - Q_i - k\delta A_i \nabla_{2d}^2 T_i - h_{out} A_i (T_\infty - T_i) - \left[\sum_{j=1}^{N_V} E_j' V_j \widetilde{F}_{j-i} + \sum_{j=1}^{N_S} E_j A_j \widetilde{F}_{j-i}\right]_{T\,\text{specified}} \tag{4.5}$$

The complementary equations defined for the temperature specified and the flux specified surfaces and volumes are the same as the ones in the forward formulation, Eqs. (4.3) and (4.4).

Similarly, the equations in the given form, defining the inverse formulation are also non-linear. An iterative solution is required to cope with the non-linearity. A comprehensive discussion of solving inverse multi mode heat transfer problems is presented in França (2000) and França et al. (2000, 2002) and it is not repeated here. For the special case of radiation dominating the heat transfer, the conductive and convective terms can be neglected leading to a linear system. Then Eq. (4.5) becomes a discretized Fredholm equation of the first kind and the resulting set of equations is ill conditioned.

In order to be able to solve such a problem, the exchange factors should be calculated first. Once they are calculated using any radiation model, equations for the design and flux specified elements are written using Eqs. (4.5,3-b and 4-b), respectively. The set of equations must be solved for unknown emissive powers using regularization or filtering techniques such as CGM, TSVD or TR so that a physically reasonable, yet accurate solution can be achieved as explained in the previous chapter.

There are some regularization techniques based on iterative solution techniques such as the CGM. They produce N alternative solutions, one at the end of each iteration, N being the number of unknowns. This may pose a question mark over that statement that indicates inverse design results in a direct solution of the problems of interest as long as the problem is linear, unlike optimization or trial-and-error techniques, which result in an iterative solution. It is important to recall that using iterative techniques such as optimization or trial-and-error techniques for solution of a design problem, the governing system of equations is

solved at each iteration. If an iterative solver were used together with either of them, the solver iterates within each of the iterations of the optimization or trial-and-error technique. On the other hand, in the case of inverse design, the linear system is solved only once to achieve a direct solution. To underline the difference between the iterations of a solver and iterations required in any trial-and-error or optimization type of method, the term "step" is used in this text from here on whenever iterations of a solver are referred to.

The heat flux or source distributions for heater surfaces or temperature specified elements, and the temperatures of flux specified surfaces are then calculated through the solution of the forward problem using the calculated temperatures for the heater surfaces.

4.3 SAMPLE PROBLEMS

The applications of the solution methods discussed are presented using two boundary condition design problems. These are a two-dimensional irregular geometry problem and a three-dimensional rectangular enclosure problem. The details of each problem are as follows:

4.3.1 The Two-Dimensional Irregular Geometry Problem

An enclosure, which has an irregular cross-section formed by straight walls that include blockage and shading effects, and is very long in one dimension, is considered. Therefore, it is reasonable to approximate the enclosure as two-dimensional. The enclosure cross-section is made up of eight surfaces, which are all diffuse-gray with the heater surfaces 6,7 and 8, design surfaces 2, 3 and 4 and re-radiating surfaces 1 and 5 as shown in Fig. 4.2. The lengths

presented in the figure are non-dimensionalized using the total width of the enclosure or the length of surface 7. The emissivities along the heaters, re-radiating and design surfaces are constant over the entire surface and equal to 0.9, 0.5 and 0.9, respectively.

The design objective is to keep the temperature and the heat flux distributions along the three design surfaces (surfaces 2,3 and 4) according to the

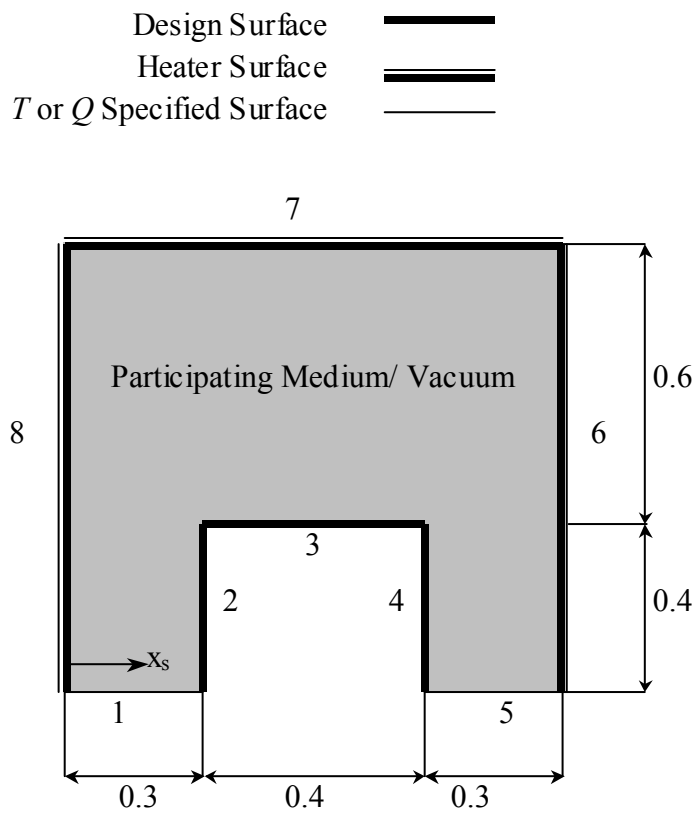

Figure 4.1: The geometry of a two-dimensional irregularly shaped enclosure problem with normalized dimensions

needs of the process. The desired distribution is usually a uniform distribution in most of the applications to overcome thermal stresses or to prevent uneven irradiation (cooking, drying, curing etc.) over the design object. For the problem under consideration, the objective is to keep the design surface at a non-dimensional uniform temperature of unity, while the non-dimensional uniform heat flux ($q''/\sigma T_o^4$, T_o being the reference temperature or the design surface temperature) equals to three.

Being the first design problem considered in the course of this study, the problem provides a means of understanding the challenges of design, and consideration of various aspects of design from a practical point of view. Therefore, the focus for this problem will be more on the physical effects of different conditions rather than the efficiency of the solutions. To accomplish this goal, different medium conditions are investigated in seven different cases, which contain transparent, absorbing-emitting and absorbing-emitting and isotropically scattering media. For all the cases with participating medium, the optical properties are considered homogeneous, the medium properties are gray and the medium is in radiative equilibrium. The values of the optical thickness based on the width of the enclosure and scattering albedo pairs for the cases considered are: $\tau = 0$; $\tau = 0.1$, $\omega = 0$; $\tau = 0.2$, $\omega = 0.5$; $\tau = 0.5$, $\omega = 0$; $\tau = 1$, $\omega = 0.5$; $\tau = 5$, $\omega = 0$ and $\tau = 10$, $\omega = 0.5$.

4.3.2 The Three-Dimensional Problem

The second design problem that is used to demonstrate the use of the inverse formulation in boundary condition design considers a three-dimensional

furnace enclosing an absorbing-emitting and anisotropically scattering medium in radiative equilibrium as displayed in Fig. 4.2. The heater surface is surface 4 (top surface), the design surface is surface 2 (bottom surface) and both of these surfaces are diffuse-gray with an emissivity 0.9. The surfaces 1,3,5 and 6 are insulated and mirror-like, therefore re-radiating and specularly reflecting with a gray emissivity of 0.15. The optical thickness for the medium based on L_y is 0.2, with a scattering albedo of 0.5 and a Henyey-Greenstein scattering phase function ($\Phi(\mu_o) = (1-g^2)/(1-g^2-2\mu_o)^{1.5}$, μ_o being the cosine of the scattering angle) with an asymmetry constant of g=0.3 (Siegel and Howell, 2002). The optical properties are considered homogeneous and gray.

The design goal is keeping the design surface at a uniform non-dimensional temperature of unity while the uniform non-dimensional net radiative

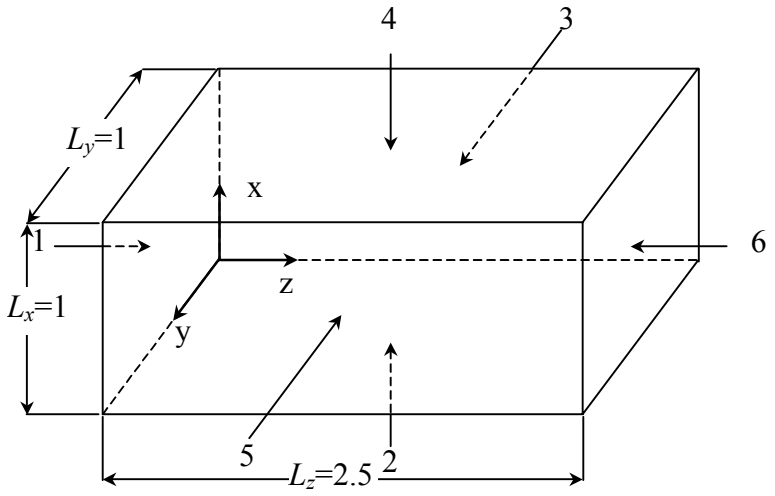

Figure 4.2: Sketch of the three-dimensional enclosure with normalized dimensions

flux over the surface is 10. The problem is solved by different solution techniques, and the alternative solutions are compared in terms of efficiency and accuracy.

4.4 RESULTS AND DISCUSSION

The design problems explained in the previous section are solved using inverse formulation and regularization techniques. As mentioned before, the analysis for the first problem is focused more on the behavior of the inverse problem, investigating how the system behaves under different conditions. The analysis of the second problem more focuses on the computational efficiency and comparison of different solution techniques.

4.4.1 The Two-Dimensional Irregular Geometry Problem

The first step in the solution of the two-dimensional irregular geometry problem is to calculate the exchange factors for every case. As the exchange factors are dependent on the optical properties of the surfaces and medium, they differ for each case. The problem considered is a challenging one with absorbing-emitting and scattering medium and blockage effects. Therefore, it is helpful to use MCM to calculate the exchange factors. The solutions presented here are calculated using a 40x40 grid resolution. It was observed that the solution for a sample forward problem is grid independent with this resolution. The MCM calculated the exchange factors using 400 million sample photon bundles, in 2161.3 seconds for the transparent case and in 3334.1 seconds for the case with τ = 10, ω = 0.5, with an Intel® Xeon™ 2 GHz processor machine.

The resulting system has 1344 volume and 192 surface elements for a case with a participating medium. The number of unknown emissive powers for a case with a participating medium becomes 1488 when full formulation is employed. A detailed explanation of differences between a full and reduced formulation are presented in the upcoming sections. For such a system, it is more reasonable to use CGM, which is known to be a very efficient solution technique.

Once the exchange factors are calculated, using Eq. (4.5) for the design surface elements, Eq. (4.3-b) for re-radiating surfaces and Eq. (4.4-b) for medium elements in radiative equilibrium, the system of equations is formed. The resulting system has 72 equations and 184 unknowns for the case without a participating medium, and 1416 equations and 1528 unknowns for the case with a participating medium.

As discussed earlier, CGM produces a number of different solutions and the adequate way to decide on the optimal solution is to use the L-curve. The L-curve for the transparent case is shown in Fig. 4.3. The solutions achieved after the 17-th CG step are useless as they are unphysical (negative emissive powers). When the figure is carefully investigated, it is recognized that the optimal solution results between 14-th and 4-th CG steps, where the corner of the L-curve lies.

The absolute percentage error based on the flux recovered over the design surface is defined as

$$\%Err_{q,i} = 100 \frac{\left| q''_{d,i} - q''_i \right|}{q''_{d,i}} \tag{4.6}$$

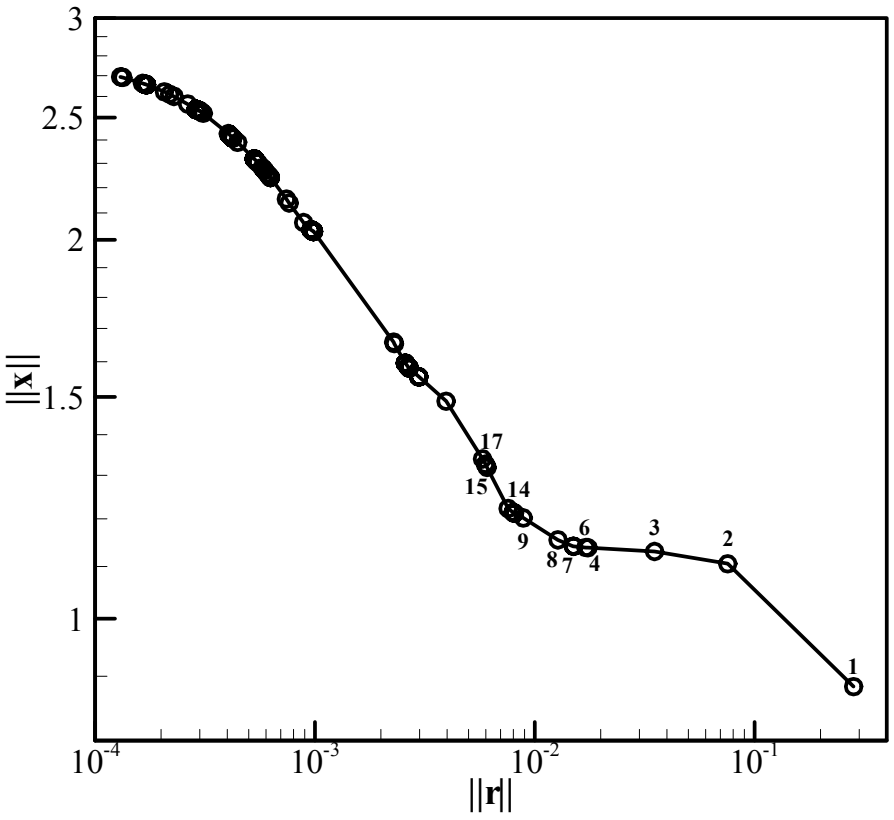

Figure 4.3: The L-curve for the solution of the problem for the case with transparent medium and no shape imposed on heater power distribution

The maximum and average of absolute percentage error based on the heat flux recovered over the design surface is 12.5 and 2.13 percent for the solution achieved at the 4-th CG step and 3.8 and 0.87 percent for the solution achieved at the 17-th CG step. The loci of the maximum error are close to the intersections of surfaces 1 and 2 together with surfaces 4 and 5.

Three alternative temperature and radiative heat flux distributions are presented in Fig. 4.4 for the transparent case. The coordinate x_s follows the enclosure surfaces in the counter-clockwise direction as shown in Fig. 4.1. It should be noted that with the missing conductive and convective terms in Eq. (4.1) for a pure radiating enclosure problem, the power input requirement Q for a heater element is the negative of the radiative heat flux.

The solutions presented in Fig. 4.4 are the results of the 17-th, 13-th and 6-th CG steps. The maximum and average errors are, 5.7 and 1.1 percent for the solution with 13 CG steps, 10 and 2 percent for solution with 6 CG steps.

It can be observed that the solution with 17 steps is slightly asymmetrical, while the other two are symmetric. It must be remembered that the exchange factors are calculated using the MCM method, which is a statistical method. Although it is possible to reduce the statistical noise by using a large number of samples, it is not possible to get rid of it completely. The exchange factors are calculated using 400 million samples, therefore the noise on the data is negligible. But one of the main characteristics of the inverse problems is that small errors or perturbations in the data used are amplified and have large effects in the solution. It is possible to discard the artificial amplification effect through adequate filtering, and as a result the symmetry can be achieved. This is demonstrated in the solutions with 13 and 6 CG steps.

In the solutions presented in Fig. 4.4, the power input varies along the heater surfaces. However, in most practical applications, a number of heaters of constant power input are used to carry out the heating. Considering such a

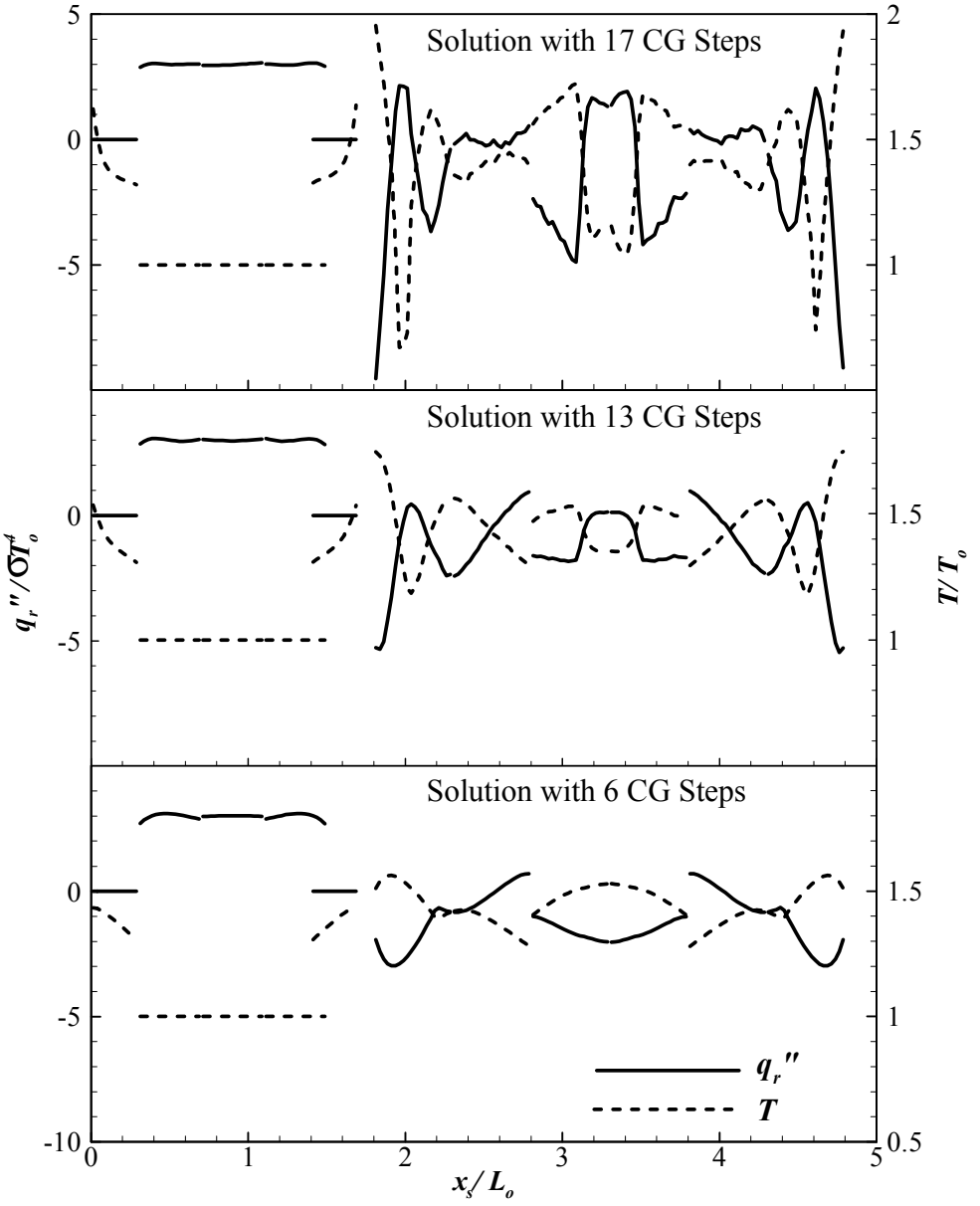

Figure 4.4: Alternative solutions using 17, 13 and 6 CG steps to the problem for the case with transparent medium and no shape imposed on heaters. (Heater elements at $1.8 \leq x_s/L_o \leq 4.8$)

practical concern, the designed system is modified to limit the number of heaters of constant power input to six, two at each heater surface. In the new configuration, the six heaters of equal length are placed along surfaces 6,7 and 8 (ordered from 1 to 6 in the counter clockwise direction). An equality relation for heat flux is written for all but one element in six heaters, so that the net radiative heat flux will be constant. This adds up 6x19 equations with the given resolution to the existing set of equations and the resulting number of equations become 186 for the transparent case, leading to an over constrained system.

The L-curve for the solution with 6 constant power heaters is shown in Fig. 4.5. Recalling Fig. 3.1, which demonstrates a typical L-curve for an ill-posed inverse problem, Fig. 4.3 looks more similar to Fig. 3.1 than Fig. 4.5. Moreover. Fig. 4.5 has only the flat part of the L-curve to the right of the curve, where the regularization error dominates the solution. It was discussed earlier that here the damping is so large that the influence of any error in the data together with some information is filtered out. This result is not surprising, as the basic idea behind regularization is imposing a shape constraint to the solution. Forcing the individual heater power input distributions to be constant performs the task without any need of further regularization.

The resulting temperature and radiative heat flux distributions are presented in Fig. 4.6 for the transparent case with constant power constraint. With the constant power constraint imposed, it is possible to achieve physically reasonable solutions using all the N steps for CGM. The solutions presented in Fig. 4.6 are the ones using 144 CG-steps and 10 CG-steps. The solutions using

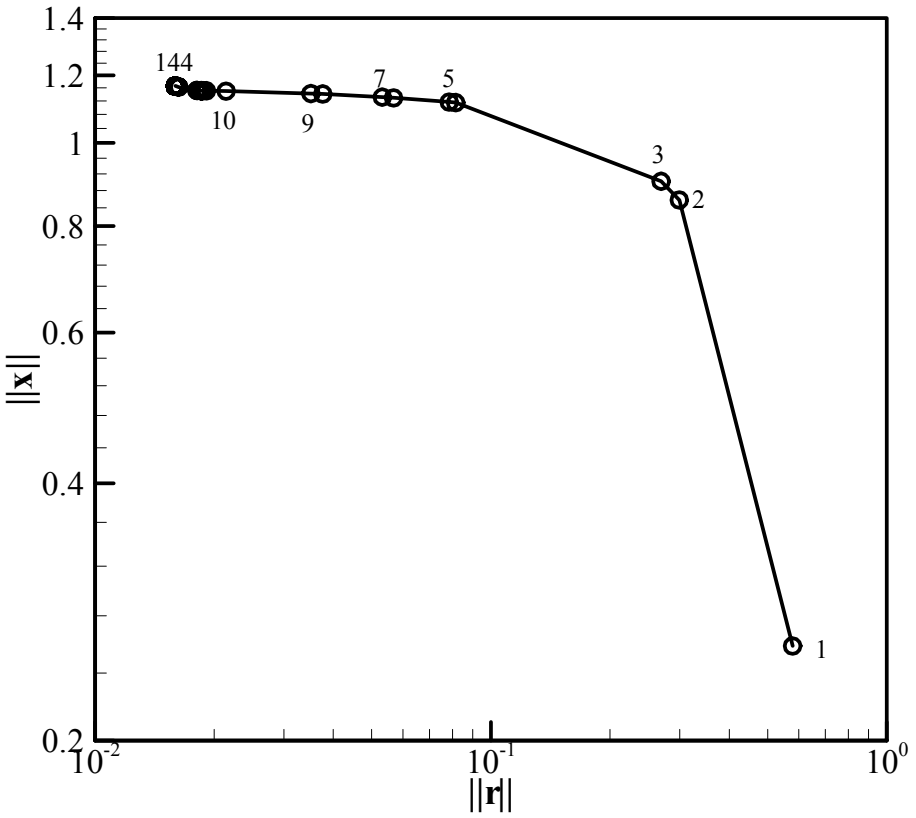

Figure 4.5: The L-curve for the solution of the problem for the case with transparent medium and constant heat flux imposed on 6 heaters

144 CG-steps have a maximum absolute error of 11.1 percent, while the average of absolute errors is 2.2 percent. This solution is the most accurate solution available for the over-constrained system as all conjugate directions are used. When compared with the solutions achieved without imposing the constant power constraint, the solution accuracy is close to the ones that are to the right of the corner point of the L-curve in Fig. 4.3.

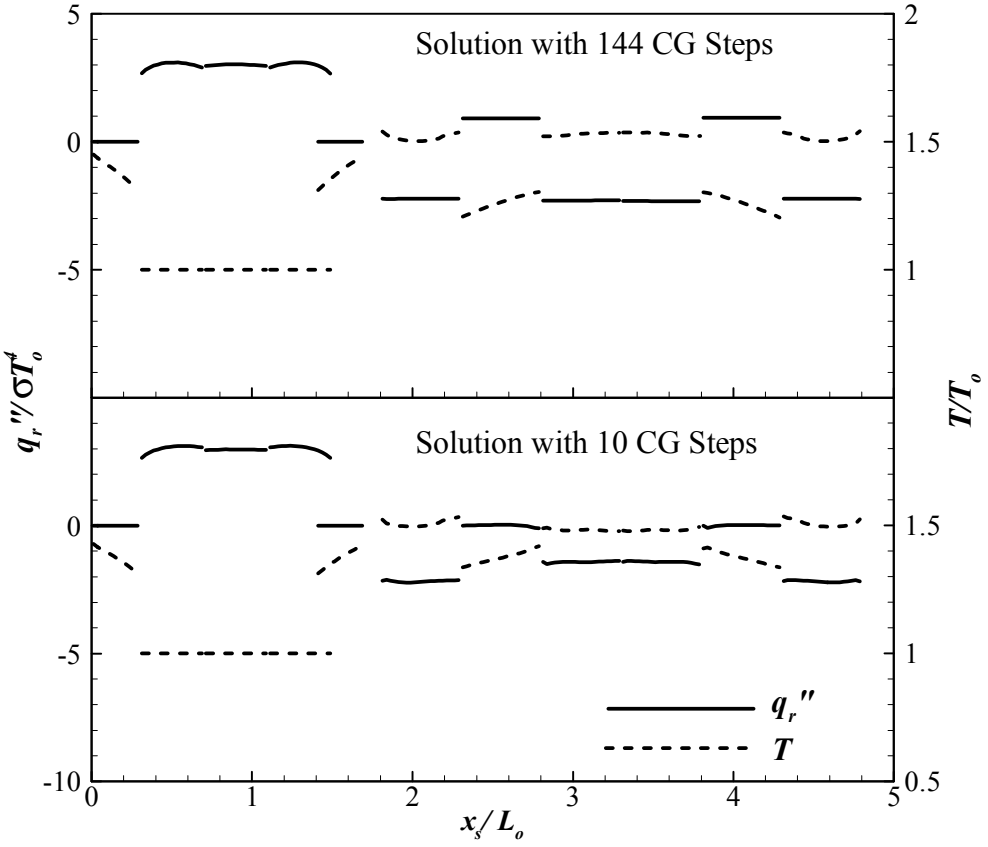

Figure 4.6: Alternative solutions using 144 and 9 CG steps to the problem for the case with transparent medium and constant power imposed on heaters. (Heater elements at $1.8 \leq x_s/L_o \leq 4.8$)

An important aspect in the thermal system design is efficiency. If the solution achieved using the constant power constraint and 144 CG-steps is used, power should be added to the heaters 1,3,4 and 6, whereas heat should be removed from heaters 2 and 5. Removing heat is not a desired condition; therefore an alternative solution is sought. The solution using 10 CG-steps

suggests that the heaters 2 and 5 can be turned-off, so that no power is added or removed from these heaters. The maximum and average absolute percentage error for this solution is 12.1 and 2.8 percent, respectively.

With this information, it is reasonable to apply the design methodology once more; this time besides using the constant power constraint, heaters 2 and 5 are turned off. The resulting temperature and radiative heat flux distributions are presented in Fig. 4.7. The maximum and average absolute errors are 12.6 and 2.4 percent, respectively. The loci of the maximum error are still close to the bottom tips of surfaces 2 and 4.

Once a suitable configuration for heaters is selected (4 heaters of constant power input with heaters 2 and 5 turned off), the design of systems with different

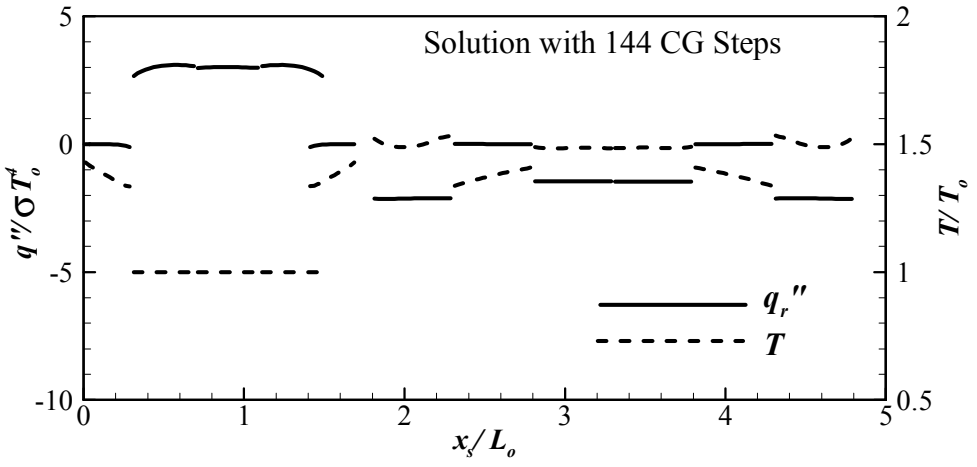

Figure 4.7: Solution using 144 CG steps to the problem for the case with transparent medium, constant power imposed on heaters, heaters 2 and 5 turned-off. (Heater elements at $1.8 \leq x_s/L_o \leq 4.8$)

medium conditions can be considered. As mentioned before, cases consider the enclosure with absorbing-emitting and absorbing-emitting and isotropically scattering media with different optical thickness. In all the cases the medium is at radiative equilibrium; i.e., the net divergence of heat flux at every volume element is zero.

The results for the cases with τ =0.1, ω =0 and τ = 0.2, ω =0.5 are presented in Fig. 4.8. When temperature and heat flux distributions are compared with the ones presented in Fig. 4.7 for the transparent medium, it is observed that there is no significant change in surface temperature or heat flux distributions. However, when the numbers are investigated more carefully, a slight increase in heater temperatures is recognized and the increase is more for the latter case with increased optical thickness.

When the optical thickness is further increased to τ=0.5, ω=0 and τ=1, ω =0.5, the increase in heater surface temperatures becomes more apparent (Fig. 4.9). Although, the total power required for the heaters is the same as the previous cases the required power input distribution change slightly. As the power required by heaters 1 and 6 increases, the power required by heaters 3 and 4 decreases, accordingly. As the optical thickness of the medium increases, the direct effect of the heaters on the thermal conditions over the design object becomes less while the effect of medium temperature distribution increases. As heaters 3 and 4 located on surface 7 are farther from the design object than heaters 1 and 6, the effect of the former heaters on the thermal conditions of the design object and the neighboring medium elements becomes smaller. Consequently, the

best system to control moves toward using the heaters with more control over the conditions.

The heater temperature increase for the medium with scattering included is again more than for the nonscattering case. For the particular problem considered with an isotropically scattering medium in radiative equilibrium, a photon

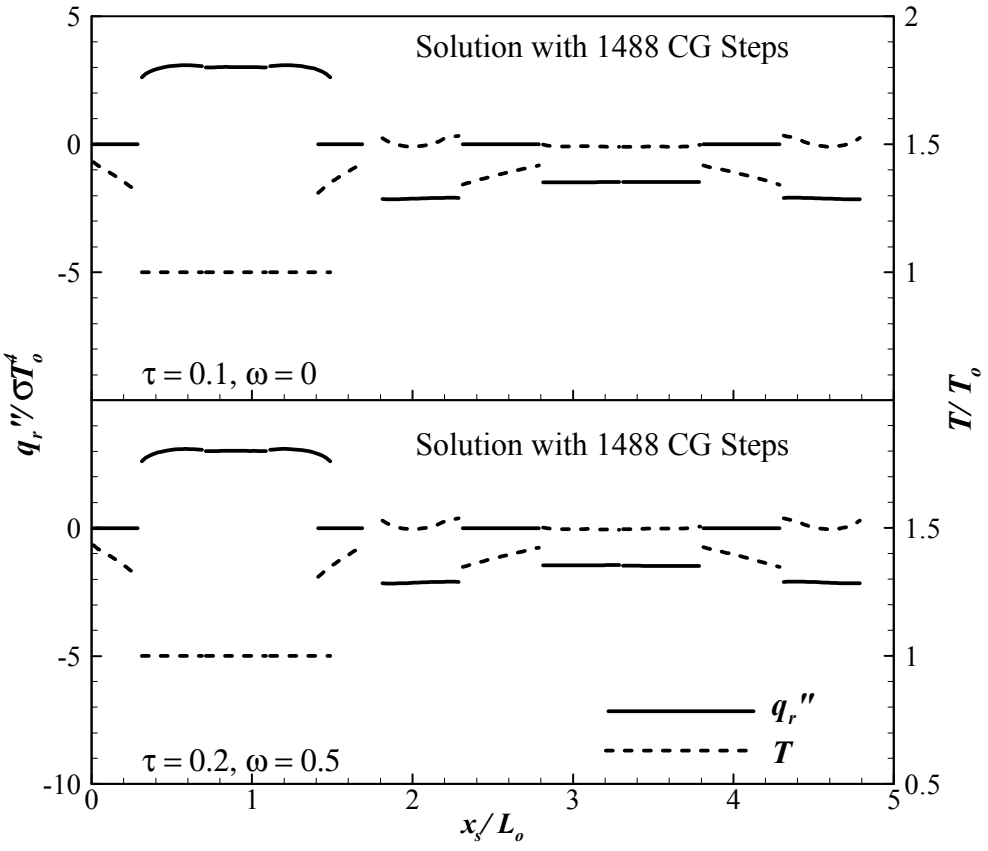

Figure 4.8: Solutions using 1488 CG steps to the problem for the cases, $\tau = 0.1$, $\omega = 0$ and $\tau = 0.2$, $\omega = 0.5$, with constant power imposed on heaters, heaters 2 and 5 turned-off. (Heater elements at $1.8 \leq x_s/L_o \leq 4.8$)

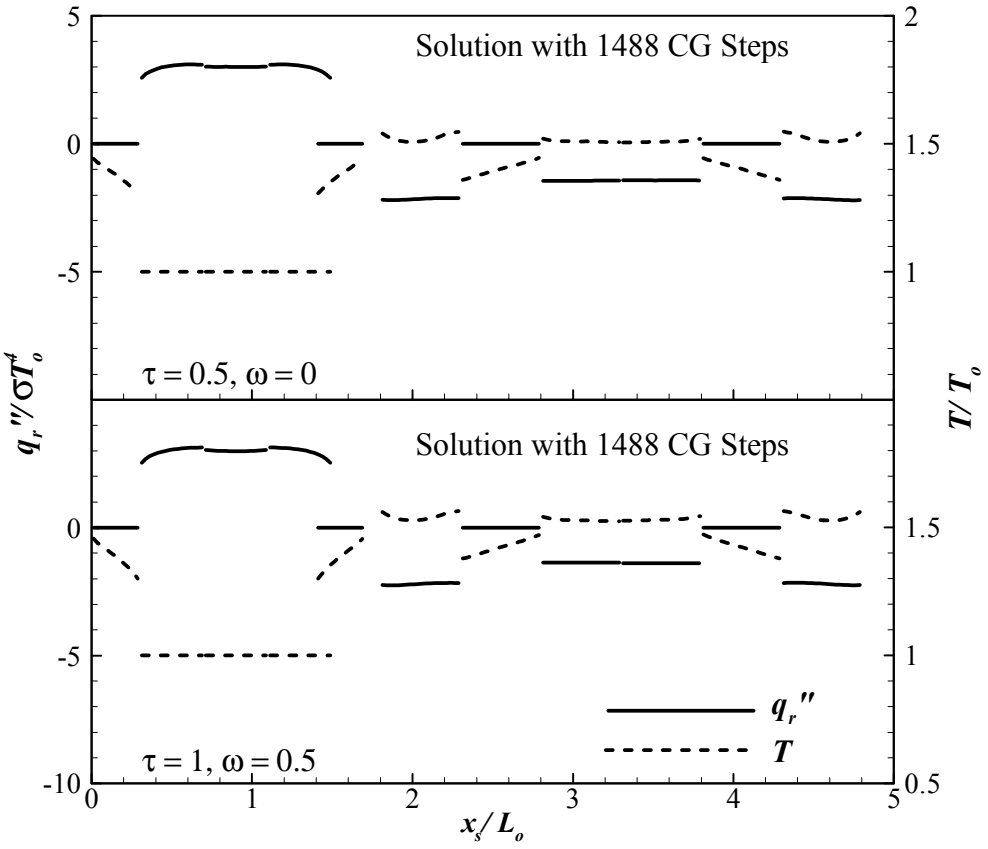

Figure 4.9: Solutions using 1488 CG steps to the problem for the cases, $\tau = 0.5$, $\omega = 0$ and $\tau = 1$, $\omega = 0.5$, with constant power imposed on heaters, heaters 2 and 5 turned-off. (Heater elements at $1.8 \leq x_s/L_o \leq 4.8$)

carrying radiative energy behaves the same whether it is absorbed or it is scattered, therefore the effects of absorption and scattering are identical. To demonstrate this, a different case with medium having $\tau = 1$, $\omega = 0$ must be considered (Fig. 4.10). It can be observed that the resulting temperature and heat

flux distributions along the surfaces are identical for the cases with τ=1, ω=0 (Fig. 4.10) and τ=1, ω=0.5 (Fig. 4.9).

Even though using surface heaters in systems containing an optically thick medium is not a common practice, the behavior of the system with an optically thick medium for cases with τ=5, ω=0 and τ=10, ω=0.5 are also investigated. In these cases, the change in heater surface temperatures is dramatic when compared with the previous ones (Fig. 4.11). The required power in heaters 3 and 4 is reduced significantly while the power required by heaters 1 and 6 increases. The maximum and average absolute percentage errors for the solutions of the cases with τ=5, ω=0 is 20 and 5.7 percent, respectively. The corresponding values are 21.8 and 8.2 percent for the case with τ=10, ω=0.5. It is observed

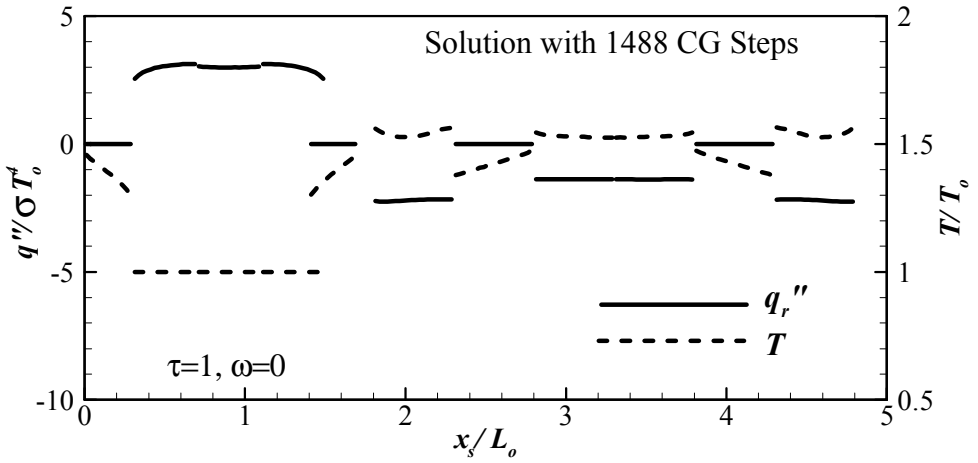

Figure 4.10: Solutions using 1488 CG steps to the problem for the cases, τ= 1, ω =0 with constant power imposed on heaters, heaters 2 and 5 turned-off. (Heater elements at $1.8 \leq x_s/L_o \leq 4.8$)

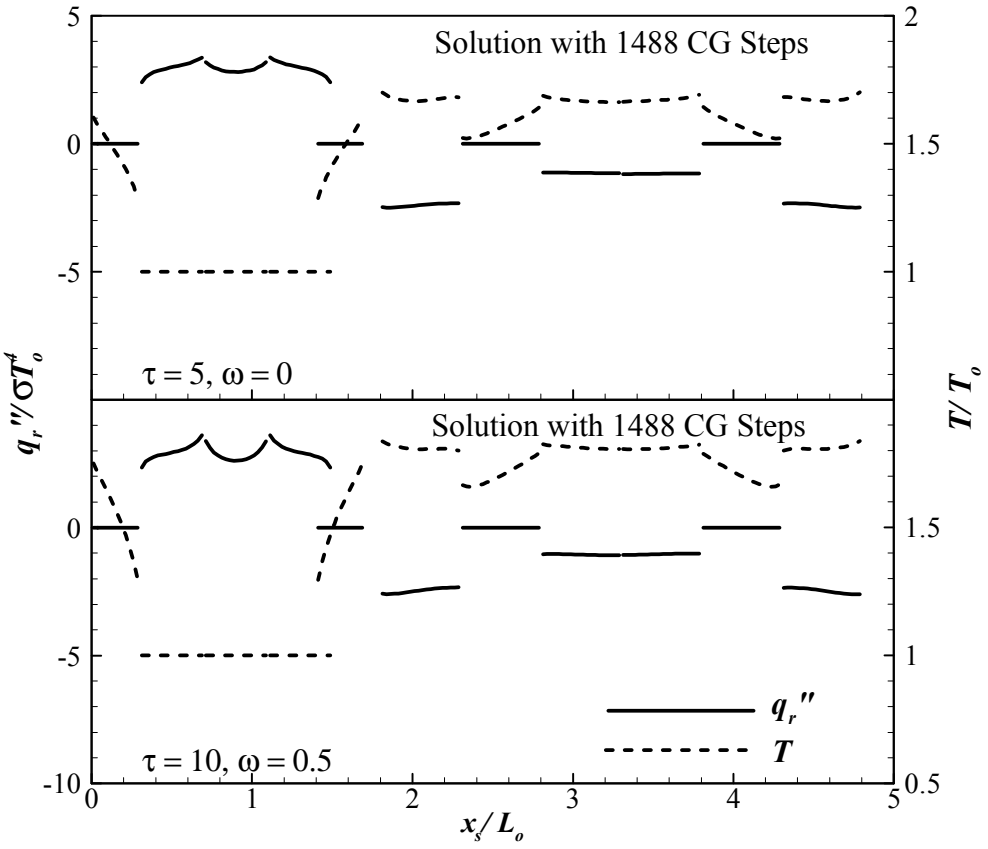

Figure 4.11: Solutions using 1488 CG steps to the problem for the cases, $\tau = 5$, $\omega = 0$ and $\tau = 10$, $\omega = 0.5$, with constant power imposed on heaters, heaters 2 and 5 turned-off. (Heater elements at $1.8 \leq x_s/L_o \leq 4.8$)

from Fig. 4.12 that the loci of the maximum error change to the corners between surfaces 2 and 3, and 3 and 4. Moreover, the error along surface 3 increases significantly.

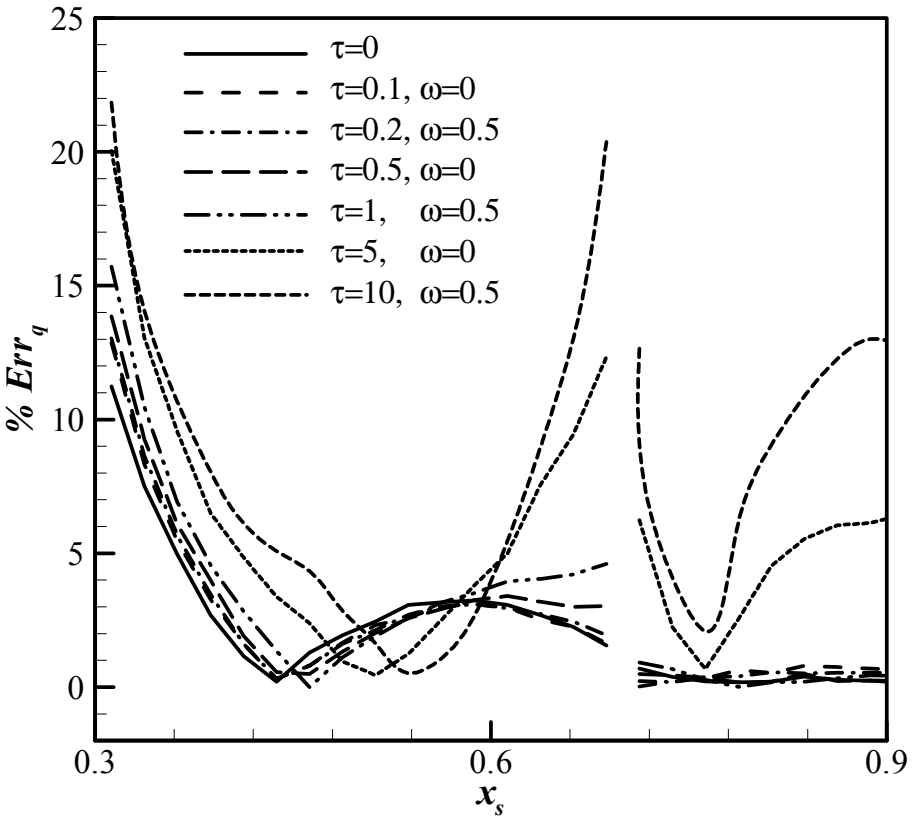

Figure 4.12: Absolute percentage error based on heat flux on the design surface for all cases with constant power constraint imposed and heaters 2 and 5 are turned off.

A summary of the results in terms of average and maximum absolute percentage errors is presented in Table 4.1. The absolute percent error distribution for the cases considered is displayed in Fig. 4.12. It can be observed that the maximum and average of absolute errors increases monotonically as the optical thickness of the medium is increased for the participating medium. This is due to the fact that the effect of the heater elements on the design object is

Table 4.1: The maximum and average of absolute percentage errors for different cases.

Optical Properties of Medium		Maximum of absolute percentage error	Average of absolute percentage error
τ	ω		
0	0	12.6	2.4
0.1	0	12.8	2.4
0.2	0.5	13.3	2.5
0.5	0	13.9	2.6
1	0.5	15.7	3.1
5	0	20	5.7
10	0.5	21.8	8.2

reduced as the optical thickness increases, resulting in a more ill-conditioned system. The influence of the medium elements neighboring the design elements increases. For the latter two cases, the radiative transfer in the participating medium becomes a diffusive phenomenon ($\tau \geq 5$). With increased optical thickness, the heaters can only control the neighboring volume elements and their resulting diffusive effect over the elements neighboring the design object. As a result of the weak dependence, the resulting solutions are subject to higher errors.

4.4.2 Three-Dimensional Problem

The three-dimensional problem explained in Section 4.3.2 is solved to compare the solutions and the performance of different regularization techniques. The reduced and full formulations are used for the solutions. In the case of the reduced formulation, the system governing the problem consists of equations written for design elements and the only unknowns are the variables of the heater

or burner elements. Alternatively, the equations for all of the elements in the system are considered in the full formulation. Therefore, the resulting system with the full formulation is much larger than it is for the reduced formulation when the same grid resolutions are considered. The reduced formulation is applicable in certain cases such as when all the temperatures except on the heaters are specified, whereas the full formulation is a more generalized approach.

4.4.2.1 The Results with the Reduced Formulation

The problem considered has four re-radiating surfaces and a participating medium in radiative equilibrium. Therefore, the exchange factors can be calculated so that the effects of these boundary conditions are included in the exchange factors. When the exchange factors are calculated using the MCM, this can simply be accomplished by immediately emitting a photon bundle whenever a re-radiating surface element or a medium element that is in radiative equilibrium absorbs one. This results in satisfying the specified boundary conditions for these surface or volume elements exactly leading to a reduced formulation. The equations that define the system are Eq. (4.5), written for the elements of surface 2. These equations are discretized Fredholm equations of the first kind, and the resulting system is ill-conditioned.

The exchange factors for the system are calculated with the MCM using 100 million sample photon bundles emitted from each of the heater and the design surface. The solutions presented are calculated using an 8x8x20 grid along the x, y and z coordinates of the enclosure. This grid resolution is tested using a

forward problem comparing the predictions with solutions of a 16x16x40 grid, and based on the comparisons the solutions are grid independent.

The system is analyzed by SVD, and the singular values for the system are presented in Fig. 4.13. It can be observed that the singular values decay from 0.76 to 4.86×10^{-6}. The continuous decay is a characteristic of a discrete ill-posed problem (Hansen, 1998) and the high condition number (1.56×10^{5}) of the system indicates how ill-conditioned the problem is.

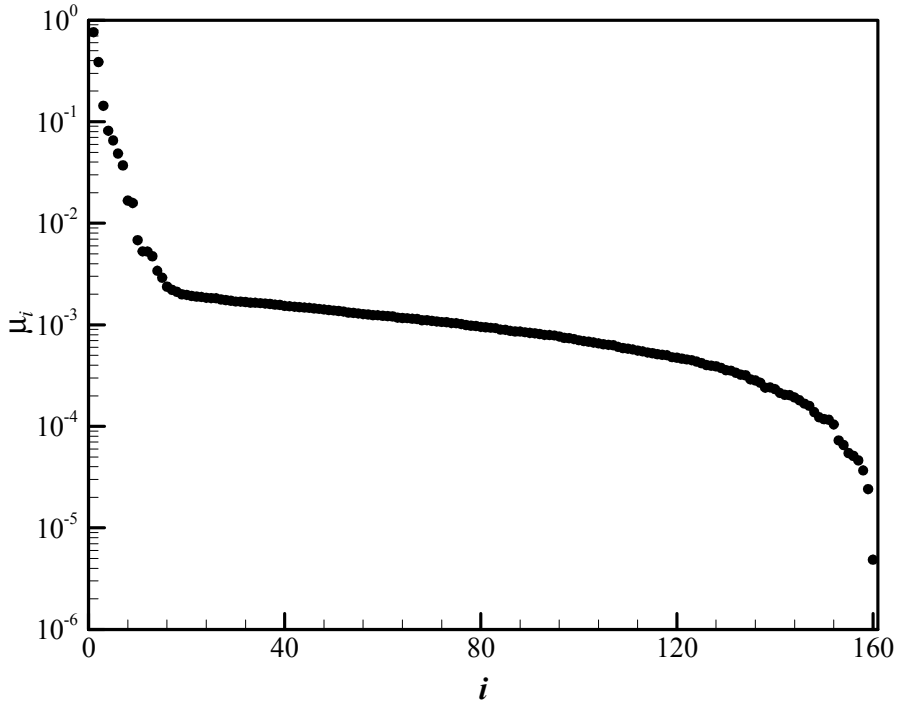

Figure 4.13: The singular values for the reduced formulation with 8x8x20 resolution

Solutions with the CGM and TSVD are considered for the reduced formulation. Both of these methods produce a number of different solutions based on the regularization level and in order to choose the "best" or the "optimal" solution among them, the L-curve for solutions produced with each method must be considered. The L-curves are presented in Fig. 4.14. The CGM produces solutions with physical meaning up to the 9-th step; further steps produce negative emissive powers. The corresponding number of singular values is 10 for TSVD. When the CGM solutions are considered, the slope of the L-

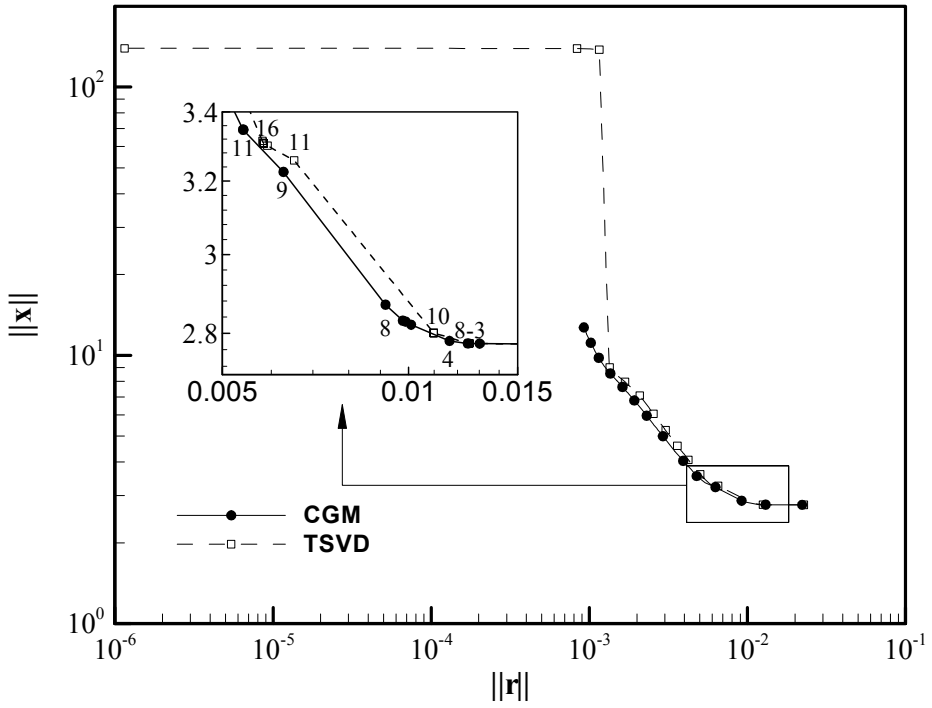

Figure 4.14: The L-curve for solutions with CGM and TSVD using reduced formulation

curve does not change significantly up to the 4-th step. After the 4-th step the slope starts increasing and therefore, the solution calculated by the 4-th step has acceptable accuracy and shape characteristics. The similar trend can be observed with TSVD solutions. The solutions with 3 to 8 singular values are located very close on the L-curve and the any of the solutions using 3 to 8 singular values can be considered to have optimal accuracy and shape characteristics.

The resulting distributions displayed in Fig. 4.15 are calculated using the fourth step of the CGM and TSVD utilizing four singular values. The distributions along two lines y=0.0625 and y=0.4375 is presented along the furnace axial length. Due to the highly specularly reflecting and re-radiating sidewalls the required temperature distribution along the heater surface is nearly isothermal. It can also be observed that the resulting temperature distributions calculated by TSVD and CGM look almost identical. The average and maximum absolute percent errors based on the imposed and the obtained heat flux on the design surface as defined in Eq. (4.6) are 0.53 and 1.8 percent for both the CGM and TSVD solutions presented.

Using the reduced formulation there is slight difference in the computation time as the resulting system is very small. For the particular problem with a grid resolution of 8x8x20, the resulting system has 160 unknowns with 160 equations. The CGM presented in the previous chapter requires a computation time of 0.016 second to calculate the 8-th step and 160 steps takes 0.094 second. The TSVD solver that uses the SVD routine presented in Press et al. (1992) uses 0.42 seconds

while 0.34 of that time is spent for SVD, with an Intel® Xeon™ 2 GHz processor system.

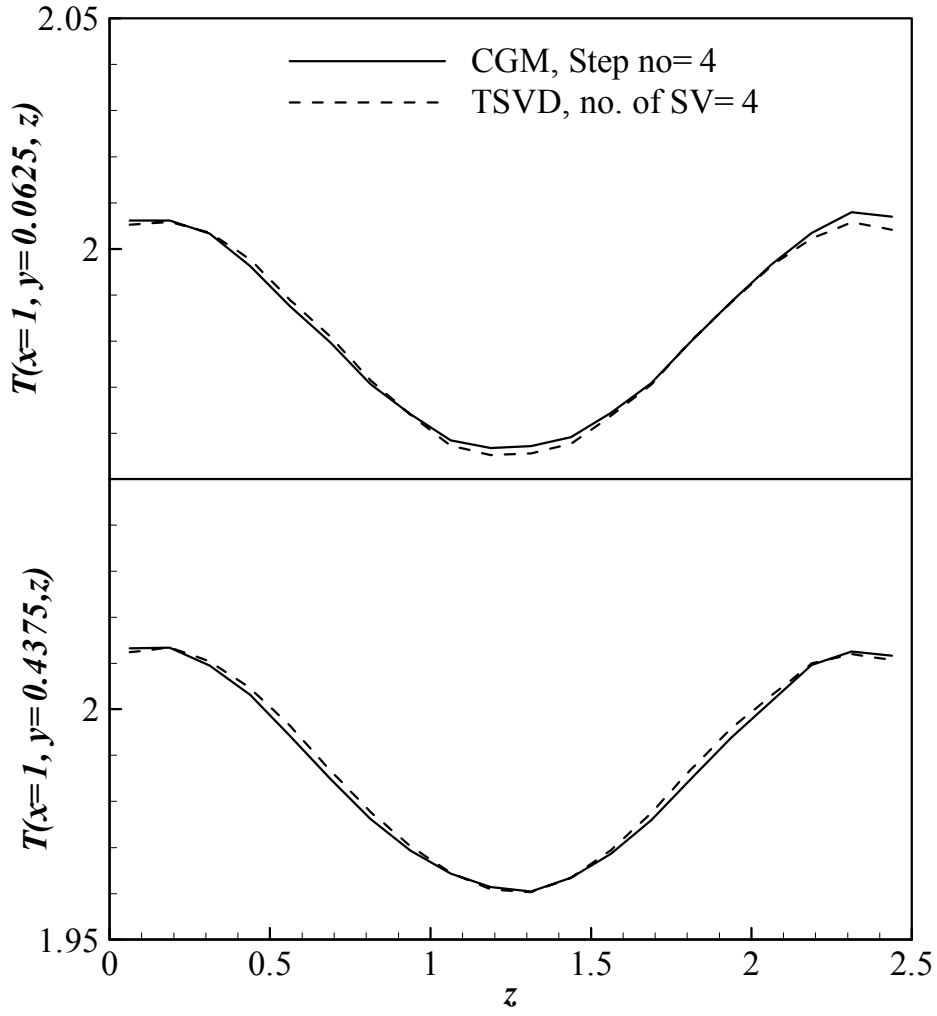

Figure 4.15: The solutions with reduced formulation with CGM using 4 steps and TSVD using 4 singular values following two different lines along furnace length.

While CGM requires an approximate memory size of $MN+2(M+N)$, TSVD utilizes $2MN+N^2+2(N+M)$ for a system with M equations and N unknowns. The memory required by TSVD is approximately three times the memory required by the CGM algorithm. For the solution with reduced formulation, the resulting system is small, and the differences in the CPU time and required memory are not significant. But as the size of the system increases, the differences in the computational time and the required memory highlights the advantages of the CGM over TSVD.

4.4.2.2 The Results with the Full Formulation

The full formulation includes additional equations to those used in the reduced formulation. The additional equations are Eq. (4.3-b) for the re-radiating surface elements and Eq. (4.4-b) for the medium elements in radiative equilibrium. As the effects of the re-radiating surfaces and medium are included in the governing system through added equations, the generic exchange factors are used for the formulation that are only dependent on geometry and optical properties. Hence, the exchange factors used do not include the effects of boundary conditions as in the case of exchange factors used in the reduced formulation. This leads to a more generalized approach that can be applied whenever thermal radiation dominates the heat transfer or other modes of heat transfer are negligible.

Using the same resolution of 8x8x20, the resulting system has 160 discretized Fredholm equations of the first kind for the design surface as before, 448 discretized Fredholm equations of the second kind for the re-radiating

surfaces (64 equations for each of surfaces 1 and 6, 160 equations for each of surfaces 2 and 4) and another 1280 discretized Fredholm equations of the second kind for the medium elements. The resulting set has 1888 equations and 1888 unknowns (160 emissive powers for the heater surface, 64 emissive powers each for surfaces 1 and 6, 160 emissive powers each for surfaces 2 and 3, and 1280 emissive powers for medium).

Once more, in order to analyze how ill-conditioned the system is, the most convenient tool would be SVD. Once the SVD is performed, and the distribution of the singular values is displayed, the characteristics of the system can be defined more easily.

The singular values of the linear system governing the problem using the full formulation are presented Fig. 4.16. The pattern of decay for the displayed singular values is quite different from the one presented in Fig. 4.13. The singular numbers for full formulation decay from 1.49 to 0.89 until the 1728-th singular value, and then there begins a steep decay to 1.42×10^{-6}, leading to a condition number of 1.05×10^{6}. It is not a coincidence that the number of discretized Fredholm equations of the second kind in the system is also 1728. Moreover, the decay pattern for the remaining 160 singular values shown in Fig. 4.16 after the 1728-th singular value is identical to the one presented in Fig. 4.13.

Alternative solutions are calculated using CGM, TSVD and 0-th order TR. L-curves are plotted for all three methods in order to choose the optimal solution with each method among the available alternative solutions. The L-curves for solutions with all three methods are presented in Fig. 4.17. When compared with

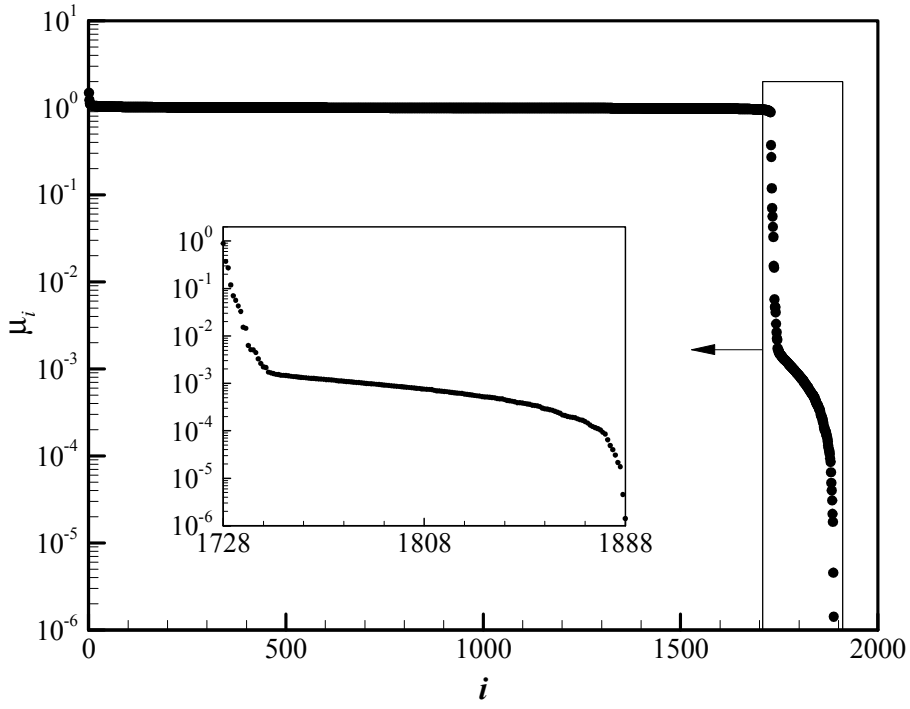

Figure 4.16: The singular values for the full formulation with 8x8x20 resolution

Fig. 4.14, the L-curve for TSVD solutions differs slightly. The very first point identified on the right is actually 1728 coincident points. This simply means that truncation of singular values that represent the well-posed part of the system leads to solutions with unacceptable accuracy. When 1729 singular values are used for the solution, a sudden increase in the accuracy together with an increase in solution norm is observed. At this point, the L-curve for the TSVD solutions converges to the L-curves of CGM and 0-th order TR solutions. This point also is the beginning of the plateau where the optimal solution is generally located. At the end of the plateau the solution norm increases suddenly without improving the

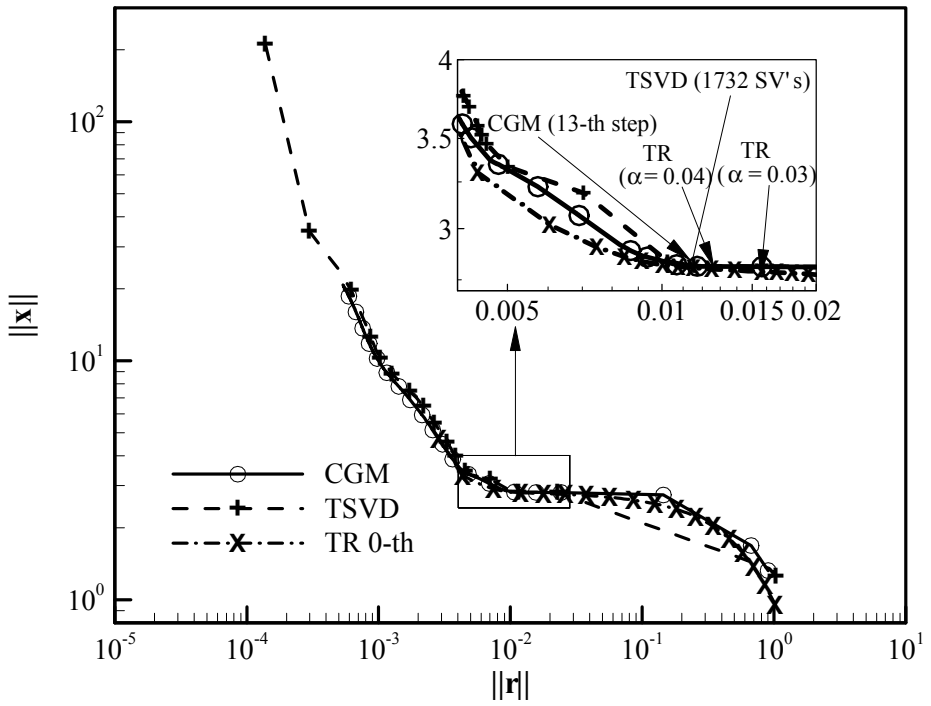

Figure 4.17: The L-curve for solutions with CGM, TSVD and 0-th order TR using full formulation

accuracy significantly. The final solution that is physically acceptable is the one that uses 1738 singular values and is located just after the corner of the L-curve. Although they are presented in the L-curve here, the solutions for more singular values are useless, suggesting negative emissive powers.

The L-curve for the CGM solutions follows a more familiar pattern to the L-curve of CGM solutions using the reduced formulation. The major difference is that it takes four steps to reach the plateau where reasonable solutions lie, whereas in the previous case a solution with similar accuracy is achieved as a

result of the very first step. Then the CGM L-curve follows a similar pattern with the TSVD L-curve and reaches the corner around the 20-th step. No physically reasonable solutions are achieved after the 39-th step.

The 0-th order TR is applied by solving Eq. (3.21) using the CGM using all available conjugate directions, which is equal to the number of unknowns. As explained earlier in Chapter 3, CGM using all conjugate directions yields an exact solution of the linear system. The right hand side of the L-curve for the solutions with 0-th order TR is very similar to the one shown in Fig. 3.1. It follows the similar trend reaching the plateau around α=0.2 and then the corner around α=0.015. Solutions using regularization parameters smaller than 0.001 are unphysical.

One interesting observation on the L-curves presented in Figs. 4.14 and 4.17 is that the maximum solution accuracy achieved by TSVD is higher than it is with CGM and the maximum solution accuracy achieved by CGM is higher than it is with 0-th order TR. This is really not an important aspect as these mathematically accurate solutions are dominated by fluctuations and are unphysical. Nevertheless, an explanation of this behavior is sought so that these methods can confidently be used. The reason can be explained as follows: The generalized CGM algorithm that is used, presented in Fig. 3.2, does not solve the system as it is. For a system given as Eq. (3.13) it solves the linear system $\mathbf{A}^T(\mathbf{Ax}=\mathbf{b})$, which is supposed to have an identical answer. Moreover, for the 0-th order TR solution with α=0 that uses a CGM solver, the solved system becomes $(\mathbf{A}^T\mathbf{A})^T$ $(\mathbf{A}^T\mathbf{Ax}=\mathbf{A}^T\mathbf{b})$. Therefore, it is concluded that due to the modifications in

the solved linear system, additional round-off error is introduced in the calculations of the CGM and 0-th order TR that uses CGM as a linear solver. The result is L-curves being "shorter" than the TSVD L-curve in the region where the round-off error is important.

Once the L-curves are analyzed thoroughly, solutions with optimal characteristics can be selected. These solutions are presented in Fig. 4.18. The TSVD solution presented uses 1732 singular values and the CGM solution is the one calculated using the 13-th step. These solutions are very similar to those presented in Fig. 4.14 and have similar accuracy characteristics. The maximum and average absolute percentage errors are 1.60 and 0.52 percent for the CGM solution and 1.58 and 0.52 percent for the TSVD solution.

The 0-th order TR solutions presented are for regularization parameters 0.03 and 0.04, and the resulting profiles differ slightly from the others presented. The required temperature distribution along the heater surface has a more significant gradient across the furnace width. The maximum and average absolute percentage errors are 2.12 and 0.66 percent for α=0.03, and 2.67 and 1.07 percent for α=0.04.

It was stated earlier that the full formulation for the problem requires more memory and more computation time. Therefore, the performance of the solver becomes more critical with the increasing demand for computation time and memory. In this regard, the full formulation constitutes a better benchmark problem where the performance of the regularized solution techniques can be compared than the reduced formulation.

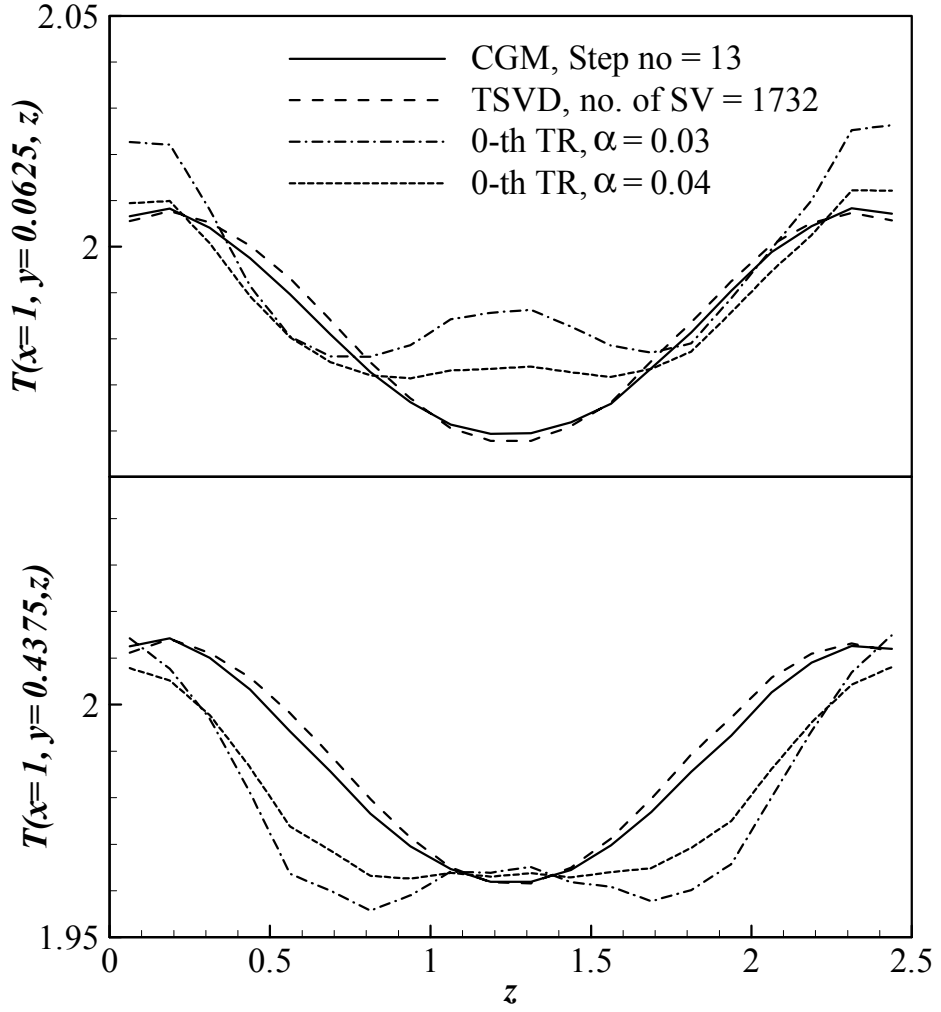

Figure 4.18: The solutions with full formulation with CGM using 13 steps, with TSVD using 1732 singular values, with 0-th order TR using α= 0.03 and α=0.04 for two different lines along furnace length.

For the resolution of 8x8x20, or a linear system size of 1888x1888, the CGM produces exact solution using all 1888 steps that are required to plot the L-

curve and uses a CPU time of 726.4 seconds. The CGM solution presented in Fig. 4.18 is the result produced by the 13-th step and the first 13 steps uses a CPU time of 5.2 seconds. Similarly, plotting the TSVD L-curve takes 1200 seconds. In order to plot the L-curve, the SVD must be performed following 1888 back substitutions using different levels of truncation. The solution presented that uses 1732 singular values requires 565.2 seconds, and it is the SVD routine that absorbs the greater part with 565 seconds.

The 0-th order TR consists of two parts. First the linear system must be modified imposing the shape constraints and then the modified linear system must be solved by using any appropriate solver. As the CGM had proved itself as a very reliable and efficient solver, CGM is used as mentioned earlier. The 0-th order TR L-curve is plotted using 100 different solutions using regularization parameters varying from 1 to 0 following the function

$$\alpha_i = 1 - \frac{\log i}{\log N},\ i=1..N \tag{4.7}$$

where N is the number of points in the L-curve.

The calculation for 100 different solutions using different regularization parameters with 0-th order TR takes 15779.8 seconds. During the calculations the convergence criteria for the CGM was that the norm of the residual vector must be reduced below 10^{-20}. The solutions presented in Fig. 4.18, uses 215.2 and 177.6 seconds using 451 and 356 CG steps for α=0.03 and 0.04, respectively. The CPU times presented are for an Intel® Xeon™ processor computer with a processor speed of 2 GHz.

One last comment must be made on the memory requirements. As mentioned earlier for a MxN system CGM and TSVD uses an allocation size of $MN+2(N+M)$ and $2MN+N^2+2(M+N)$, respectively. The required size for 0-th order TR that uses CGM as a linear solver is $MN+2N^2+M+4N$. Therefore, 0-th order TR that uses CGM as a linear solver has similar memory requirements to the TSVD that in turn requires almost three times as much memory as the CGM. Therefore, it can be concluded that CGM is the most efficient and economic among the methods used, in terms of both computation time and memory requirement.

CHAPTER 5

Design of Transient Thermal Systems

5.1 INTRODUCTION

The objective of a thermal system like a process furnace is to handle an engineering process. Examples are furnaces and ovens for annealing, curing of paint or surface coating, industrial baking and manufacturing through chemical deposition applications. The process takes place as long as the design environment satisfies specific thermal conditions. In many applications the quality of the product depends on the how accurately the thermal conditions are satisfied. The necessary design conditions are prescribed as a desired temperature distribution over the design surface in many cases. For a transient system where design is considered along a specific time interval, the net heat flux on the design environment provides an additional constraint due to the effect of thermal capacities. Two conditions are thus specified for the design environment while no condition is prescribed in the heater section.

In this chapter, an inverse design methodology, which is developed to tackle the design problem of transient heating of an object using radiant heaters, is presented together with its applications on two different problems. The first problem involves heating of a stationary object following a specified heating history in a two-dimensional process furnace. The second problem is about heating of an object as it moves along a rectangular process furnace.

5.2 INVERSE DESIGN METHODOLOGY AND FORMULATION

The transient heating problem in a radiating enclosure is a challenging one as it considers transient, combined mode heat transfer that is highly non-linear. The governing relation includes the radiative transfer equation, an integral equation that has absolute temperature to the power four terms, together with the transient energy equation, which is a partial differential equation that includes derivatives of absolute temperature to the first power.

The main difference between the transient problem and the steady problem is that in the steady problem the objective is to satisfy a certain temperature and heat flux distribution over the design environment, while in the transient problem the goal is to follow a specified temperature history with temperature and heat flux distributions specified at each time throughout the history. Due to the change in energy storage based on the required temperature history, the objective at a specific time is not much different than it is in the steady problem, as it is still desired to satisfy a certain heat flux distribution combined with certain temperature distribution. It is then possible to formulate the transient problem as a series of steady problems solved along time that are dependent on each other.

Consider the discretized energy equation on a design surface element:

$$\left[\sum_{j=1}^{N_S} {E_j}^n A_j \widetilde{F}_{j-i}\right]_{T^n\ unknown} = \rho_i c_{p_i} \delta A_i \frac{T_i^{n+1} - T_i^n}{\Delta t} - {q_{cd_i}}^n - {q_{cv_i}}^n - \left[\sum_{k=1}^{N_S} {E_k}^n A_k \widetilde{F}_{k-i}\right]_{T^n\ known} + E_i^n A_i \tag{5.1}$$

The summation inside $[\ ]_{T^n\ unkown}$ denotes the surface elements with unknown temperatures for the n-th time step and the summation inside $[\ ]_{T^n\ kown}$

denotes the surface elements with known temperatures in Eq. (5.1). The form of energy equation presented here is discretized in time using an explicit Euler scheme and in the given form all the terms on the right hand side are the known terms from the available information, while the terms on the left hand side are the unknowns. The T_i^{n+1} term of the design surface is the value defined by the objective function or the temperature history that is followed at the n+1-st time step.

With known exchange factors, this equation at each time is a set of discretized Fredholm equations of the first kind. When written for all design surface elements, they constitute the ill-conditioned set of equations and in order to achieve a reasonable solution for a system of equations of this type, the system must be regularized by any regularization technique explained in Chapter 3.

By using the explicit Euler discretization scheme, the resulting system of equations becomes linear, keeping all the conductive, convective and heat capacitance terms that generate the non-linearity in the right hand side vector of the linear system of equations. If another scheme is preferred such as an implicit Euler scheme or an Adams-Bashforth scheme, the resulting system of equations will have unknown terms both in absolute temperatures and absolute temperature to power four leading to a non-linearity.

Once the distribution at the n-th time step is known for all surfaces but the heaters, Eq. (5.1) can be solved for the required temperature distribution in the heaters for the n-th time step. This is followed by the calculation of the required power input for the heaters

$$Q_i^{n-1} = \rho_i c_{p_i} \delta_i A_i \frac{T_i^n - T_i^{n-1}}{\Delta t} - {q_{cd_i}}^{n-1} - {q_{cv_i}}^{n-1} - \sum_{j=1}^{N_S} {E_j}^{n-1} A_j \widetilde{F}_{j-i} + {E_i}^{n-1} A_i \tag{5.2}$$

where summation over N_S denotes summation over all the surface elements. The convective and diffusive terms in Eq. (5.2) are all in the (n-1)-th time step, for which the values of temperatures are known.

It should be noted that based on the objective temperature distribution, the history chosen and the accuracy of the solutions produced in the previous time steps, it is quite possible for the system to demand removal of heat from some elements of the system. This situation is reflected in the solutions as the values of the power input being negative for some of the heaters. Such conditions are not acceptable, as adding and removing heat at the same time is not desired.

In such a situation, the simplest solution is just to turn off the heaters which demand removal of heat, or in other words to set power input for these elements $Q_j = 0$. This will lead to some error between the resulting and desired conditions in the design surface, depending on the system considered. If the power input value is modified for some heater elements, it will not be possible for those heaters to reach the temperature distribution estimated from the solution of Eq. (5.1). Instead, the temperature distribution achieved will be

$$T_i^n = T_i^{n-1} + \frac{\Delta t}{\rho_i c_{p_i} \delta_i A_i} \left({q_{cd_i}}^{n-1} + {q_{cv_i}}^{n-1} + \sum_{j=1}^{N_S} {E_j}^{n-1} A_j \widetilde{F}_{j-i} - {E_i}^{n-1} A_i \right) \tag{5.3}$$

Once the temperature distribution of the heaters is known for the n-th time step, the net heat flux over all surfaces and therefore the resulting temperature distribution at the n+1-st step can be calculated using

$$T_i^{n+1} = T_i^n + \frac{\Delta t}{\rho_i c_{p_i} \delta_i A_i} \left({q_{cd_i}}^n + {q_{cv_i}}^n + \sum_{j=1}^{N_S} {E_j}^n A_j \widetilde{F}_{j-i} - {E_i}^n A_i \right) \qquad (5.4)$$

The procedure described is applied from the initial time step, where the design, reflector and the heater surfaces are all at a prescribed initial condition. An outline of the procedure is presented in the flowchart in Fig. 5.1.

The algorithm presented in Fig. 5.1 applies as long as the properties or the geometry of the enclosure does not change. If the geometry of the enclosure or the configuration inside the enclosure changes, the exchange factors must be recalculated at every time step for the new configuration. The availability of the exchange factors in each time step is critical for computational efficiency. Depending on the nature of the problem, instead of using an exchange factor formulation, the use of the configuration factor formulation could be more advantageous.

Moreover, for a problem where the object is moving along a surface for the processing of a material as it is moved using a conveyor belt, the changes in the total energy of the control volumes must also be considered.

For such a problem, it is reasonable to consider the design object using moving coordinates attached to it while the rest of the system can be modeled using coordinates with respect to a fixed reference point. The energy equation for a moving design object can be defined using the partial derivative with respect to

time while it is defined using the substantial derivative for all other moving parts. Therefore, Eq. (5.1) is the energy equation for the design surface while the governing equation related to the moving parts can be written as:

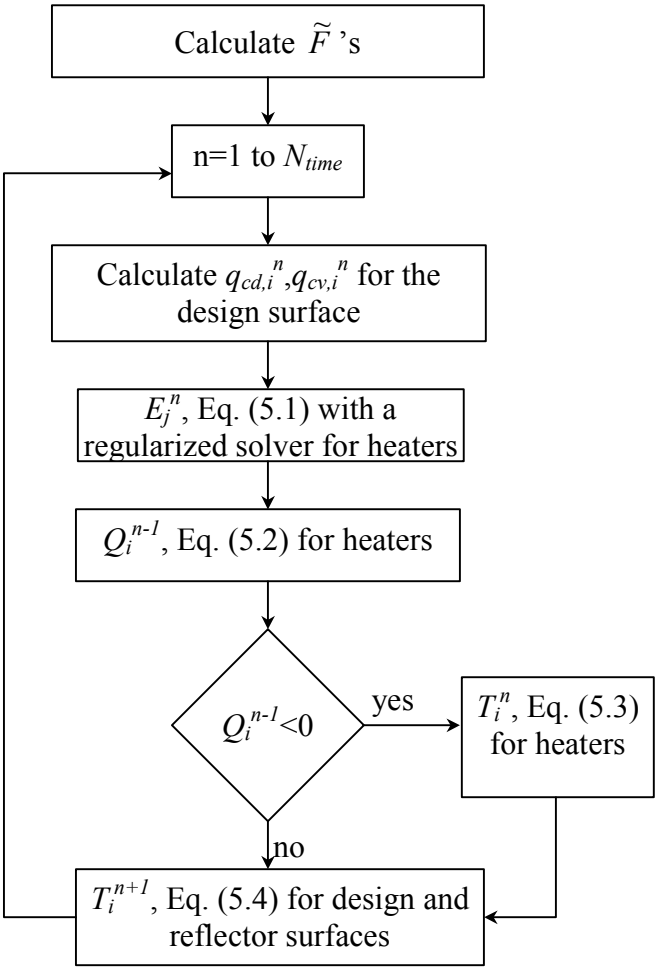

Figure 5.1: The flowchart of the solution algorithm

$$\sum_{j=1}^{N_S} E_j{}^n A_j{}^n \widetilde{F}_{j-i}{}^n - E_i{}^n A_i{}^n + q_{cv,i}{}^n + q_{cd,i}{}^n + U\rho_i c_{pi}\delta_i \frac{A_i^n}{\Delta y}\left(T_{i-1}{}^n - T_{i+1}{}^n\right) = \rho_i c_{p,i}\delta_i A_i{}^n \frac{T_i^{n+1} - T_i^n}{\Delta t} \tag{5.5}$$

where U is the velocity of the surface and Δy represents the grid size perpendicular to the velocity direction. Although Eq. (5.5) uses exchange factor formulation for radiation as before, the exchange factors are dependent on the time.

5.3 PROBLEM STATEMENTS

Two sample problems are considered to display the use of the algorithms explained in the previous section. These are transient heating in a two-dimensional enclosure and transient heating of a moving object. The first problem considers the basic problem of a transient thermal boundary condition design. The method is applied and the solution is analyzed extensively for different cases that modify the main problem. The second problem considers a special case of the first problem where the geometric configuration inside changes as the design object moves along the furnace.

5.3.1 Transient Heating in a Two-Dimensional Enclosure

The problem considered first is a transient thermal boundary condition estimation problem, in which the designer aims at controlling the thermal conditions in the design environment by setting the necessary thermal conditions on the heater surfaces. The design surface is to be heated from an initial state to a

final steady state, while it is kept at a spatially uniform temperature, following a specified heating profile.

A two-dimensional evacuated furnace with heater surfaces 5, 6 and 7, design surface 2 and reflector surfaces 1, 3, 4 and 8 is shown in Fig. 5.2. The heater surfaces have the properties of nichrome with an oxidized rough surface leading to diffusely reflecting surfaces. The reflector surfaces have the properties of polished aluminum, and are therefore specularly reflecting with a higher reflectivity than the heater and design surfaces. The design surface has the properties of silicon carbide, which is diffusely reflecting. The heater surfaces are made up of 30 uniform temperature strip heaters that are slightly separated from each other. The backside of the design surface is insulated and it does not touch the reflector surfaces at the edges. Thus, the thermal radiation is the only means

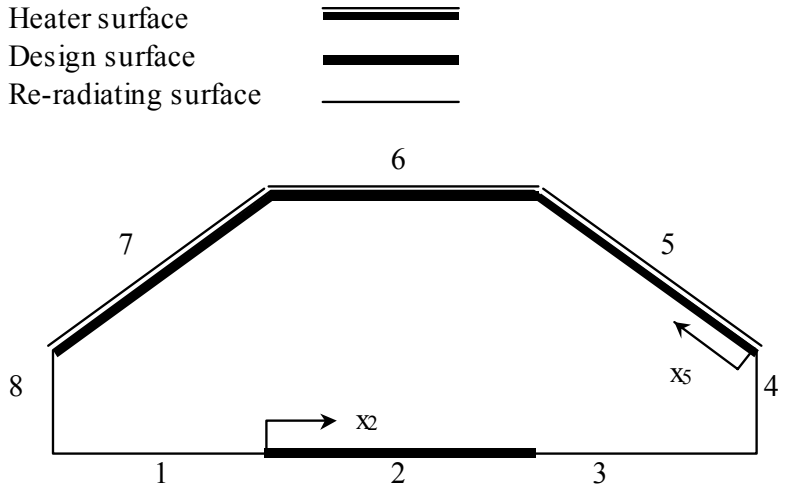

Figure 5.2: The geometry of the furnace in the transient heating in a two-dimensional enclosure

of exchanging heat from the design surface to its surroundings. Furthermore, it is assumed that the conduction across the plate thickness is negligible when compared with the thermal radiation exchange on the inside of the enclosure and conduction along the plate so that the surface can be approximated as isothermal across the plate thickness. The other assumptions considered for the solution are: all the thermal properties are assumed to be constant and independent of the temperature variations in the system, all the radiative properties are gray and the system is considered to be at local thermodynamic equilibrium at all times.

The desired design surface heating history is presented in Fig. 5.3 and is defined in terms of a smooth polynomial from an initial temperature of 300 K to a final temperature of 1000 K and $T_d(t)$ is uniform across surface 2. The geometric data and required thermal properties of the surfaces are presented in Table 5.1.

Table 5.1: The geometric and thermal parameters that define surfaces for the transient heating in a two-dimensional enclosure problem.

Surface	δ (m)	ρ(kg/m^3)	c_p (J/kgK)	L (m)	k (W/mK)	ε
1	0.001	2702	903	0.8	227	0.05
2	0.001	3160	675	1	454	0.9
3	0.001	2702	903	0.8	227	0.05
4	0.001	2702	903	0.4	227	0.05
5	0.0001	7870	447	1		0.95
6	0.0001	7870	447	1		0.95
7	0.0001	7870	447	1		0.95
8	0.001	2702	903	0.4	227	0.05

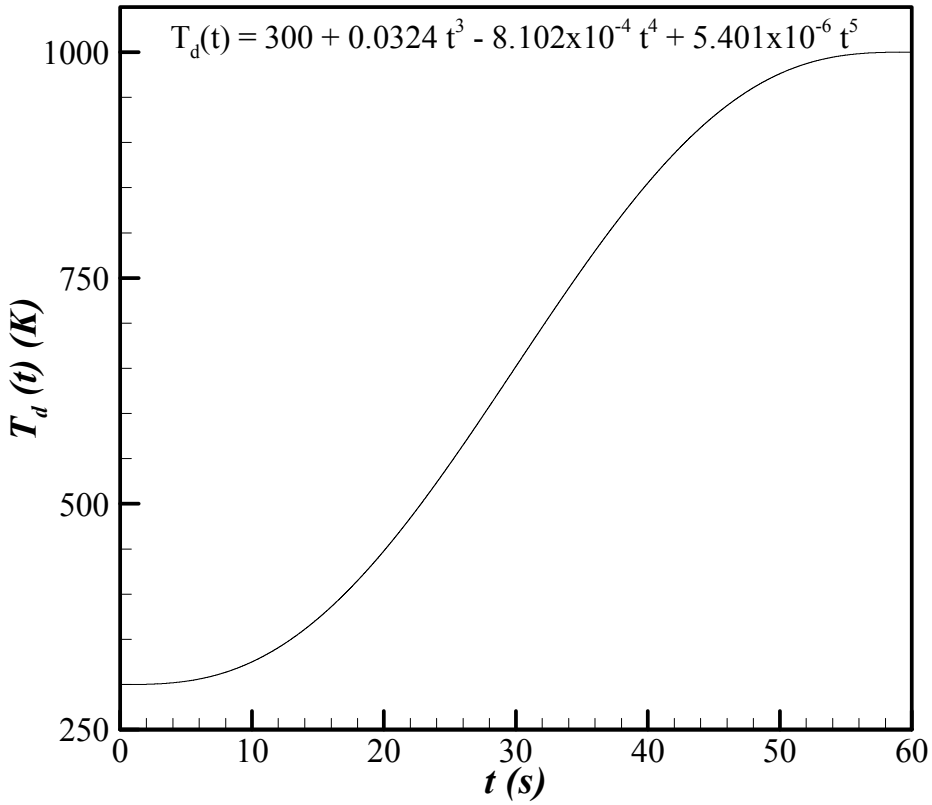

Figure 5.3: The desired design surface temperature history for the transient heating in a two-dimensional enclosure problem.

5.2.2 Transient Heating of a Moving Object

The second example problem considers the design of a tunnel-shaped process furnace with heaters on top and a design surface that is to be heated as it is moving along the furnace at the bottom and with reflector walls on the sides. This problem can be classified as a transient boundary condition estimation problem and it resembles the typical furnace that can be used for industrial

annealing, preheating, baking, drying or curing where the object to be processed enters the furnace, is heated based on the heating history required by the particular process while it is moving towards the exit and then leaves the furnace. In such a furnace that uses surface heaters, thermal radiation is the dominant mode of heat transfer when there is no forced flow inside.

This problem is very similar to the preceding problem where a stationary object is heated along time. It includes an additional complexity in terms of a moving object.

The evacuated tunnel-shaped furnace is displayed in Fig. 5.4. Surface 4 (top surface) is the heater, the shaded surface at the bottom is the design object, surfaces 5 and 3 are reflectors and surfaces 1 and 6 are the surfaces that allow the

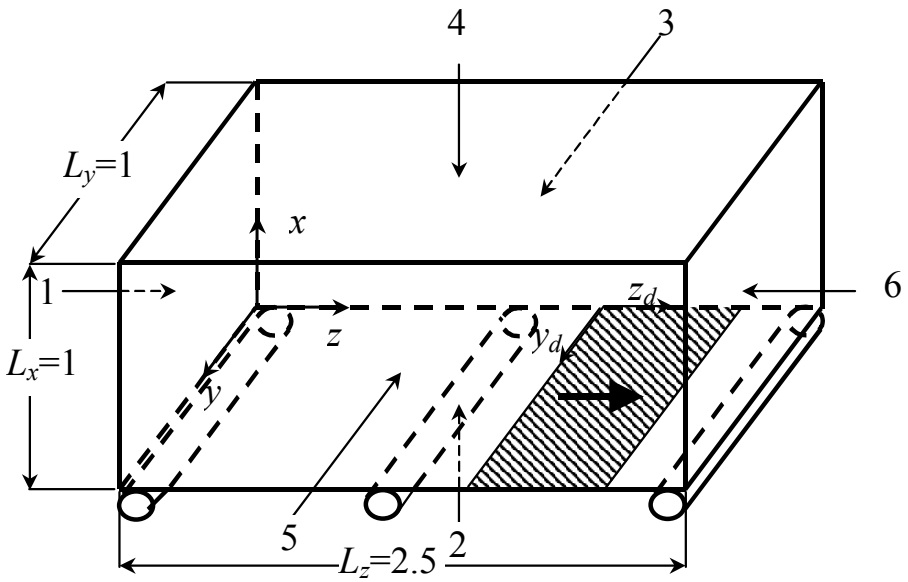

Figure 5.4: The geometry of the furnace in the transient heating of a moving object problem (dimensions are given in meters)

design object to enter and exit the furnace. The unshaded portion of surface 2 represents the conveyor that moves along with the design object. The heater surface is made up of isothermal oxidized-nichrome heater plates with a diffusely reflecting surface. The plates are slightly separated from each other so that there is no diffusive heat transmission between them. The reflector surfaces are specularly reflecting polished aluminum (k=227 W/m K). The design surface is silicon carbide (k=454 W/m K), the conveyor, the inlet and exit surfaces are made up of coated aluminum (k=227 W/m K), which are all diffusely reflecting.

All the surfaces other than 1 and 6, the inlet and exit surfaces, are insulated from the outside so that they do not lose heat to the environment (T_∞ = 300 K), whereas the convective heat loss from surfaces 1 and 6 can be approximated by the use of an average convective heat transfer coefficient (h= 5 W/m^2 K).

Furthermore, it is assumed that the conduction across the plates is negligible; therefore, the plates are considered as isothermal across the plate thickness. The other assumptions considered are: the interface between the design surface and the conveyor is well insulated so that the heat diffusion due to physical contact is prevented, all radiative properties are gray, all the thermal properties are assumed to be constant and independent of the temperature variations in the system and local thermodynamic equilibrium is assumed to be present everywhere at a given time.

The design surface is one-fifth the length of the total furnace along the z-axis and it starts moving near surface 1, located at z=0, as the heaters are turned

on. The furnace is heated from a uniform initial temperature that equals to the ambient temperature as the design surface moves so that the design surface is heated uniformly as it is kept isothermal, spatially. The uniform heating is a common design constraint sought in many processes to prevent thermal stresses or provide uniform baking, curing or drying. The design surface follows a heating history as defined by a polynomial similar to the previous problem. It smoothly connects the initial temperature 300 K and the final temperature 600 K (Fig. 5.5). When the leading edge of the design surface reaches the end of the furnace, surface 6, the design surface temperature should also reach the final temperature, 600 K, and the heating process ends.

The rest of the data required to define the characteristics of the furnace of this test problem are presented in Table 5.2. In Table 5.2, the properties of surface 2 are defined separately for the design and the conveyor surfaces.

Table 5.2: The thermal parameters that define surfaces for the transient heating of the moving object

Surface	δ (m)	ρ(kg/m^3)	c_p (J/kgK)	k (W/mK)	ε
1	0.01	2702	903	227	0.05
Conveyor	0.01	2702	903	227	0.9
Design	0.001	3160	675	454	0.9
3	0.01	2702	903	227	0.05
4	0.0001	7870	447		0.95
5	0.01	2702	903	227	0.05
6	0.01	2702	903	227	0.05

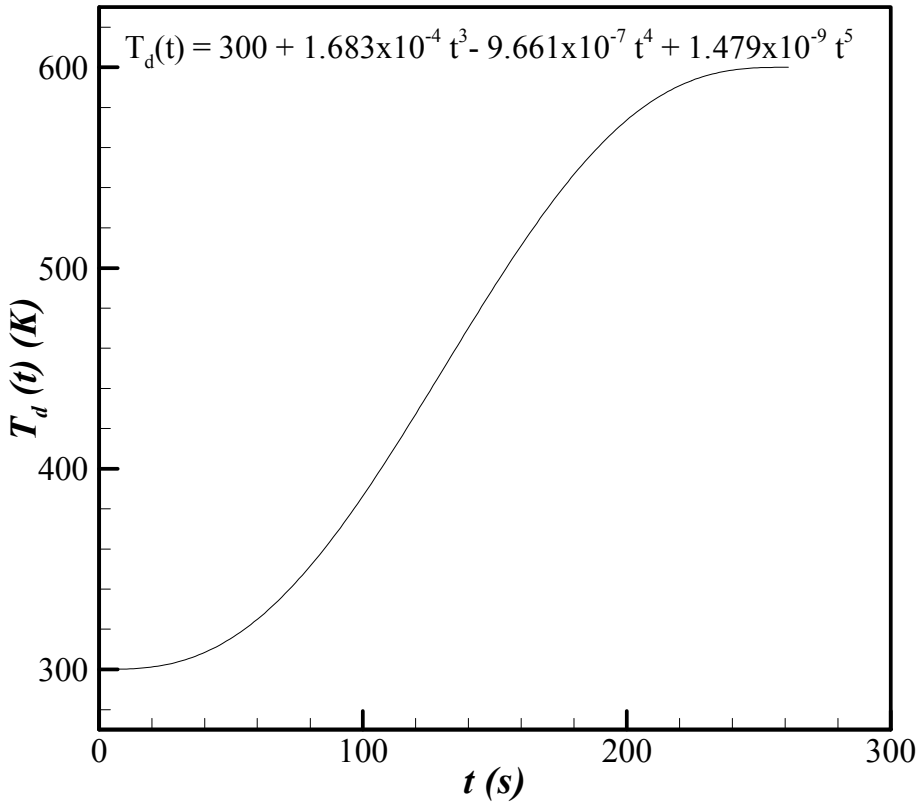

Figure 5.5: The desired design surface temperature history for the transient heating of a moving object problem

5.4 RESULTS AND DISCUSSION

The two sample problems are solved using the inverse design methodology explained in the preceding section. The results achieved are as follows:

5.4.1 Transient Heating in a Two-Dimensional Enclosure

The problem of transient heating of the design object is solved to evaluate the necessary power input for the 30 individual strip heaters (10 on each surfaces 5, 6 and 7 of Fig. 5.2) to provide the necessary radiative flux for the design surface so that it will be heated spatially isothermal, following the specified temperature history presented in Fig. 5.3 in a total time of $t_{tot} = 60$ seconds.

Certain considerations should be underlined regarding the solutions, so that the results can be discussed more clearly.

The MCM is used to calculate the exchange factors and as it is a statistical solution technique the solutions obtained by the method are subject to statistical noise. Even though it is possible to reduce the noise through increasing the number of samples used for the simulation, it is impossible to get rid of it completely unless the symmetry is forced through modifications. In a forward problem or even in a steady inverse problem as long as enough samples are used, the resulting slight noise does not affect the solution (Ertürk et al., 2000). On the other hand, in the transient inverse problem under consideration it was observed that the slight noise in the exchange factors is amplified through inverse solutions at each time step resulting in slight asymmetry in the solution at certain time steps. In order to get rid of this behavior completely, symmetry must be forced in the exchange factors. This kind of re-adjustment of exchange factors is not considered in this study, as the asymmetry is not significant.

The conjugate gradient method is used to produce regularized solutions as explained in the previous section. The method produces a number of different

solutions, which have different levels of accuracy, smoothness characteristics, and shape. If the optimal CG-step is sought for each time step, significant fluctuations in the variables along time result, as the CG-step yielding the optimal solution may change at each time step, while the solution is repeated. In order to get a smooth distribution along time, solutions must be produced using a fixed CG-step for each time step rather than by using the optimal solution at each step. This leads to a loss in accuracy at certain time steps where a more accurate and still smooth solution might be available from the use of more CGM steps.

The resulting temperature distribution over the design environment (surface 2) based on the designed system, evaluated by the proposed algorithm is displayed in Fig. 5.6. Figure 5.7 displays the error of the achieved temperature distribution along the design surface throughout the process, which is defined as

$$\%E_{T_i} = 100\frac{\left|T_i - T_d(t)\right|}{T_d(t)} \tag{5.5}$$

It may be observed from Fig. 5.7 that the accumulated errors affect the system the most when the non-dimensional time is about 27 s (t/60 s = 0.46), reaching a maximum error of 0.45 percent, where the average error is 0.12 percent. The maximum and average error decreases to 0.16 and 0.07 percent, respectively, as the system reaches the steady state. It should be remembered that the solution accuracy is still limited by the assumptions considered for the formulation, the available property values and the radiation solver used. It can be observed that the locus of the maximum error is usually at the edges of the design surface. This information can be used by the designer to reconfigure the heater or

enclosure geometry to achieve better agreement with the prescribed design environment.

The conditions on the design surface, demonstrated in Fig. 5.6, are achieved when the temperature of the heater strip surfaces satisfies the values displayed in Fig. 5.8, which displays the necessary heater temperatures for 30 strip heaters, along the heating process. It can be observed that the temperature of

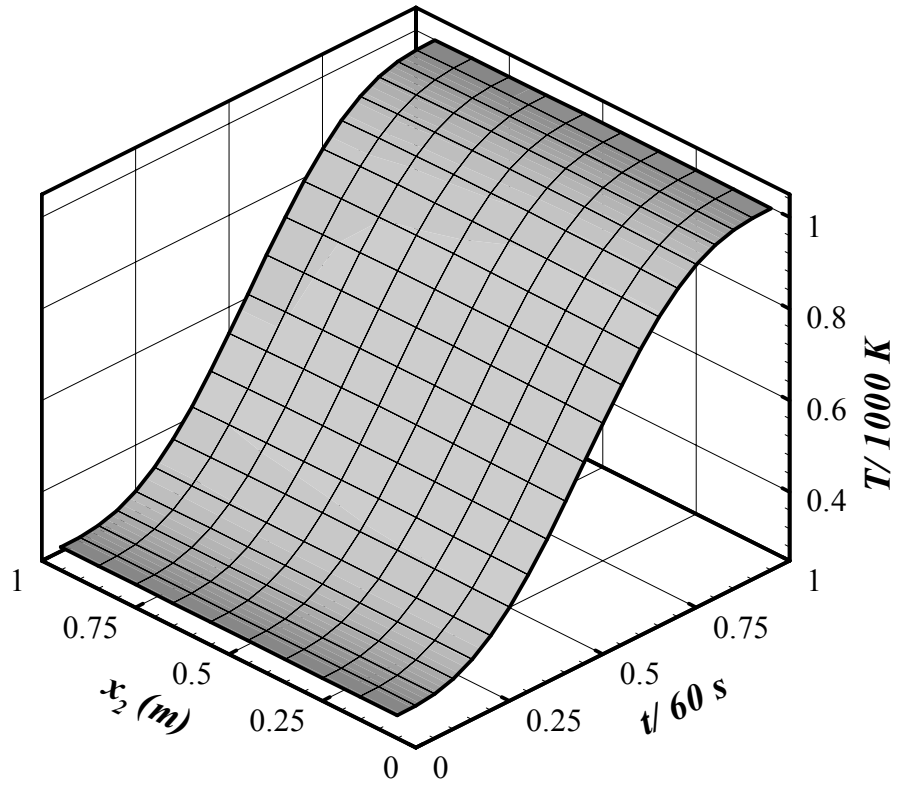

Figure 5.6: The resulting design temperature distribution based on the heater conditions determined from inverse analysis

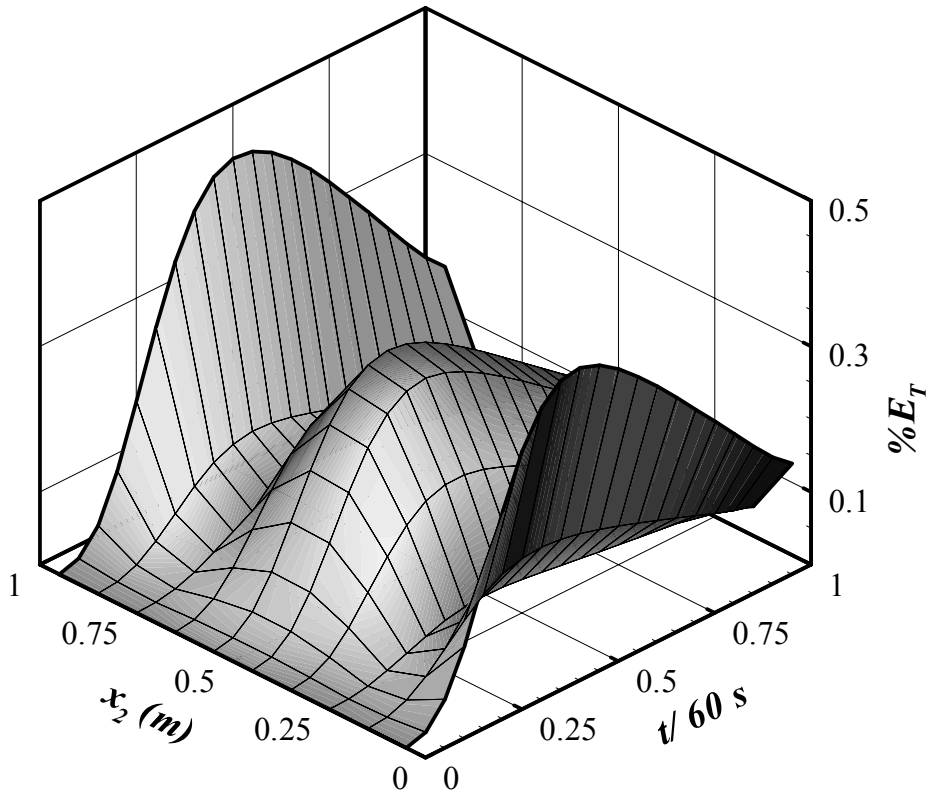

Figure 5.7: The errors based on design surface temperature and design specification

the heater strips is slightly above the temperature of the design surface at all times so that they can radiatively heat the design surface in the amount necessary to follow the design objective as specified by $T_d\ (t)$. Furthermore, the distribution along the heater strips is such that when combined with the resulting design and reflector surface temperature distributions, the spatially uniform heat flux and temperature condition is satisfied on the design surface. The temperature of the

heater strips increases until it peaks around 39 seconds at a value about T= 1100 K and then decreases to the steady state temperature of the design surface.

The 30 heater strips exchange energy through thermal radiation with other surfaces and each other, and receive energy as an input. In order to control the temperature distribution of the heater strips that controls the temperature distribution on the design surface, the input power distribution is varied. The necessary power input to keep the temperatures of the strip heaters as shown in

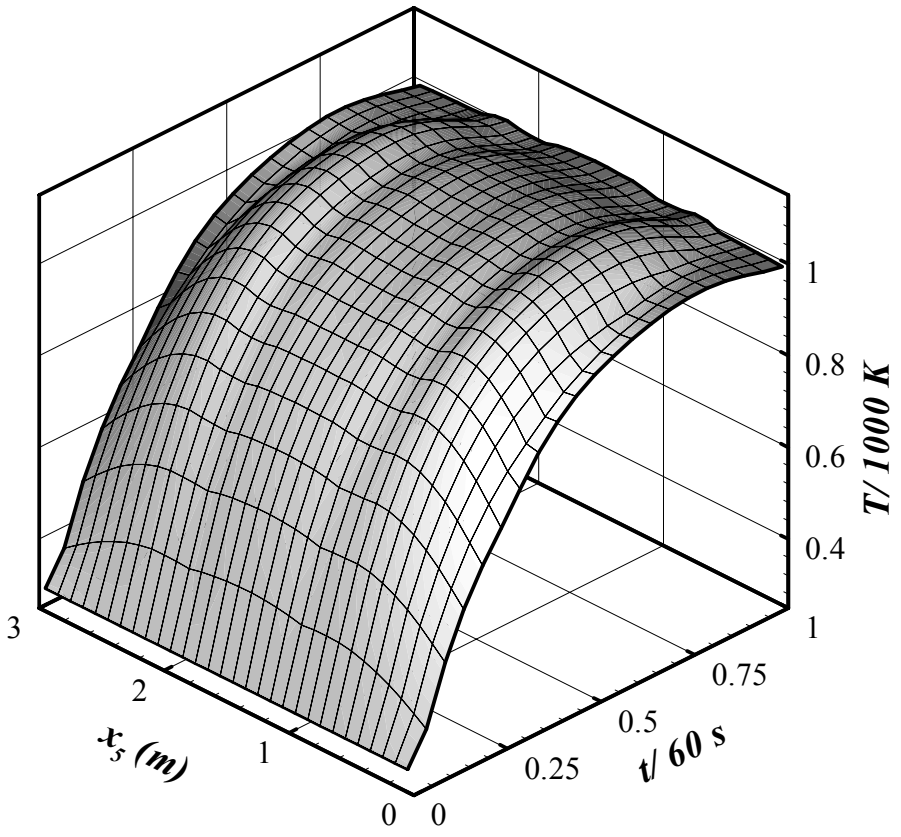

Figure 5.8: The temperatures of thirty heater strips along the heating process

Fig. 5.8 is displayed in Fig. 5.9. To obtain the distribution presented in Fig. 5.9 an additional constraint is used for the initial time step. For this problem, the required initial net heat flux on the design surface is zero with all initial design and reflector surface temperatures being 300 K. It is apparent that a uniform distribution of 300 K, identical to the initial condition, along 30 heater strips will satisfy the design constraints exactly. However, the regularized inverse solution predicts a heater profile that has a slight gradient. The heater strips close to the

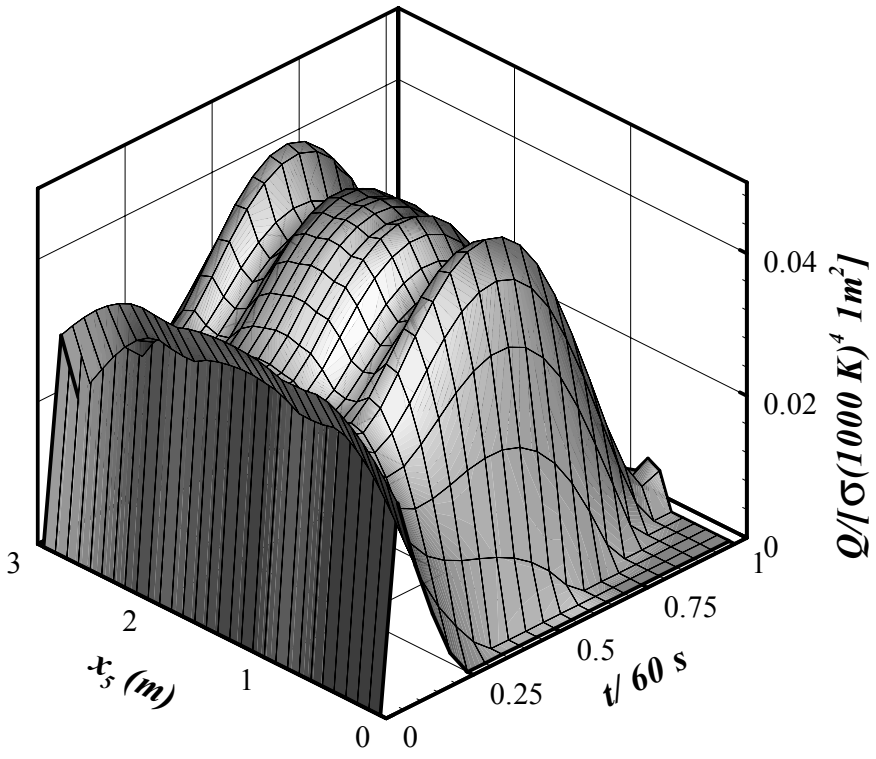

Figure 5.9: The necessary power input for thirty heater strips

edges tend to have values slightly lower than 300 K and the ones close to the middle larger than 300 K so that the energy equation is satisfied at every location. When the design constraint that restricts the energy removal from the strips is applied, the values of the temperature below 300 K are corrected to 300 K leaving the ones above 300 K as they are. This sudden change at the end of the initial time step due to the regularization error necessitates a large amount of power input per time step to account for the heat capacity of the heaters, especially for simulations utilizing a very small time step ($\Delta t < 0.376$ seconds). This apparent sudden increase in heater power requirement is due solely to regularization error. Therefore, a second constraint is applied for the initial time step to remove the "artificial" need for the power input that has nothing to do with the physical needs of the system. This constraint is simply not turning the power on for all heater strip elements for the initial time step leading the heater strips not to change their temperature.

All the results presented in Figs. 5.6-9 are obtained using a time step size of $\Delta t = 0.0226$ seconds and 64 surface elements with a 26x10 grid resolution. The exchange factors are calculated by MCM using 400 million sample photon bundles. The result from the first CG-step was used in order to obtain physical solutions with smooth spatial and time profiles, during the entire heating process. It was observed that identical solutions result when the grid resolution is doubled, utilizing 128 surface elements with a 52x20 grid.

Although the accuracy of the inverse solutions could have been improved by using the results of further CG-steps, this increases the norm of the solution as

displayed in the L-curve. The L-curve represents the variation of the residual of the solution with the norm of the solution for a single time step and a sample L-curve of the solution presented in Figs. 5.6-9 is displayed for the 665-th time step in Fig. 5.10. Every point in Fig. 5.10 represents a possible solution resulting at the end of a different CG-step for the 665-th time step. While the decrease in the norm of the residual represents the increase in solution accuracy, the

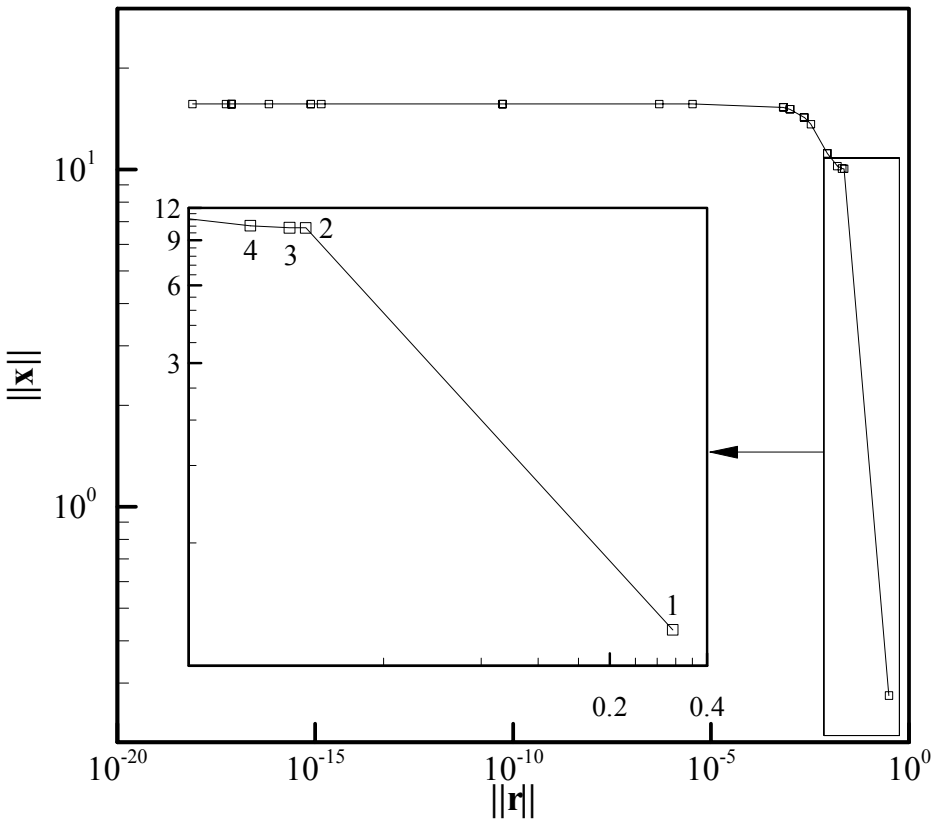

Figure 5.10: The L-curve, variation of the norm of the solution with norm of the residual for time step 665

corresponding increase in the norm of the solution represents the decrease in the smoothness of the solution. Therefore, the solutions produced by the use of further CG-steps are more accurate but have a greater tendency to produce non-physical solutions than the earlier CG-steps.

In order to investigate the effect of the CG-step used in the solution of the sample design problem, the maximum percentage error of solutions produced using different CG-steps and time step sizes are compared in Fig. 5.11. It can be observed that the time step size is an important parameter that affects the level of accuracy in the solution. The discretization error in Eqs.(5.1-4) dominates the solution when a large time step is used. Therefore, for time steps larger than 3.76 seconds the system at some point overheats the design surface due to time discretization errors in such an amount that satisfying the design goal becomes numerically impossible using positive emissive power on the heater elements. As a result, no physical result is available. On the other hand, when the time step size is decreased, the total number of time steps used for the solution increases. This simply results in increasing the cumulative effect of regularization errors leading the system to a state where it is also impossible to maintain a physical solution as stated above. Therefore, the algorithm cannot produce any solution when the time step is reduced below some value.

The range of time steps where it is possible to produce a physically meaningful solution differs for solutions that use the results of a different number of CG-steps. This range is from 3.76 to 0.0226, 3.76 to 0.301 and 3.76 to 0.0188 seconds when the results of the first, second and third CG-step are used,

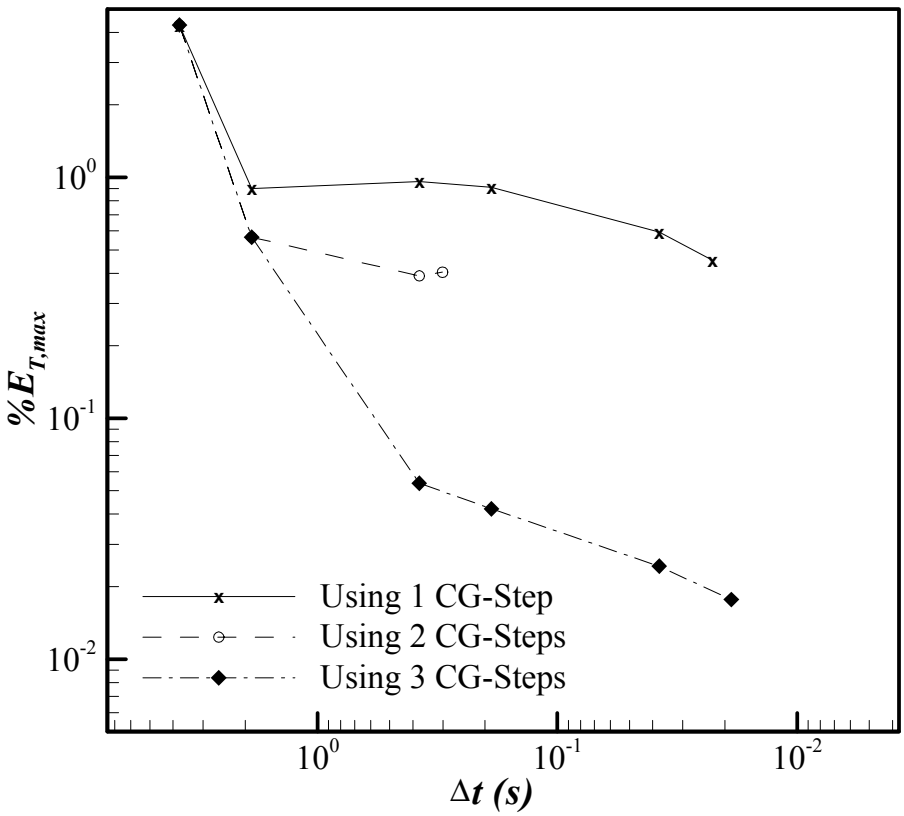

Figure 5.11: The change in solution accuracy with the result of CG-step used and time step size

respectively. The solutions that use the results of the first and the third CG-steps have a larger time step size range than the solution that uses the result of the second CG-step. This is because the solution evaluated using the result of the first CG-step is the smoothest; thus, even though it is affected most by the cumulative effect of the regularization error as the number of time steps used increases, it still can produce physically reasonable solutions up to some point.

On the other hand, the solution evaluated using the result of the third CG-step is subject to the least regularization error among the three solutions and the cumulative effect of the regularization error starts affecting the system later than the other two although it produces the least smooth solutions. The solution using the results of the second CG-step satisfies neither of the conditions, and as a result has the smallest range of useful time increment size. Thus, as the overall solution accuracy increases with decreasing norm of residual, the smoothness decreases with the use of more CG-steps. This is a basic trade-off in most inverse problems, and the choice of the CGM step is dependent on the process and the problem considered.

One of the main characteristics of inverse problems is that the solutions are very sensitive to perturbations in input. For that reason, it is customary to test the solution procedures for inverse problems by introducing some perturbation to the input data (Özışık and Orlande, 2000). In a measurement problem, the perturbations are often in the form of random noise in the measured data. A similar effect is encountered when slight changes in the designed system is considered. One should be very careful when introducing perturbations, as this can lead to a problem that has no solution within an acceptable level of accuracy.

Two tests with perturbations in the system are considered in this study; the first is the use of reflector surfaces that have larger emissivity (ε =0.5) and the second is replacing the slab design surface with a two-dimensional surface so that the furnace geometry becomes as displayed in Fig. 5.12. The lengths of surfaces 2-a and c in Fig. 5.12 is 0.3 m and the new design surface introduces blockage

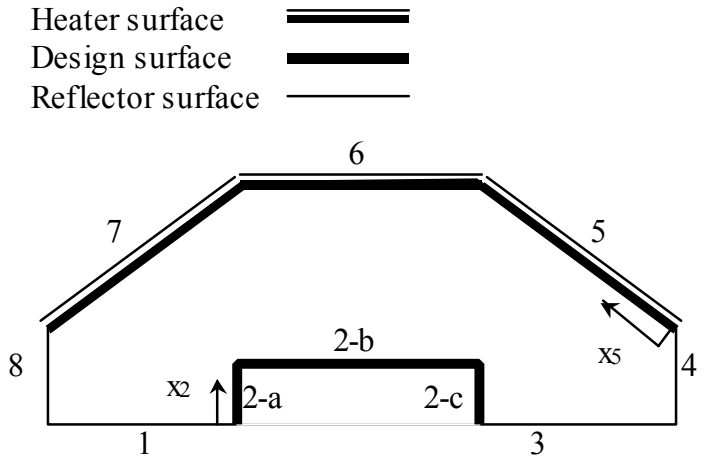

Figure 5.12: The geometry of the furnace for the second perturbed case

into the problem. Attaining spatially isothermal heating of the surface is more difficult than it was in the previous case. The rest of the conditions for the materials used, geometry, and the design objective are unchanged.

Figure 5.13 displays the required heater temperature distribution along the process, for the case with reflector surfaces having ε =0.5. The distribution is calculated using the results of the first CG-step and a time step size of Δt = 0.0226 seconds. The corresponding percentage error based on the temperature of the design surface is presented in Fig. 5.14. The maximum error in the achieved temperature of the design surface is less than 0.6 percent. When Figs. 5.8 and 5.13 are compared, it can be observed that the temperature gradient along the heater strips is greater in the case where reflector surfaces have ε =0.5, and from Figs. 5.7 and 5.14, it can be concluded that the original case (with ε =0.05) is more likely to be the preferred configuration, both in terms of achieving the

design goal more accurately and in terms of efficiency considerations, as in the original case the reflector surfaces absorb less energy. The results are in agreement with physical intuition, as highly specularly reflecting sidewalls will make it easier to achieve spatially uniform distributions.

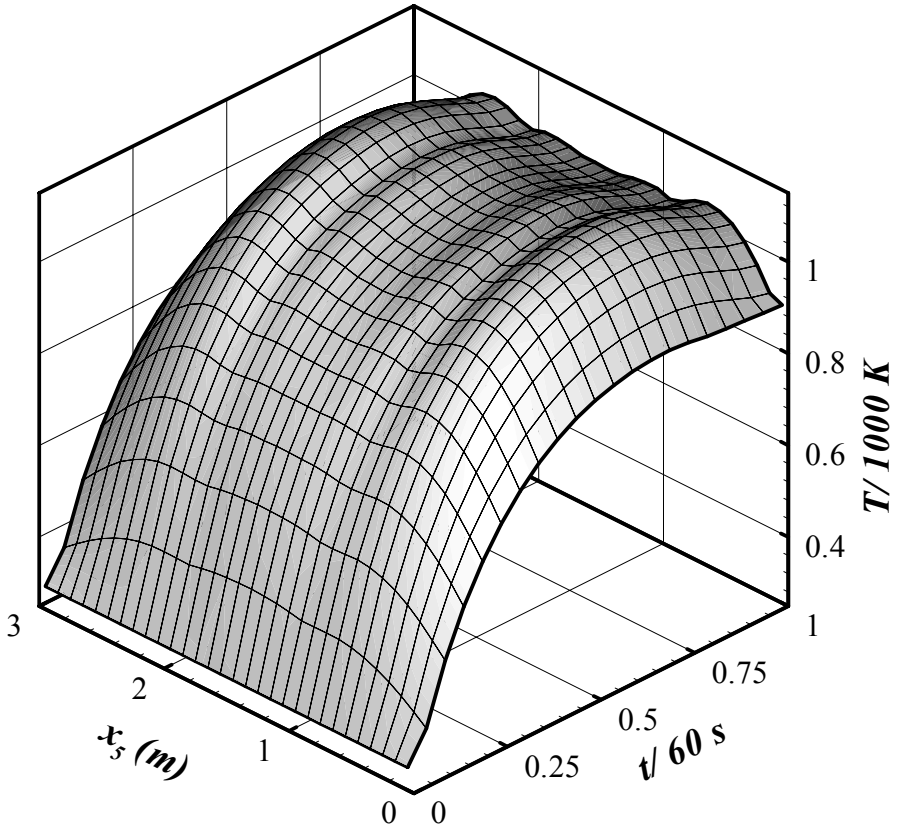

Figure 5.13: The temperatures of thirty heater strips along the heating process for the problem with reflector surfaces having ε=0.5

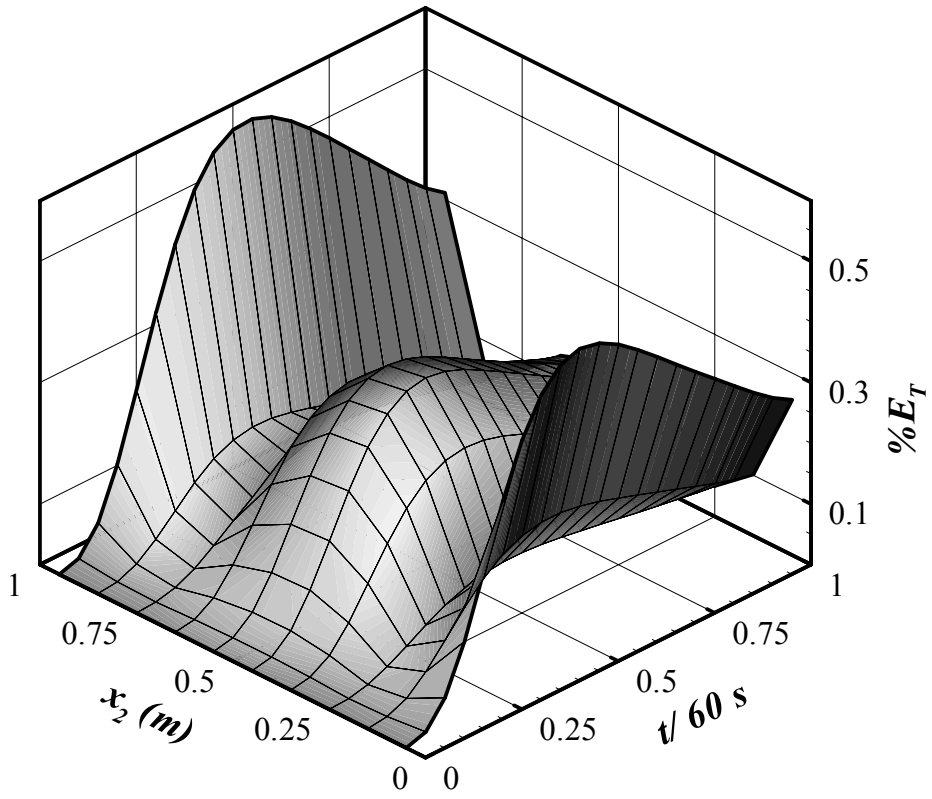

Figure 5.14: The errors based on design surface temperature and design specification for the problem with reflector surfaces having ε=0.5

The second perturbation considered is the change in the design surface geometry as shown in Fig. 5.12. The required temperature distributions along the design surface temperature based on the designed system is plotted in Fig. 5.16. The maximum error for the final case is less than 0.5 percent, which can be a heater strips are displayed in Fig. 5.15. The corresponding error in the achieved significant error for applications like RTP or CVD but can be considered to be

within acceptable limits when the governing assumptions are considered. The solution presented in Figs. 5.15 and 5.16 are produced using the results of a single CG-step with a time step size of $\Delta t = 0.0376$ seconds, which is the limiting value for the case. In order to further improve the solutions, the designer should consider other changes, either in geometry or the materials used.

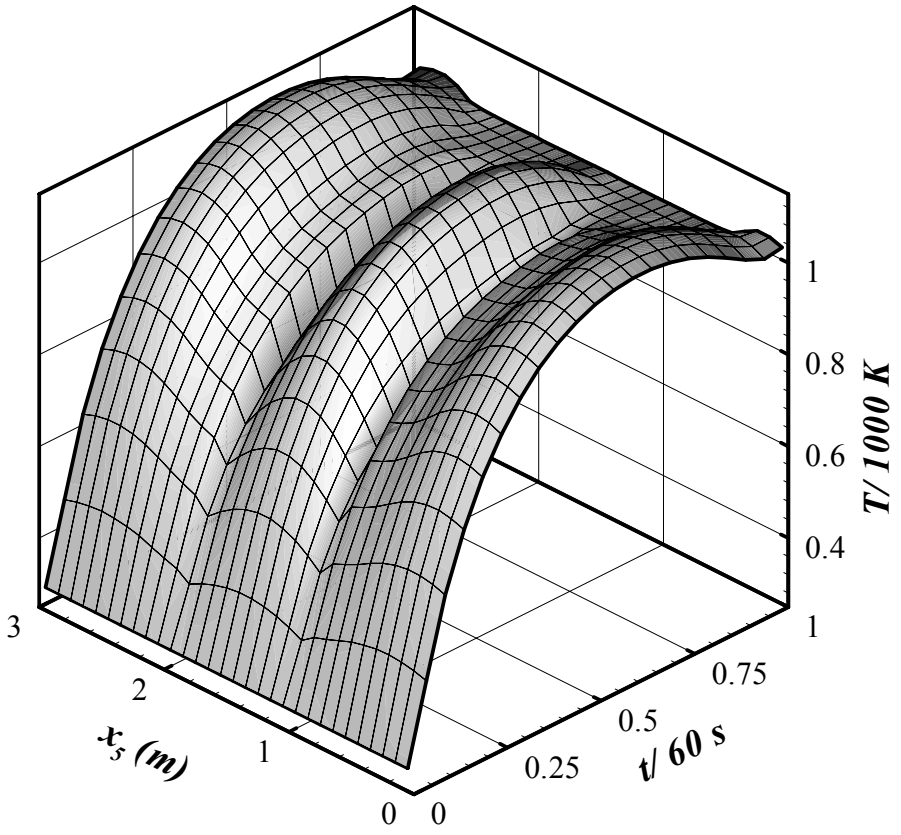

Figure 5.15: The temperatures of thirty heater strips along the heating process for the furnace geometry displayed in Fig. 5.12

The main advantage of the proposed procedure is that it can produce a direct solution and it can be applied with any similar regularization technique instead of CGM or any other method to formulate the radiation transfer instead of MCM with the limitations outlined. When the temperature dependency of the radiative properties becomes important the solution technique could be modified by either of two different approaches. Both of these approaches require the

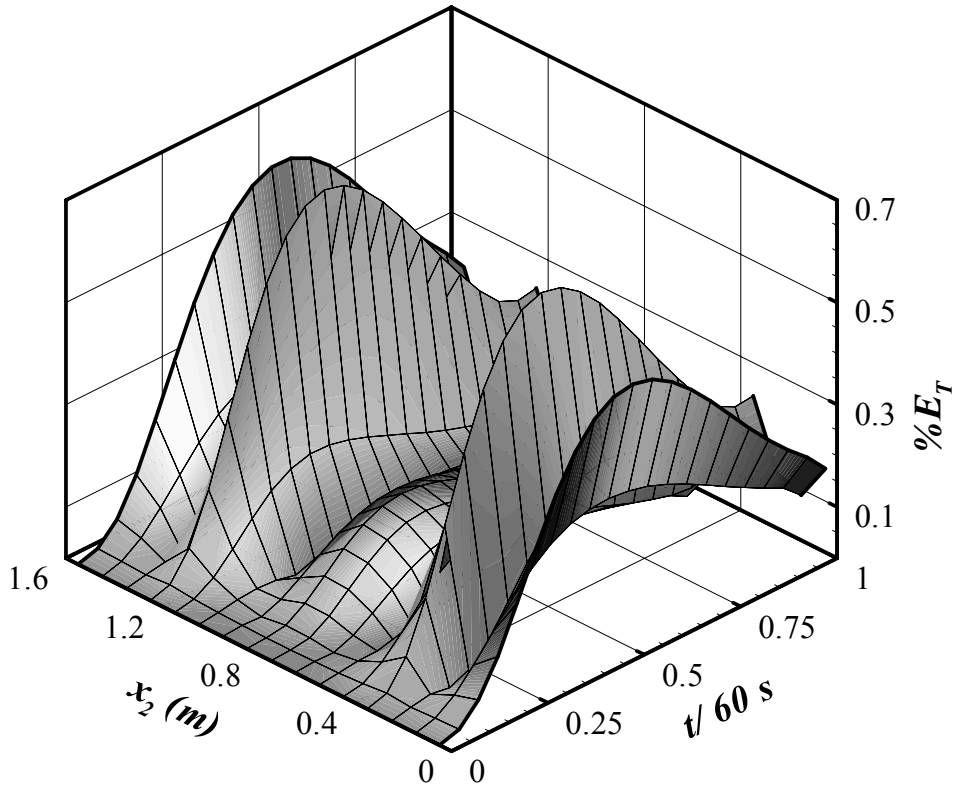

Figure 5.16: The errors based on the achieved design surface temperature and desired design surface temperature history for the furnace geometry displayed in Fig. 5.12

calculation of configuration factors instead of the exchange factors at the beginning. The first approach is to calculate the exchange factors at each time step based on the radiative properties varying with changing temperature distributions and following the rest of the steps in the procedure as outlined in Fig. 5.1. The burden of the calculation with this approach is the calculation of exchange factors from configuration factors. An alternative approach is using the configurations factors in the formulation directly, i.e. using the discretized form of Eq. (2.11) instead of the discretized form of Eq. (2.13) leading to a larger number of simultaneous equations to solve at each time step.

5.4.2 Transient Heating of a Moving Object

The design problem of the transient heating of a moving object is now solved to evaluate the necessary power input to the heaters so that the moving surface is heated isothermally from an initial temperature to a final temperature following a specific temperature history. At the initial condition, the non-dimensional temperature of all surfaces is 300 K and the trailing edge of the design surface is at the position $z = 0$. The surface moves along the furnace at a constant speed of 27.5 m/hours, and it takes the leading edge of the surface 262 seconds to arrive at the exit. The leading edge arrives at position $z = 2.5$ at the end of the heating as the temperature reaches a value of 600 K.

The MCM is used to calculate the exchange factors for the system. As in the case of the previous problem, symmetry is not forced and any resulting asymmetry around $y = 0.5$ is a result of the amplification of the slight noise in the

exchange factors that are obtained through a MC simulation that makes use of 100 million sample photon bundles.

The exchange factors for the design surface change as it moves, therefore they must be re-calculated at each time step. If a new simulation for every configuration is done the computational expense will be tremendously high due to the high cost of the method used. Instead, the exchange factors for the design surface are derived at each time step using simple geometric relationships from the exchange factors to the whole bottom surface evaluated by the MC simulation. This is possible because the emissivity of the conveyor and the design surfaces are the same. Otherwise, one of the two approaches explained in Section 5.2 should be followed.

Due to the changing exchange factors, the coefficient matrix of the system of equations governing the inverse design changes with time. Therefore, the use of the CGM is not only advantageous because it provides regularized solutions but also due to its computational economy. As mentioned before, the solutions produced at the end of different CG steps can have extremely different shapes. If the same number of CG-steps is not used at each time step, significant fluctuations in the variables along time result, as in the case of the previous problem. Therefore, a solution that is produced with a fixed number of CG steps is used rather than using the optimal solution that could be evaluated for each time step.

Obtaining the desired heating history is the design goal. The temperature values obtained at the points (y_d =0.9375, z_d =0.0625) and (y_d =0.5625, z_d

=0.4375) are displayed in Fig. 5.17. These points are the ones close to the corner trailing and the middle of the design surface, respectively.

The average and maximum of the absolute percentage errors based on the design surface temperature change are displayed in Fig. 5.18 along the process. The absolute percentage error based on the design surface temperature is defined by Eq. (5.5)

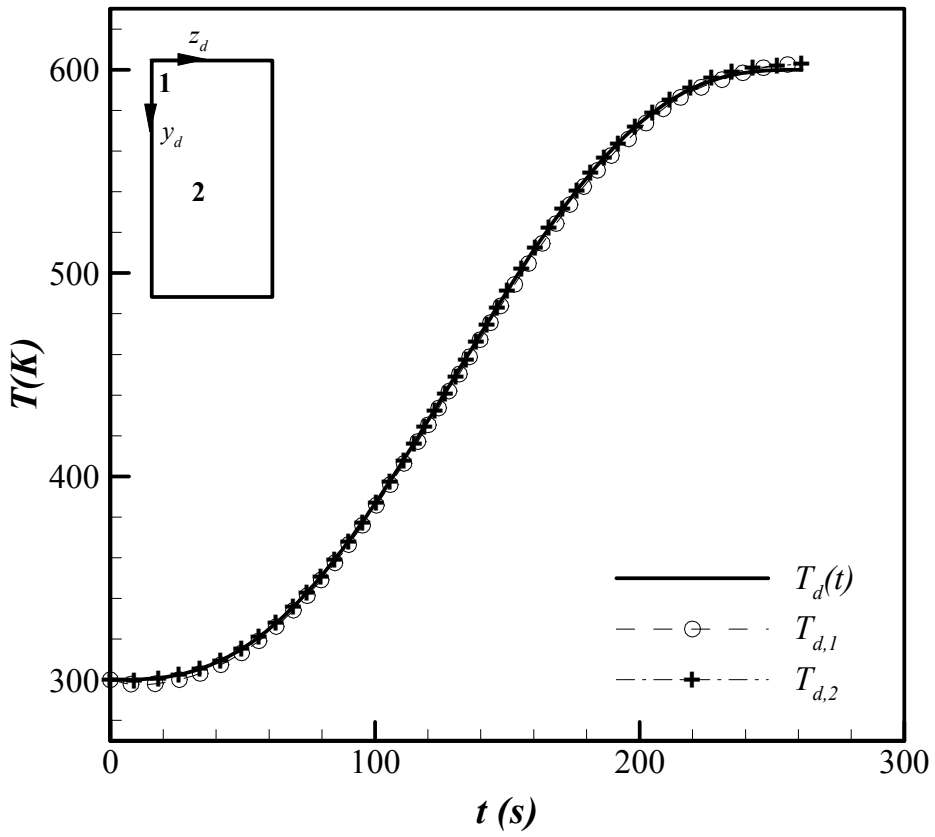

Figure 5.17: The change of temperature in the design surface with time along points 1 and 2 compared with design objective.

From Fig. 5.18, it is observed that the errors are largest at the beginning and at the end of the process when the required net heat transfer to the design surface is very small. The maximum and average of the absolute percentage error reaches 0.9 and 0.5 percent at the very beginning of the heating at time 8.71 seconds. The design surface is under-heated slightly at both points. The corresponding error values decrease and stay below 0.7 and 0.3 percent,

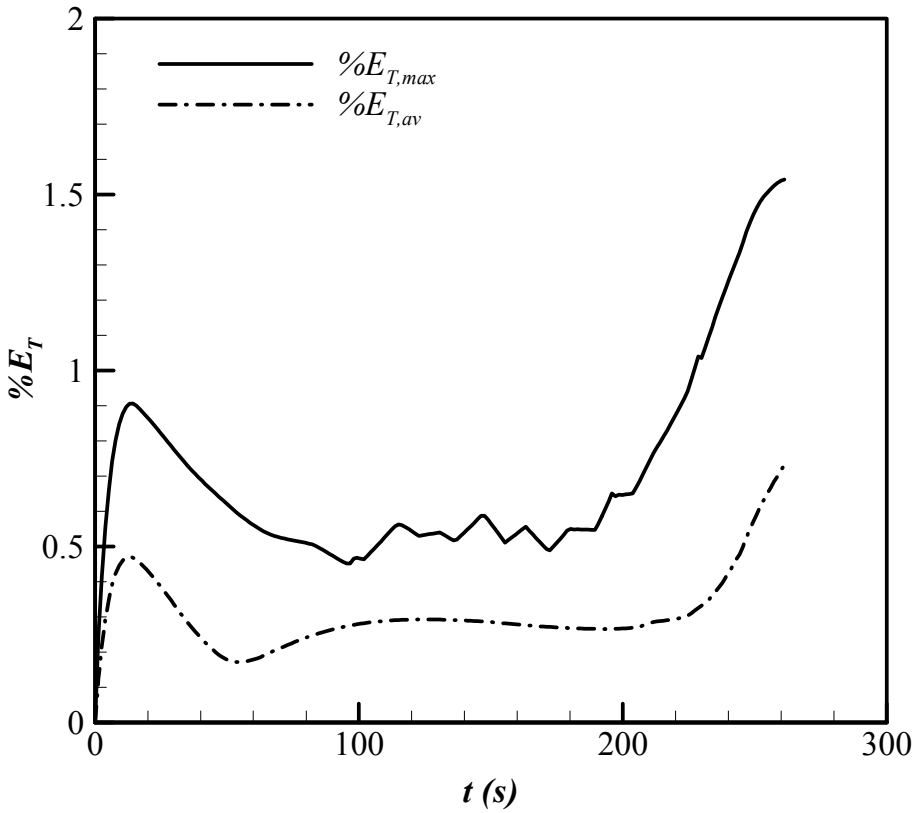

Figure 5.18: The maximum and average of absolute percentage errors based on design surface temperature and design specification

respectively as the design surface moves towards the exit surface. There, the corresponding error values increase sharply towards the end of heating, exceeding 1.5 and 0.6 percent at the end of the process.

From Fig. 5.17, it can be observed that the design surface is over-heated at the two points mentioned above. Examining these two plots, one can note that as the heating rate of the design surface decreases so that it will reach zero at the end, the thermal inertia of the system requires more heat rejection in the system so that the rate of temperature increase could slow down sufficiently. This could not be done because of the thermal inertia of the heaters, and leads to over-heating on the surface resulting in maximum errors reached by system.

The furnace is controlled by the temperature distribution on the heater surfaces. The temperature distributions evaluated by the inverse design approach necessary to attain the conditions displayed in Fig. 5.17 are shown in Figs. 5.19 and 5.20. The temperature variations of six heaters located at (1, 0.0625, 0.0625), (1, 0.0625, 1.1875), (1, 0.0625, 2.4375), (1, 0.4375, 0.0625), (1, 0.4375, 1.1875) and (1, 0.4375, 2.4375) are displayed in Fig. 5.19. These heater elements are the heaters near the edge at the inlet, mid furnace length, the exit and near the mid furnace width at the inlet, mid furnace length and the exit, respectively. The complementary Fig. 5.20 displays the variations of dimensionless temperature of the heaters along the furnace length along y =0.0625 and y =0.4375 at times t =0, 1.31, 130.6 and 262 seconds. From both figures, it can be observed that due to the presence of highly specularly reflecting sidewalls, the temperature distribution on the heater surfaces is nearly independent of the y-direction. As expected, the

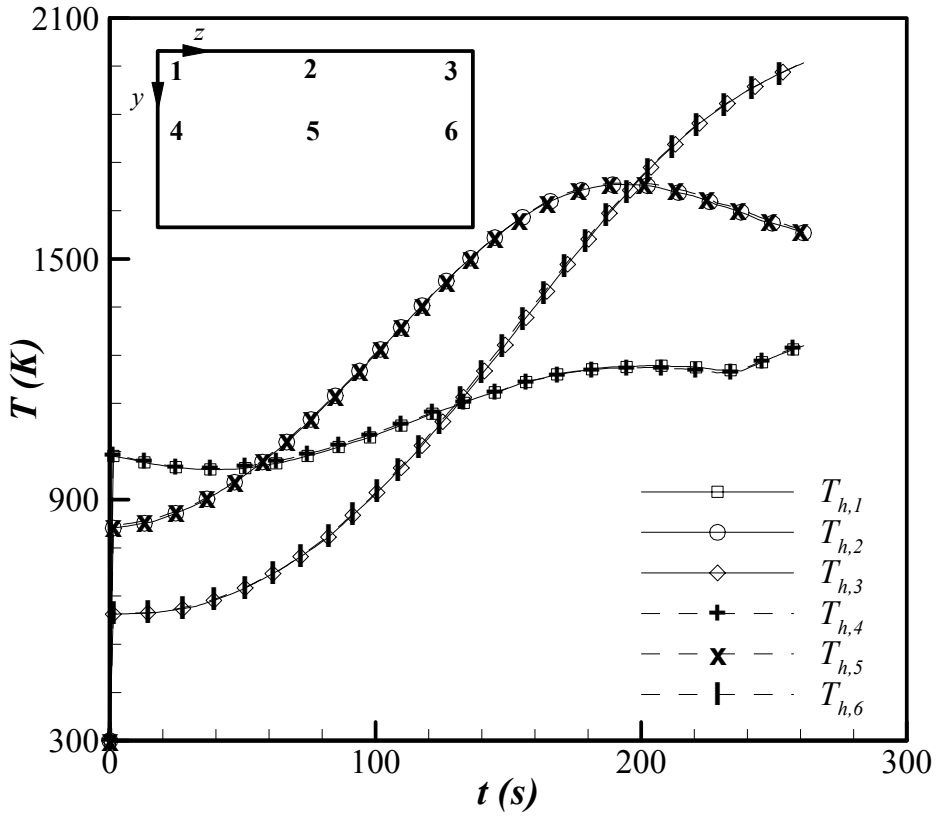

Figure 5.19: The temperatures of six heater elements along the heating process

locus of the maximum temperature changes with the locus of the design surface so that the temperature peaks at the heater elements closest to the design surface at a given time. This trend can also be observed from Fig. 5.19, and it is due to the domination of the system of equations by the greatest exchange factors.

A discontinuity can be observed in the temperature variation near the furnace exit for the two heater elements located close to the inlet of the furnace. This can be explained with the help of Figs. 5.21 and 5.22, which display the

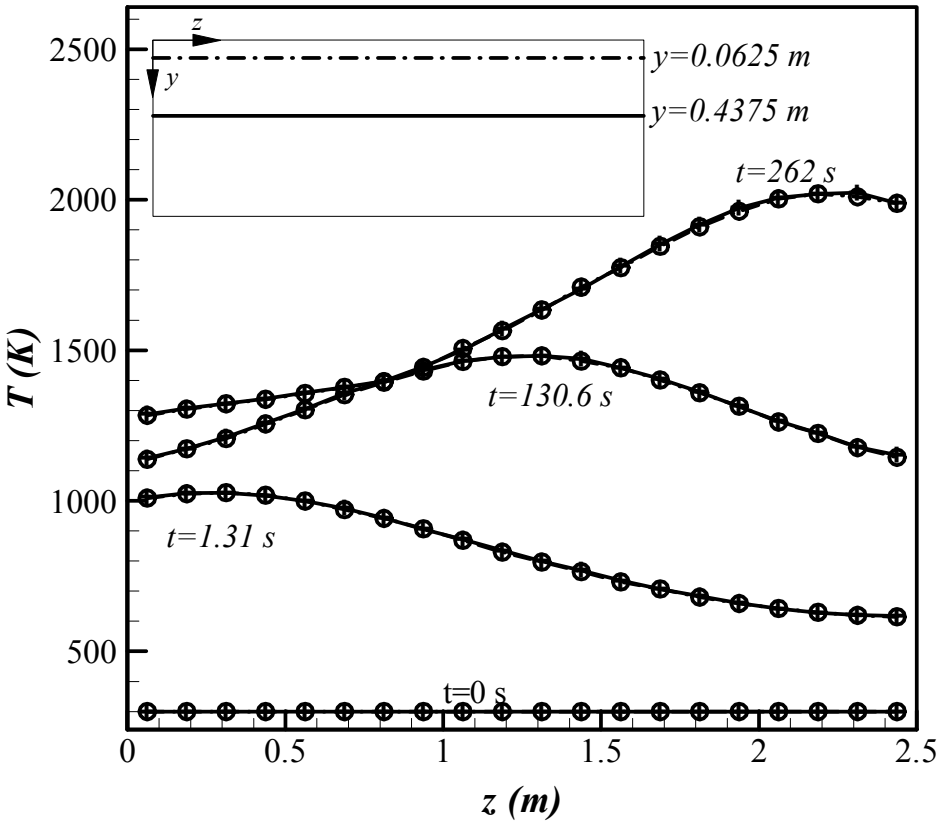

Figure 5.20: The necessary temperatures for heater elements along lines y = 0.0625 and y =0.4375 at three different times

heater energy input required to reach the temperature distributions displayed in Figs. 5.19 and 5.20, for the particular furnace problem.

Figure 5.21 displays the variation of the necessary energy input to the heater elements mentioned above, so that they will be able to follow the variation presented in Fig. 5.19. The variations of required energy input in Fig. 5.22 is

similar to variations in the temperature of the corresponding heater elements displayed in Fig. 5.20.

It can be observed from both figures that the heater strips close to the furnace inlet do not require further heat input to follow the design temperature profile. This result is due to the design constraint set so that the heat input can only be greater than or equal to zero, and heat rejection from the heater elements

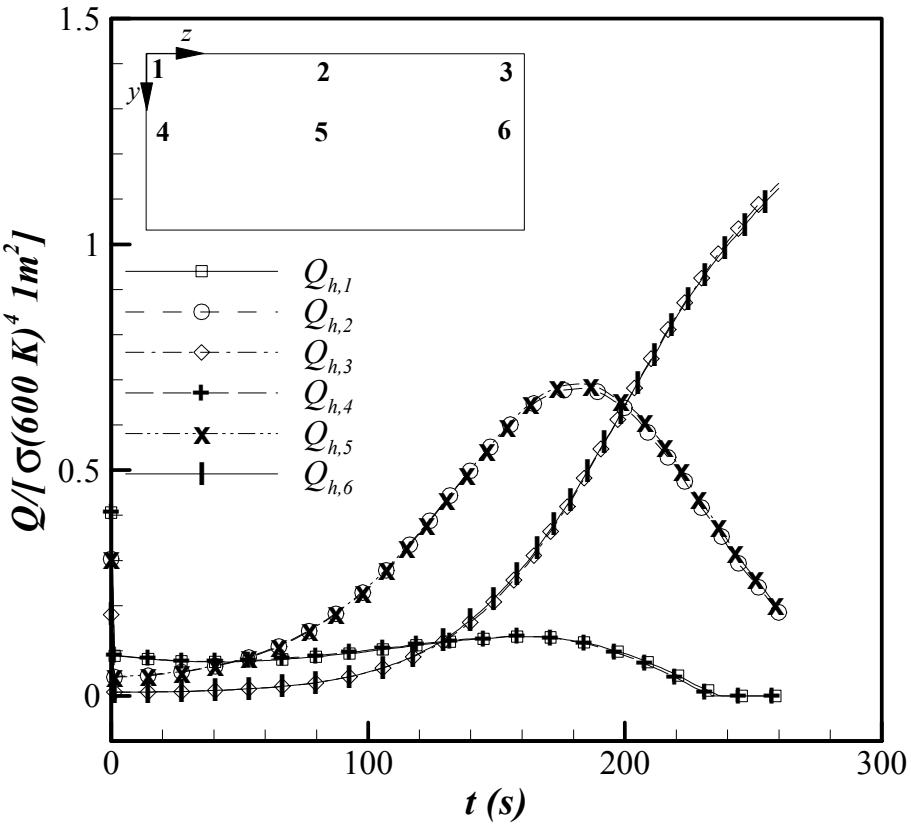

Figure 5.21: The necessary heat input for six heater elements along the heating process

by a cooling device is not allowed. If this constraint, which introduces the discontinuity in the variations along time, were not applied the corresponding heater elements, the cooling trend would be continuous. This is also the reason of the sharp increase in the average and maximum errors displayed in Fig. 5.18 as the design surfaces comes close to the exit surface. In order to attain higher accuracy the designer can consider increasing the convection rate at the inlet

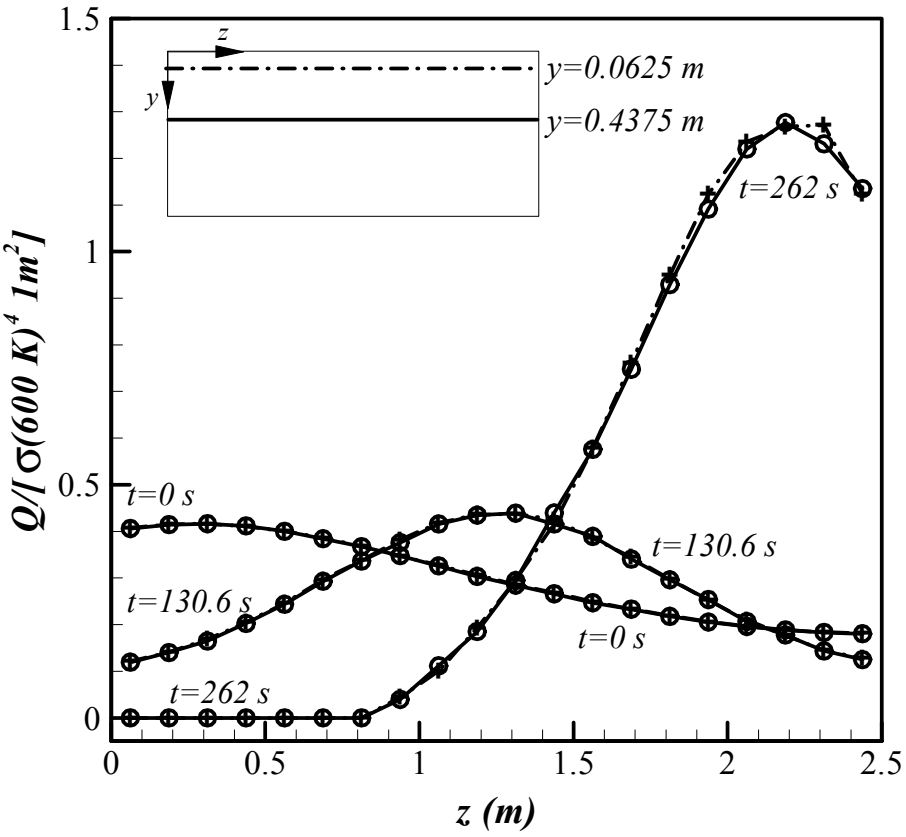

Figure 5.22: The necessary heat input for heater elements along lines y =0.0625 and y =0.4375 at three different times

surface as the design surface moves away to the exit surface so that more heat would be rejected from the heater elements close to the entrance.

The numerical solution was carried out by using a dimensionless time step of 1.31 seconds, with a grid resolution of 8x8x20 along the x, y and z-axes, respectively. The heater temperatures presented are calculated by using CG method using the result of the first CG-step.

From Figs. 5.19 and 5.22 it can be observed that 20 heater strips that have a non-dimensional size of 1x0.125 along the y and z-axes, respectively, located along the furnace length will be adequate to perform the heating.

CHAPTER 6

Control of Transient Thermal Systems

6.1 INTRODUCTION

The boundary condition design of thermal systems using inverse formulation for steady and transient thermal systems was discussed in Chapters 4 and 5, respectively. In both cases, the inverse formulation was coupled with mathematical models of the physical systems to be designed. The systems considered in this study are radiating systems as mentioned earlier. The corresponding models used were presented in the Chapter 2, where it was discussed that they are based on various assumptions and approximations. As a result, the predictions of the models are subject to some deviation from the response of the physical system no matter how many complex phenomena are included in the model. Moreover, the level of accuracy of the radiative property data itself is often questionable, which further increases the uncertainty of the predictions.

In order to be able to use the inverse design approach that is based on the mathematical models of the physical systems considered, some means of correction for the predicted responses should be developed. This can be accomplished through the use of a control algorithm.

Several alternative approaches can be employed to perform this task. One of these can be to develop some means of correcting the model so that the

differences between the model predictions and the system response are reduced. Another alternative can be using a feedback control algorithm that estimates the required input based on the system response.

Of these, the use of the first approach is demonstrated in this study. The control algorithm is implemented through the use of artificial neural networks, which are trained using the predictions of the inverse design and the responses of the physical system. Brief information about artificial neural networks is presented next. That is followed with the description of the control algorithm and the application of it.

6.2 ARTIFICIAL NEURAL NETWORKS

In this research, the goal is not to investigate, improve or develop the state-of-art of artificial neural networks (ANN). The ANN's are just used as a control tool, and this section briefly introduces ANN's without giving details that are available in the literature (Demuth and Beale, 2001; Nelson and Illingworth, 1993).

Artificial neural networks are a relatively new information processing technique that has its basis in simulating living nerve systems. They are basically parallel processing architectures where the knowledge is represented in terms of weights between input and output layers.

A simple neural net structure is represented as in Fig. 6.1, which has N layers, R inputs and P outputs. As indicated in Fig. 6.1, the relation between the inputs **I** and outputs **O** is represented in terms of the biases (**b**) and the transfer functions (f) of the layers and the weights (**W**) between the nodes of the adjacent

layers. The most commonly used transfer functions are the unit step function, pure linear functions and the sigmoid functions; the so-called "logsig" and "tansig" (identical to hyperbolic-tangent) functions. These functions are presented in Fig. 6.2.

The main significance of the ANN's when compared with traditional programming is the ability of learning through the process called training. By training, the ANN is taught to adjust the weights and biases to follow or repeat what it has learned. The weights and biases are modified so that the average squared error between the target outputs and the network outputs is minimized (Fig. 6.3). In order to perform this minimization, optimization methods are used.

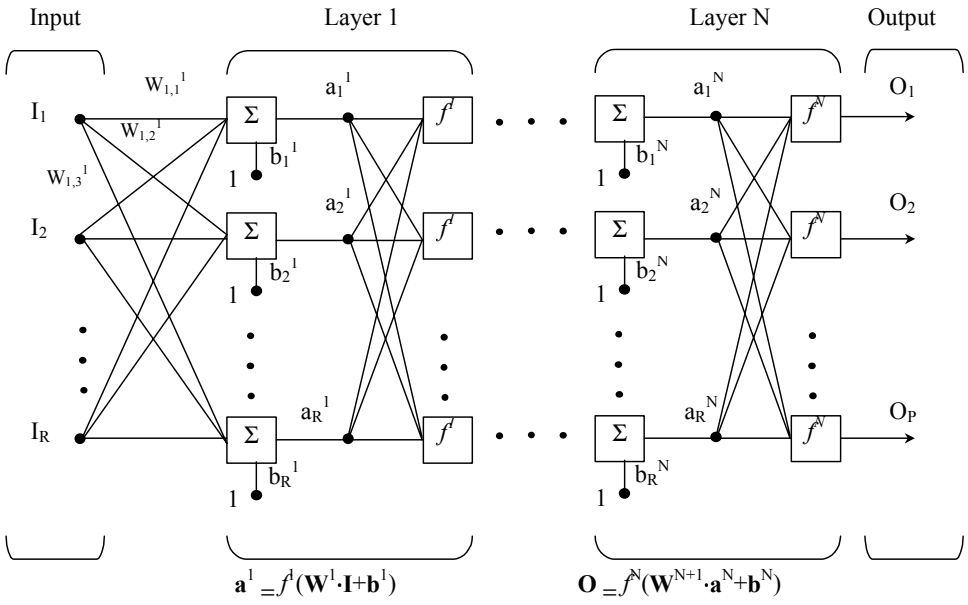

Figure 6.1: An N-layered artificial neural network architecture

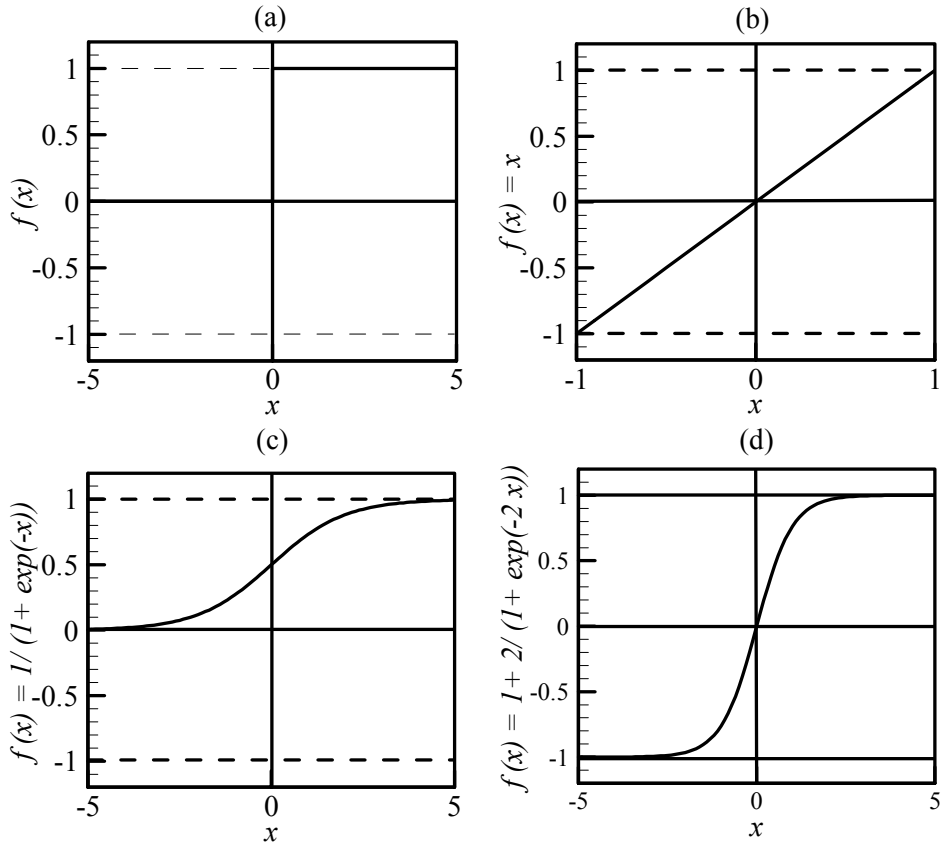

Figure 6.2: The transfer functions: (a) the unit step function, (b) the pure linear, (c) logsig, and (d) tansig

When the ANN faces an input for the first time it simply estimates the output for the input based on the experience it has, or the training. If the input lies within the input data range it has trained with, it is probable that the estimation will be relatively successful. On the other hand, if the ANN extrapolates rather than interpolates, the accuracy and the reliability for inputs are always in question.

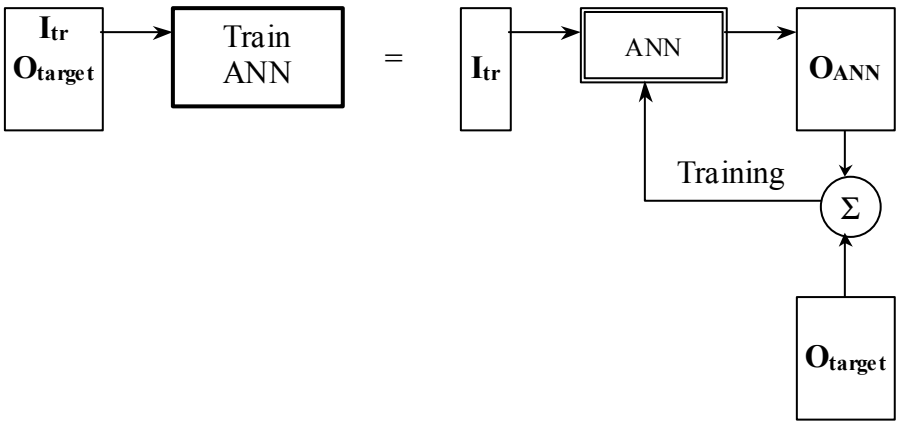

Figure 6.3: Training of ANN

6.3 METHODOLOGY

Control using neural networks or simply neurocontrol has been attracting interest since the late 1980s. Werbos (1992) classifies the basic control algorithms that use ANNs into five categories:

1. Supervised control: ANN's are trained using a database that contains correct data from the physical system.
2. Direct inverse control: ANN's learn the mapping from desired response of the physical system to the control signals that yield these responses
3. Neural adaptive control: ANN's are used instead of linear mappings in the standard adaptive control.

4. The backprobagation of utility: Maximizes some measure of performance over time. They cannot efficiently account for noise and it is difficult to provide real-time learning for large problems.
5. Adaptive critical methods: Methods that approximate optimal control over time in noisy, nonlinear environments.

Anyone of the listed approaches can be used to control a system such as the ones described in the previous chapters. However, as stated earlier the emphasis in this study is on correcting the model using the responses of the physical system. Then the corrected model can be used to predict the required input to achieve the desired response from the system. To accomplish the task, a hybrid of the first two approaches, supervised control that uses the correct data from the physical system and direct inverse control will be used. This is done in three steps:

6.3.1 Step 1: Inverse Design

Inverse design is based on a mathematical model that estimates the required input for the system, so that the desired system response is satisfied. The inverse boundary condition design for a transient system is explained in the previous chapter.

6.3.2 Step 2: Training of ANN

For model based training, the data are generated from inverse design. Due to the approximations inherent to the mathematical model, the uncertainties in the property data used, and the regularization error due to the inverse formulation,

there will be a certain level of discrepancy between the estimations of the numerical model and the actual conditions achieved in the physical system.

Therefore, the training data consists of the estimated inputs and the corresponding physical system response along the process, which is different from the desired response. At the end of the training, the ANN simulates the physical system, as long as an adequate network architecture and training method are used. The accuracy of the simulation with ANN is primarily limited by the interpolation ability of the trained ANN. This depends on the quality of training, which is the ability to recover all the target points for the given input values.

6.3.3 Step 3: Control using the ANN

Once the ANN is trained it could be used to control the system so that the required input could be estimated based on the desired response from the system. A well-trained ANN estimates the input that results in the desired response from the system more accurately than the inverse design based on a mathematical model.

However, the interpolation ability of the trained ANN might not be enough. In such a case, using the estimates of the ANN trained for the input and the corresponding responses from the physical system, the training data can be enlarged. The enlarged data can be used to train another ANN, which models the physical system more accurately when compared with the previous one. This procedure can be repeated until an ANN with required accuracy is accomplished. It should be noted that too many iterations, which leads to training using a very large data set or simply over training, must be avoided. Over training limits the

interpolation ability of the network. The algorithm is illustrated in Fig. 6.4. The addition of the training data simply means enlarging the data set in every iteration rather than vector addition.

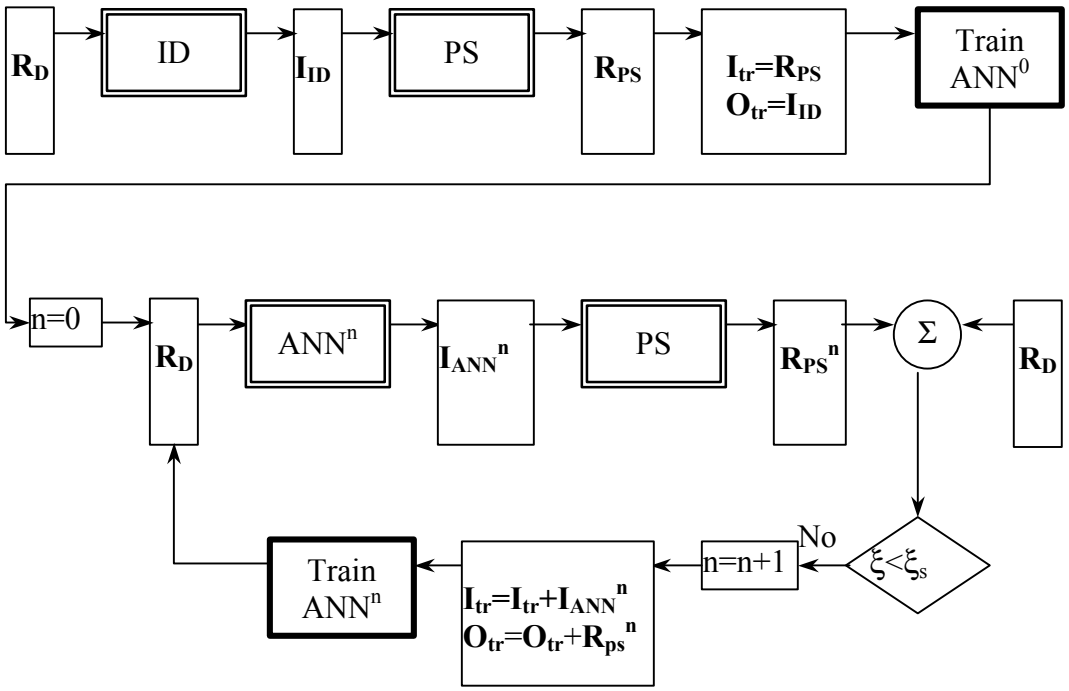

PS : Physical system
ID : Inverse design based on numerical model
$\mathbf{R_D}$: Desired response
$\mathbf{I_{ID}}$: Input based on inverse design
$\mathbf{R_{PS}}$: Response of physical system
$\mathbf{I_{ANN}}^n$: Input based on ANN^n
$\mathbf{I_{tr}}$: Input data for training
$\mathbf{O_{tr}}$: Output targets for training
ξ : Error based on desired response
ξ_s : Acceptable error

Figure 6.4: The control algorithm to correct the model using an ANN.

6.4 APPLICATION OF THE ALGORITHM

It is reasonable to discuss the basis of the discrepancies between the mathematical or the numerical models with the measurements from the physical system before explaining the details about how the algorithm is applied. There are three major sources of discrepancy between a mathematical model and the measurements of physical system. These are:

1. The discrepancies due to approximations or assumptions.
2. The discrepancies due to estimated or approximated property data used in the mathematical model.
3. The uncertainties in the measurement or the measurement error.

As a numerical model replaces an analytical model, additional discrepancies due to numerical discretization emerge. For statistical models, such as the Monte Carlo method explained in Chapter 2, statistical errors are also present.

In the absence of a physical system to implement the algorithm, the application of the algorithm can be demonstrated through numerical experiments. A simplified numerical model is used for the inverse design and a more accurate numerical model simulates the physical system. The deviation between the simple and accurate models is similar to the one between the physical system and a numerical model simulating it.

The control algorithm is applied to the transient heating in a two-dimensional enclosure problem explained in the previous chapter where the solution using inverse design is also presented. The radiation model used for the

solution of the problem was the Monte Carlo method. The method was preferred so that all the radiation property dependence and geometric effects listed in the problem statement can be considered with ease, but it will also be possible to simplify some of them.

In the application, the simple model considers the reflector surfaces to be diffusely reflecting instead of specularly reflecting. That introduces some difference with respect to the complex model representing the physical system. Moreover, the emissivity of the reflector surfaces is 0.075 instead of 0.05, introducing the effect of erroneous property data. Besides, using a statistical numerical model for both the simplified (or erroneous) and the complex model introduces some additional discrepancy due to statistical error, which has an effect similar to the measurement uncertainties.

6.5 RESULTS AND DISCUSSION

The solution of the problem using inverse design methodology is presented in the previous chapter. For both the simple and complex model the Monte Carlo model is used here with a 10x26 resolution. As stated in the previous chapter the solution with this resolution is grid independent. When inverse design is performed with Δt = 0.3762 seconds, the achieved temperature distribution on the design surface is subject to a maximum error of 1.24 percent using the simple numerical model.

When the initial conditions and the power input values estimated by the inverse design using the erroneous simple model are used as inputs to the accurate numerical model representing the physical system, the maximum percentage error

becomes 6.92 percent. The goal of the control system developed is to reduce this to a more reasonable level.

In order to implement the control system, MATLAB® software with the neural net toolbox is used for generating and simulating the ANN's. The training data consist of one set of input and target data for every time step in the inverse design. For $\Delta t = 0.3762$ seconds, there are 159 input and target sets. Each input set consists of emissive power values at a time t gathered at three points (two at the edges and one in the middle) on the design surface of the system with the accurate numerical model together with the achieved emissive power on the design surface for the same points at time $t+\Delta t$. Therefore, the 159 input vectors of 6 elements are matched with the 30 power inputs applied to the system at time t, leading to 159 target vectors of 30 elements.

The algorithm was used iteratively as explained. After the first iteration is performed, the training data were expanded with additional data sets gathered during step 3. Then the combined set can be used for training the neural net and the control can be performed. Each iteration step expands the training data sets by the number of time steps the simulation uses in step 3.

A two-layered ANN is used with the transfer functions for the first and second layers being "tansig" and pure linear, respectively. The first layer has 6 input, 18 output nodes while the second has 18 input and 30 output nodes. The conjugate gradient optimization with Powell-Beale restart is used to minimize the mean square error between the targets and outputs of ANN (Demuth and Beale,

2001). The optimization routine uses 1500 steps to minimize the mean square error between the targets and outputs for all iterations.

Through the use of ANN outlined, the maximum error was reduced to 1.18 percent at the end of six iterations as displayed in Fig. 6.4, where the power input displayed in Fig. 6.5 is required. The conditions displayed in Fig. 6.5 differ from those presented in Fig. 5.9; the sudden demand in power input at the beginning is smoothened out, the locus of the maximum power requirement is now the middle of heater surface 6, and the profile has changed significantly. Moreover, there is no power required for the heater elements close to the edges in Fig. 5.9, whereas this is not the case in Fig. 6.5.

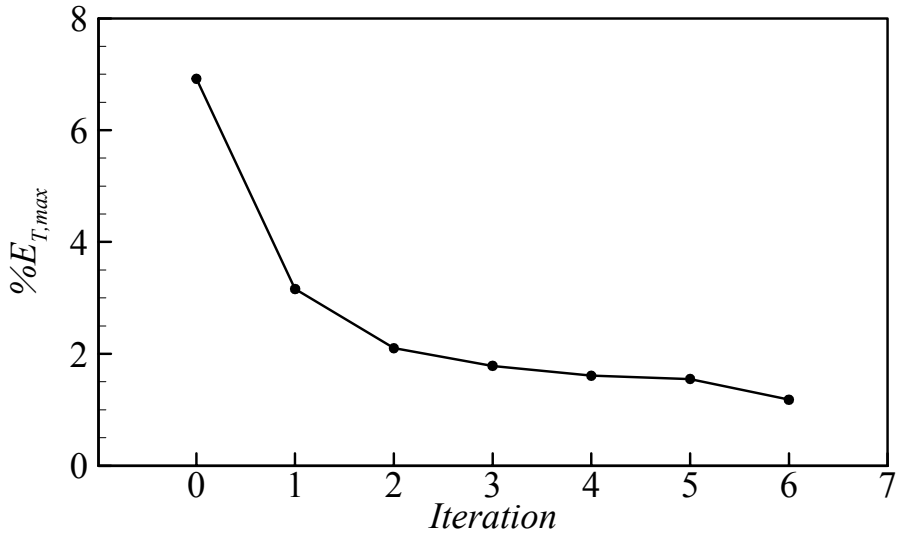

Figure 6.4: The convergence of the trained ANN's in terms of maximum absolute percentage error

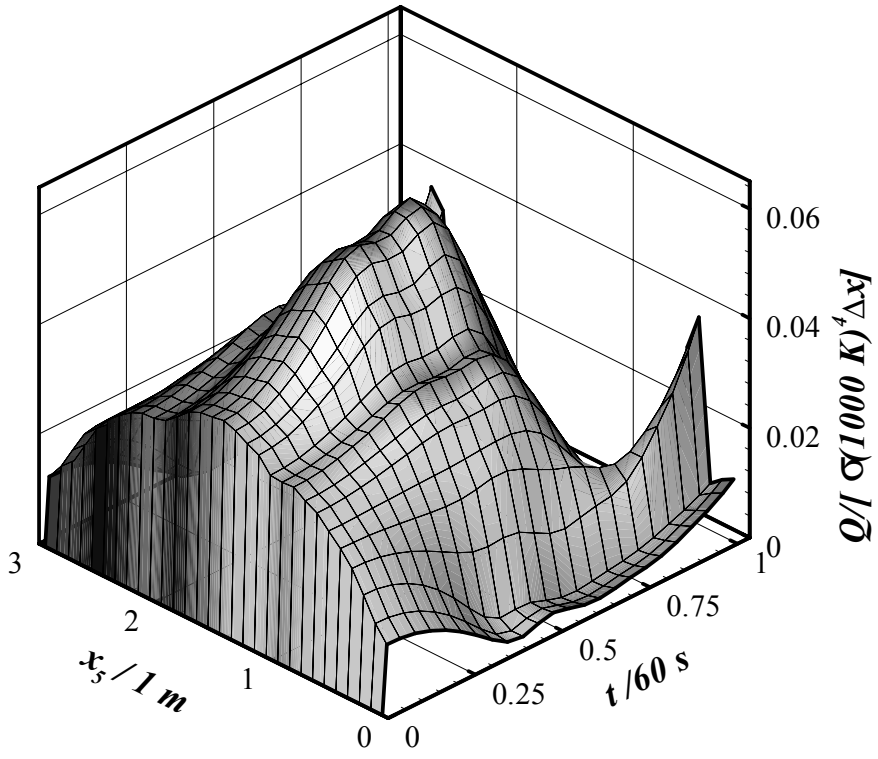

Figure 6.5: Required radiant heater power input

The changes in the power requirement in the heaters affect the resulting system accuracy. As can be observed from Fig. 6.6 the locus of the maximum error has moved to the middle of the design surface from the edges. The maximum error occurs twice at times 10.9 seconds (*t/60 s* = 0.182) at the edge of the design surface and 24.2 seconds (*t/60 s* = 0.403) in the middle of the design surface.

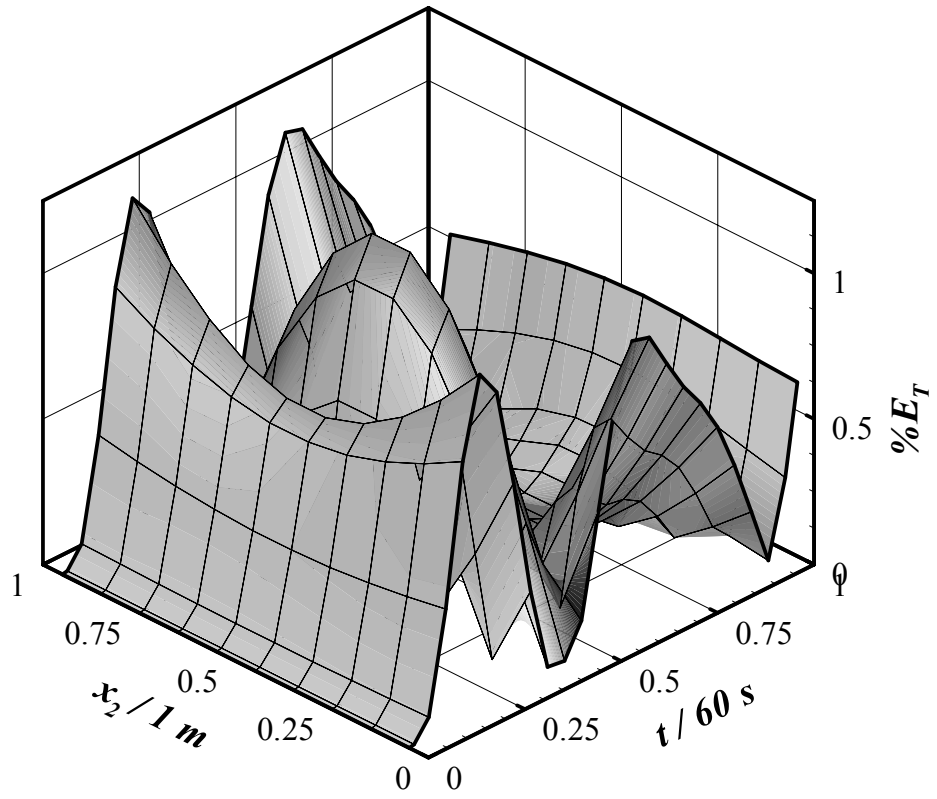

Figure 6.6: Error in temperature on design surface at iteration 6

For the application considered, less accuracy is achieved by the control algorithm than the inverse design based on the complex (more correct) model. However, it should be noted that the control algorithm used a simplified model with erroneous property data, as will be the case in practical problems. For a real system the limitations of accuracy for the control algorithm will be the training of the ANN that represents the ANN's ability to simulate a physical system and the measurement accuracy, which effects the quality of the training data.

CHAPTER 7

Application on a Thermometry Test Bed

7.1 INTRODUCTION

The applications of inverse design have been demonstrated for various boundary condition design problems in the preceding chapters. Some of these problems were steady state problems where maintaining the design surface at a certain thermal condition is of interest (Chapter 4). Others were transient problems, in which the objective was to heat an object uniformly from an initial to a final condition following a specific heating history (Chapters 5 and 6). Although the use of the inverse formulation was successfully demonstrated in the design problems mentioned, none of these problems are based on existing systems. As a result experimental validation was not possible.

In this chapter, the design approaches together with the modeling techniques explained before are applied to an experimental rig to verify the numerical model and inverse design approach. A thermal system that is built as a thermometry test rig and instrumented accordingly is used to achieve this goal. Using the system, an instrumented semiconductor wafer can be heated isothermally and the temperature distribution across the wafer can be measured using a light pipe thermometer.

For production of semiconductor chips with high reliability and quality, uniform deposition of material is required across the whole wafer. As the

deposition is dependent on the thermal conditions, a uniform temperature is desired across the surface of the wafer, as any slight temperature gradient can lead to non-uniformities on the wafer. Therefore, it is of vital importance for the industry to be able to measure the temperature distribution across the wafer accurately. The thermometry test bed was built as a calibration tool to achieve this task.

Although the thermometry test bed has different characteristics than the systems used for rapid thermal processing of semiconductor wafers, it is desired to keep the wafer isothermal in both applications. Thus, the demonstration of the use of inverse design for heating a semiconductor wafer in the thermometry test bed can prove its applicability for rapid thermal processing systems, which have a vital economic importance.

For that reason, the steady boundary condition design problem is solved to predict the required power input for the heaters in order to verify the design methodologies explained in the previous chapters. The next sections present a detailed explanation of the test rig, the solution methodology and the results.

7.2 THE TEST RIG

The experimental apparatus used is an axisymmetric vacuum chamber that is used as a thermometry test bed and developed by The University of Texas, the National Institute of Standards and Technology, the SensArray Corporation and International SEMATECH (Geyling et al., 2000; Ball et al., 2001). The rig has been extensively used in the past and currently for calibration of commercial temperature sensors used in the semiconductor industry.

The chamber consists of an outer and of an inner assembly. Figure 7.1 shows a schematic view of the system. The outer assembly is formed by a

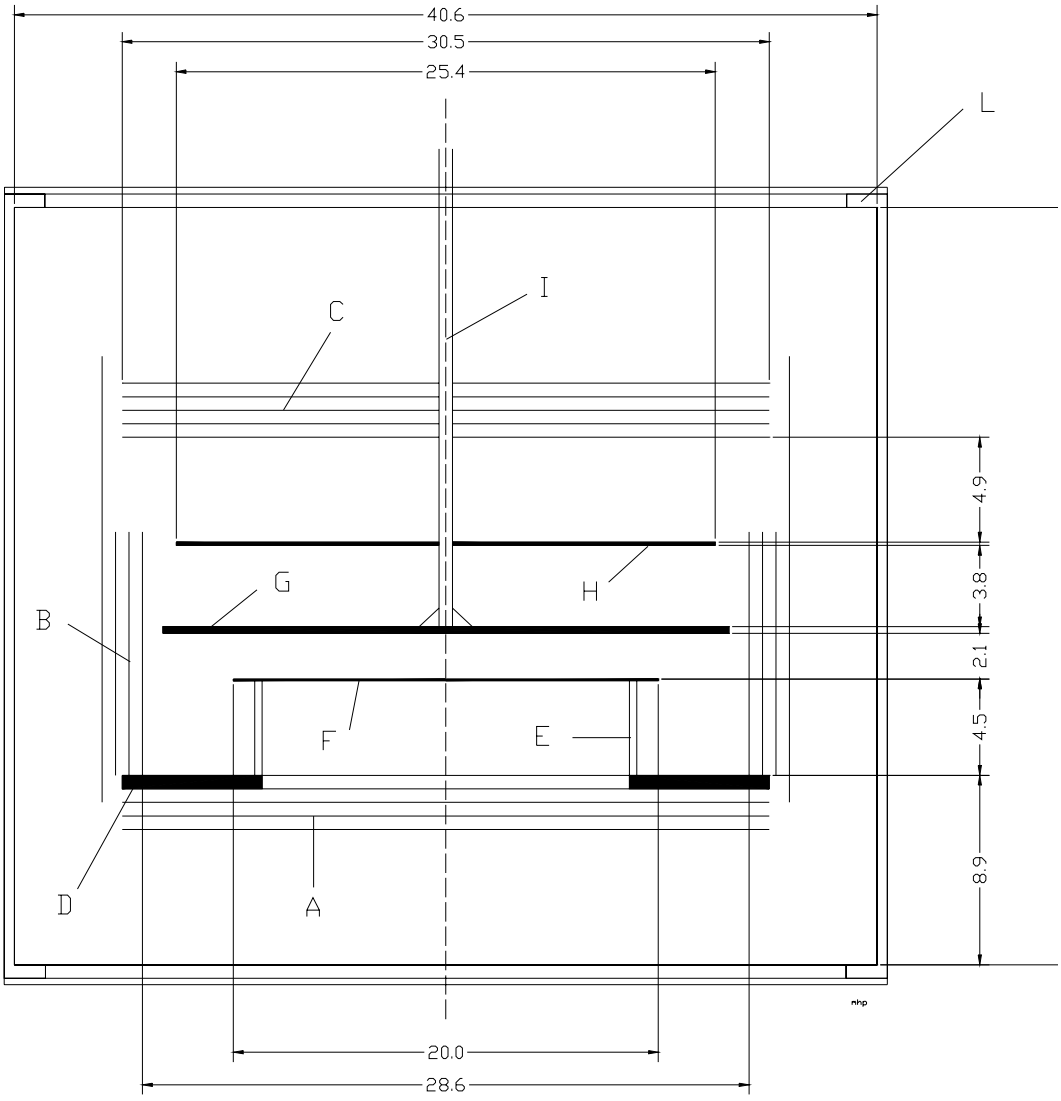

Figure 7.1: Sketch of the assembly. The main components are: A, bottom shields; B, side shields; C, top shields; D, Inconel ring; E, quartz wafer support; F, silicon wafer; G, zirconia diffuser; H, heater; I, rotating shaft; L, outer vacuum chamber.

cylindrical stainless steel vacuum chamber 35.6 cm tall and 40.6 cm in diameter closed at the ends with two main flanges. The sealing between the cylinder and the main flanges is provided by O-rings. A mechanical (roughing) pump and a diffusion pump are connected to the vacuum chamber to ensure a vacuum level greater that 10^{-5} Torr. The walls of the vacuum chamber are water-cooled to keep them at or below room temperature to avoid overheating of the elements that are fed through the sub-flanges and through the sealing O-rings.

The inner assembly is formed by a ceramic heater (H in Fig. 7.1), a zirconia diffuser (G), a silicon wafer (F) and a quartz wafer support (E). To minimize heat loss from the inner assembly and to thermally protect the vacuum chamber walls and fittings, the inner assembly is shielded all around with a series of molybdenum radiation shields (A, B and C). The side shields and the quartz wafer support are supported by an Inconel circular ring (D) elevated in the center of the vacuum chamber by three legs.

The heater is a Boralectric™ ceramic heater with three independently powered concentric zones controlled by a microprocessor-based power controller that provides voltage regulation and repeatability (Ball et al., 2001). Three pins connected to the top main flange support the heater. Although the heater has three heating zones, only the inner and outer ones are usually used, since it has been observed that a better radial temperature distribution can be imposed with this setting (Geyling et al., 2000; Ball et al., 2001).

The wafer used for this experiment is a 200 mm silicon wafer provided by NIST. It is supported by a cylindrical quartz support of about 17.3 cm in diameter and 4.4 cm in height that is seated on the top of the Inconel ring.

The test rig was designed to create a system that can be used to determine a reference procedure to calibrate commercial temperature sensors for the semiconductor industry. Therefore, it was crucial to develop a system that could impose a uniform temperature field on the wafer. In order to ensure a uniform temperature field across the wafer, a conductive circular diffuser plate has been placed between the heater and the wafer so that it would absorb and re-radiate energy. The diffuser plate should have high thermal resistance in the radial direction so that the radial distribution provided by the heater to ensure wafer temperature uniformity can be maintained through the diffuser. Moreover, the thermal resistance in the axial and azimuthal directions should be relatively lower so that the diffuser will be efficient and axisymmetry over the wafer temperature distribution is satisfied, respectively. These conditions are achieved using a thin diffuser disc of high thermal resistance material that rotates to ensure axisymmetry. Therefore, a 3.2 mm thick zirconia disc supported by a rotating shaft fed through the top main flange is used.

The radiation shields surround the parts listed above to reduce the radiative heat losses from the hot components of the inner assembly to the cold outer assembly. They play an important role in the experimental setup since they govern the energy loss and the heat exchange in the system. The radiation shields are composed of a set of multiple layers of 0.13 mm thick pure molybdenum foil.

Molybdenum was chosen because of its high reflectivity and its ability to stand high temperature. The heater-diffuser-wafer-quartz wafer support assembly is surrounded on the side by four concentric cylindrical shields (referred as the side shields) spaced 6.5 mm apart and the first layer having a diameter of about 28.5 cm and a height of about 11.7 cm. The side shields seat on the Inconel ring. The top and the bottom are shielded respectively by five and three circular shields spaced 6.5 mm apart (referred as top and bottom shields, respectively). With this configuration the actual inner chamber where the important radiative energy exchange occurs is limited by a cylindrical volume 28.6 cm in diameter and 24.2 cm in height where the heater, diffuser and wafer are placed.

7.3 FORMULATION

The design problem considered is calculating the required steady state power input distribution to the heaters so that the silicon wafer is kept at a specified uniform temperature. The solution of the steady thermal energy equation for the system is required and the following assumptions are considered for the solution.

As the chamber is evacuated to a pressure of 10^{-5} Torr, convective effects can be neglected. For a design problem that considers keeping the wafer surface at an isothermal temperature of 600 °C the characteristic temperature will be 873 K. Based on this characteristic temperature, the Inconel ring has the greatest conduction radiation parameter, $N_{cr}=k\delta/\sigma T_o^3 R_o^2$, that has a value of 0.09 while the value is 0.02 for the shields. The conduction radiation parameter for the zirconia diffuser is 0.009. As the wafer will be isothermal, it is already known

that there is no conduction on it. The presented values are for a characteristic length of the radius of the corresponding elements and they confirm that the diffusive effects are secondary.

The problem is a steady boundary condition estimation problem in a radiating enclosure. Therefore, the solution procedure presented in Chapter 4 may be applied. Once the radiative properties and the geometry of the system is known, the exchange factors must be calculated as the first step of the solution.

The design surface is the silicon wafer. Therefore, the governing equations for the silicon wafer are Eq. (4.5), which is the discretized energy equation written for an element where two boundary conditions are specified (temperature and heat flux). When the system reaches steady state the wafer must be adiabatic so that its temperature does not change. Here, the adiabatic term is used to explain that the net heat flux at top and bottom (or back and front) of the surface is zero. Consequently, adiabatic surface condition as explained constitutes the complementary boundary condition to the specified temperature. Similarly all the other components other than the outer chamber must balance the energy transfer on each side for the same reason. The outer chamber, which is water-cooled, is kept at a constant temperature. The energy equation for the outer chamber is Eq. (4.3-a), whereas the energy equation for all the elements other than the outer chamber, wafer and heaters is Eq. (4.3-b). Finally, additional equations must be added to the system so that the constant heat flux across each heater element can be achieved. For the system under consideration all the

convective and conductive terms are neglected and the equations are linear at every point.

7.4 SYSTEM CHARACTERIZATION AND INSTRUMENTATION

As the problem is considered as a pure radiation problem, the radiation model used and the corresponding radiative properties become crucial in the accuracy of the numerical model. For this reason, accurate radiative properties of the most important elements of the inner chamber assembly are determined experimentally.

Extensive details about the system characterization and instrumentation of the system are presented by Gamba (2002). However, a brief summary is presented here for completeness of the discussion.

7.4.1 System Characterization

The molybdenum shields and the silicon wafer have been considered as the most important elements of the system, since the shields govern the heat losses and the wafer is the design surface. The main function of the shields is to contain the radiative energy within a prescribed volume. In order to accomplish this goal, highly reflective surfaces are used. The type of reflection (i.e. diffuse or specular) must also be investigated as it influences the rate and distribution of heat transfer. The other surface elements are assumed to have less significance, and standard emissivity values reported in the literature such as Touloukian and DeWitt (1970) are used for them.

The experimental data available in the literature is limited for molybdenum. Moreover, it is observed that the molybdenum surfaces darken

when exposed to high temperatures. Therefore, it is also necessary to account for the possible changes in radiative properties as they are exposed to high temperatures in the system considered. For these reasons, an experimental determination of the reflectivity components (diffuse and specular ratios) at room temperature has been performed. The reflectivity of a standard silicon wafer was also measured.

The reflectivities are measured at room temperature in the range 0.5-5 μm using an Optronic Lab's Model 746 Infrared Radiospectrometer system. The apparatus is equipped with a Model 735IR monochromator, a Model 740-70 Integrating Sphere (with a $BaSO_4$ coating) for low wavelengths, a Model 740-70G Integrating Sphere (with gold coating) for the middle IR range, light sources (quartz-halogen lamp and IR glower) and different types of detectors (Si detector for visible range, PbS detector for near IR range and PbSe for middle IR range). This apparatus is able to measure reflectivity and transmissivity. Focusing on reflectivity, the integrating sphere allows separation of the specular component of the reflected light, thus measurements of the hemispherical and of the diffuse reflectivity are possible. The specular component can then be calculated from these two. For the particular system, the incident angle and thus the measured specular component are at 11° from the normal to the surface. As there is no other data is available, it is assumed that the specular component is independent of incident angle.

From the measured spectral data, total reflectivities are calculated by integrating over the spectrum for an approximate steady state temperature of the

heat source. For the temperature values under consideration (about 600°C) and for the spectral range where direct measurements have been possible, less than 55% of the black body energy distribution is considered. Therefore, the investigated spectral range is relatively narrow, and as a result the measured properties are only approximate. However, due to the lack of additional data, the approximate data is used for the numerical model.

Figure 7.2 displays the components of the spectral reflectivity for commercially pure, cleaned, non-oxidized molybdenum. The same data is presented for the innermost molybdenum shield, which is darker as it is exposed to high temperatures, is presented in Fig. 7.3. The reflectivity of the innermost shield is decreased especially in the regions close to the heaters. From Figs. 7.2 and 7.3, it can be observed that the trends are quite different, especially at short wavelengths. In the visible range of spectrum, the reflectivity is very low, in particular the specular component. At higher wavelengths, the reflectivity of the actual molybdenum tends to the value for the cleaned surface, although the values of the cleaned surface are never reached. Therefore, it can be concluded that due to the degradation of the surface for the innermost shields, the surfaces are more diffuse and less specular when compared with the cleaned one.

For clean molybdenum the total reflectivity at room temperature was calculated to be 0.9 ± 10% with a specular component of 0.62 ± 20%; for the oxidized molybdenum, the reflectivity is 0.73 ± 10% with a specular component of 0.37 ± 20%. The temperature dependence has been calculated from electromagnetic theory (Siegel and Howell, 2002) and the results have been

successfully compared with data tabulated in Touloukian and DeWitt (1970). Then the emissivities for the clean and oxidized molybdenum are calculated as 0.15 and 0.31 at 600 °C, respectively. The corresponding values are 0.17 and 0.37 for 800 °C.

Similar property characterization is performed for the silicon wafer. As the actual wafer could not be used to determine the spectral reflectivity profile, a

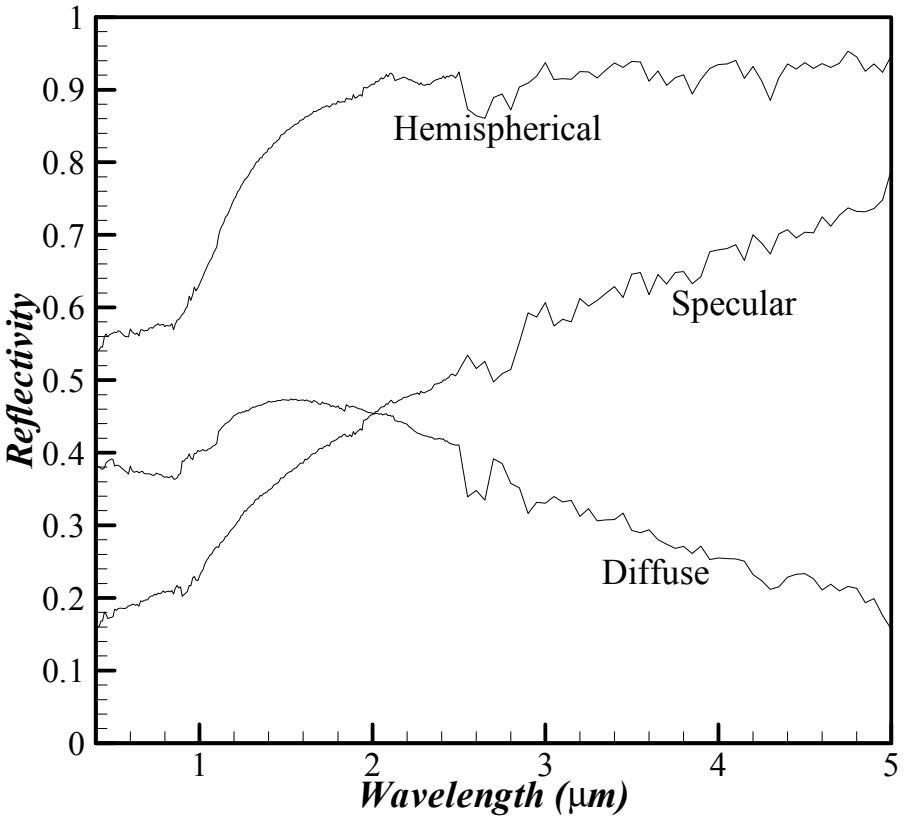

Figure 7.2: Spectral reflectivity for pure, cleaned molybdenum in the range 0.5-5 μm at room temperature

comparable sample of silicon wafer has been used. As before, three components of reflectivity (total, diffuse and specular) have been investigated on the range2-5μm at room temperature. When the transmissivity of the silicon in the room temperature is considered, it is required to use a holder capable of absorbing all the transmitted radiation (more than 99.5%) on the back of the sample.

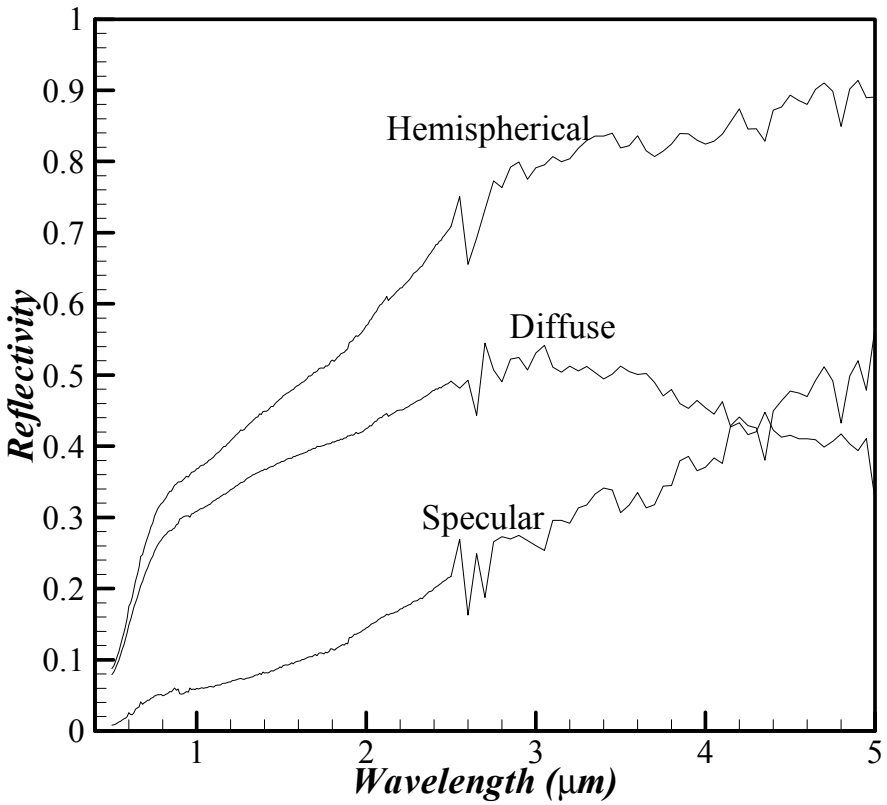

Figure 7.3: Spectral reflectivity for innermost molybdenum radiation shield in the range 0.5-5 μm at room temperature

For the silicon wafer, the total reflectivity is measured as 0.3 ±10%, and the specular component is 0.67 (±20%). This is in agreement with the emissivity of 0.68 presented in the literature (Sun et al, 1997).

The data presented in the literature (Touloukian and DeWitt, 1970) is used for the radiative properties of the other components of the system. The emissivity of the diffusely reflecting ceramic heater surface is 0.32 while it is 0.6 for the diffusely reflecting zirconia diffuser plate. The Inconel plate also reflects diffusely and has an emissivity of 0.7.

7.4.2 Instrumentation

The shields are instrumented with type K thermocouples so that the temperature on the boundaries of the inner chamber can be measured. Six thermocouples that are referred as Array A from here on are placed along the radius on the innermost shield of the bottom shields. Another array (Array B) is placed on the innermost side shield. A third array (Array C) is placed on the innermost of the top shields along the radius similar to Array A. Table 7.1 summarizes the exact position of each thermocouple.

The thermocouples used for the instrumentation of the shields are made of 24-gauge type K thermocouple wire (standard grade) insulated with Silfa Silica. This thermocouple wire is rated up to 870°C with an error of ±2.2°C or 0.75%, whichever is greater. The thermocouples have been organized in arrays in such a way that they fit between the shield layers and the thermocouple's junction contacts the innermost shield.

The wafer used for this experiment is instrumented with four Pt/Pd thin film thermocouples and with eight Pt/Rh differential thin film thermocouples embedded on the upper surface. The four Pt/Pd thermocouples are placed on the edge of the wafer and act as the reference for the differential thermocouples that are distributed on the wafer surface. The locations of the twelve thermocouples are presented in Fig. 7.4.

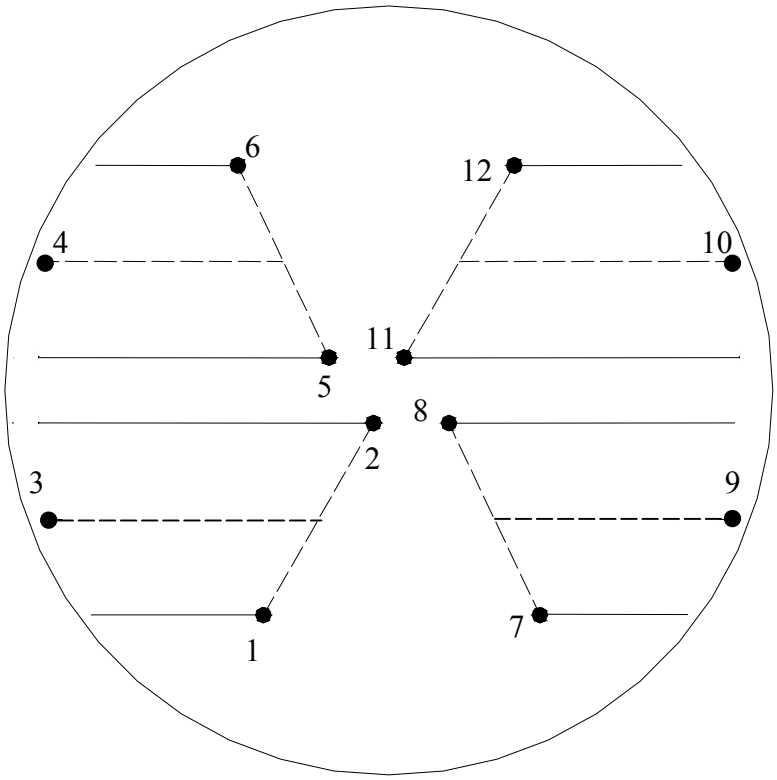

Figure 7.4: Positions of the thermocouples on the silicon wafer

Table 7.1: Summary of the locations of the thermocouples on the shields. The estimated uncertainty in the position of the thermocouples is about ±0.5 cm.

TC	Arrays A, C* (cm)	Array B** (cm)
1	0.6	1
2	1.9	2.2
3	4.4	4.1
4	7.0	6.0
5	9.5	-
6	12.4	-

* Distance from the centerline of the bottom shield
** Distance from the bottom edge of the innermost side shield.

7.5 RESULTS AND DISCUSSION

The main goal behind solving this particular design problem is to validate inverse design using an instrumented physical system. In order to be able to accomplish this goal, the numerical model must be validated first. Once the numerical model is validated, then the inverse design can be validated with confidence. The validation is carried out in two steps. First, the required heater inputs to achieve a particular uniform temperature distribution across the wafer are calculated using inverse formulation. Then using the estimated heater settings in the experimental rig, the resulting wafer temperature distribution is measured and compared with the desired temperature.

As before, the MCM is used to model the radiative transfer and in Chapter 2 verification of the MCM used in this study is presented using some benchmark solutions in the literature. It is also stated in Chapter 2 that further verifications

are available in Ertürk (1997) and Ertürk et al. (1997). However, neither in Chapter 2, nor in the references listed in Chapter 2, is validation using experimental data presented. Therefore, the developed numerical model that uses the MCM must be validated using the measurements gathered from the instrumented system. A forward problem must be solved to validate the model as it is known that forward problems are stable and well-conditioned.

7.4.1 Validation of the Numerical Model

In order to gather data for the validation of the model, a test run was performed. The inner and outer heaters were set to a power input of 354.6 W ±??% and 1187.7 W ±??%, respectively. Meanwhile, the chamber was evacuated to 10^{-4} Torr and the vacuum chamber's outer wall was cooled to about 285 K. For these settings, the temperature fields on the shields and on the wafer were recorded. The wafer was heated to an average temperature of 1054.9 K with a maximum temperature of 1064 K and a minimum temperature of 1040.8 K. For the particular test run, the diffuser plate was not rotated and consequently there exists some asymmetry in the resulting temperature distribution across the wafer.

Then the forward problem was solved using specified heater settings and the outer chamber wall temperature. All the other components of the system were considered as adiabatic as the experimental data regarding to the specified settings are gathered at steady state. Once the forward problem is solved, the temperature distributions calculated across the shields can be compared with the measured distributions.

As before, the first step of the solution is to calculate the exchange factors for the system. For the solution, the exchange factors are calculated with the MCM using one billion samples over a 24x4x12 grid along radial, polar and axial directions. The solution with this resolution is compared with the solution calculated using 48x8x24 grid and it is observed that this grid resolution yields grid independent solutions. Once the exchange factors are calculated, the forward problem can be solved.

The predictions of the forward solution for the temperature distributions are then compared with the measured values. The average of the calculated temperature across the wafer is 47.5 K larger than the average of the measured temperature, corresponding to 4.5 percent difference in absolute temperature.

It is known that the system loses heat through the bolts, supports and the junctions holding it together and the heat transfer through these parts is not accounted for in the solution. The heat transferred through these parts must be included in the analysis in order to achieve better agreement. This can be carried out by modifying the heater inputs, subtracting the heat lost through the junctions from the values applied for the physical system. As the temperature distributions for most parts are not known, an iterative solution is required. At each iteration, the heat lost through these elements must be calculated, the lost energy must be distributed to the heaters and the inputs for the heaters must be re-arranged accordingly. When the solution converges, the power input for the heater in the numerical model and the total heat lost through the bolts, supports and junctions must sum up to the applied power in the physical system.

The heat lost through these elements can be approximated by one-dimensional diffusive heat transfer expressed as

$$q_{loss} = \frac{T_{heater} - T_{out}}{R_{tot}} \tag{7.1}$$

where the total thermal resistance is $R_{tot} = \sum_{i=1}^{N_{rod}} \frac{A_i k_i}{L_i}$.

When the system is analyzed carefully, the connections where the heat is lost can be listed as follows:

1. The driving shaft that holds the diffuser plate
2. The rods supporting the Inconel ring
3. Three rods holding the heater (attached to the outer heater)
4. Leads that hold the power connections

The first three of these parts are illustrated in Fig. 7.5, and their thermal resistances can be calculated accordingly. There are a total of six, two of three different lengths of copper leads (210, 103 and 190 mm) that have identical rectangular cross-section of 0.5 mm x 10 mm.

For the given configuration, the total heat lost through these elements is 151.1 watts. This means that in order to achieve equivalent conditions using an idealized numerical model for radiation, where no heat is lost, this amount must be subtracted from the total power input. The heat lost can be distributed to the heaters as follows: The heat lost through a joint or a connecting rod attached to a heater is considered as the heat lost from that particular heater. However, the system loses heat from other parts as well. These losses are distributed to the heaters according to the power input ratio.

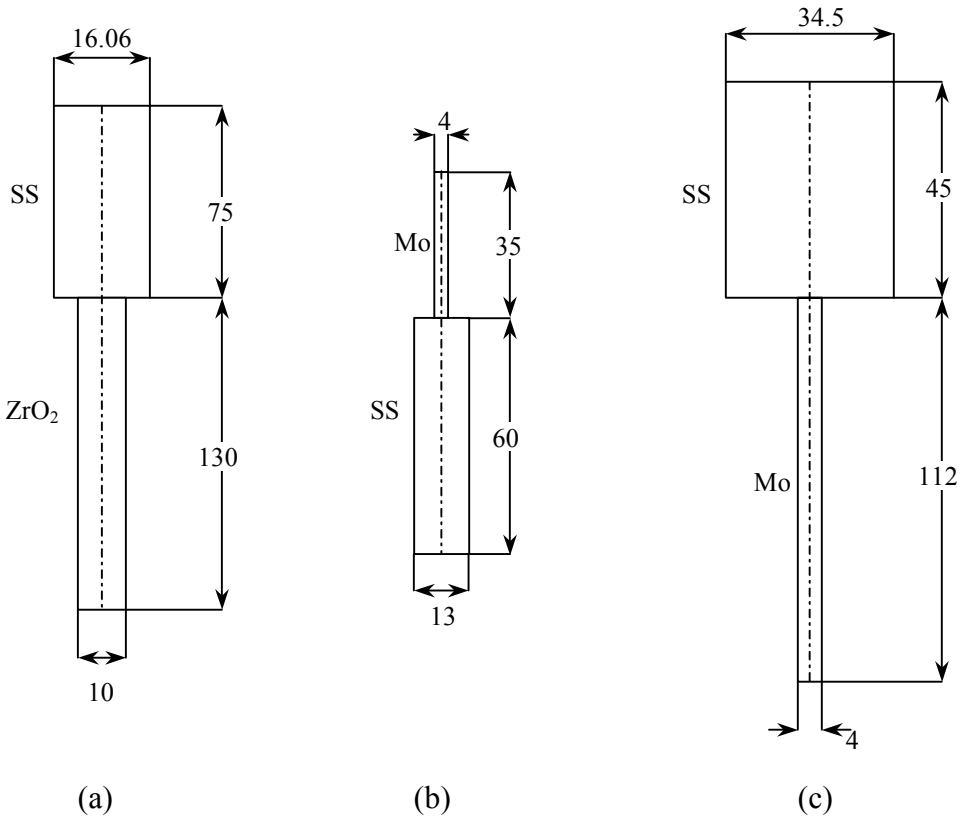

Figure 7.5: The connections, where the heat loss occurs. (a) Driving shaft, (b) Molybdenum rods supporting Inconel ring, (c) Molybdenum rod holding the heater. (SS: Stainless steel, Mo: Molybdenum and ZrO_2: Zirconia; all dimensions are in mm)

For the applied heater arrangement, the equivalent power inputs for the numerical model can be calculated as 320.6 and 1070.6 watts following the outlined procedure. The calculated wafer average temperature is 19.6 K larger than the average temperature of the wafer, which corresponds to 1.9 percent difference.

The temperature distributions along the top and bottom shields are presented in Fig. 7.6. For the top shield, the calculated distribution that considers the losses agrees with the measured values having a maximum and average discrepancy of 22 and 14.8 K, respectively. This corresponds to an error of 2.2

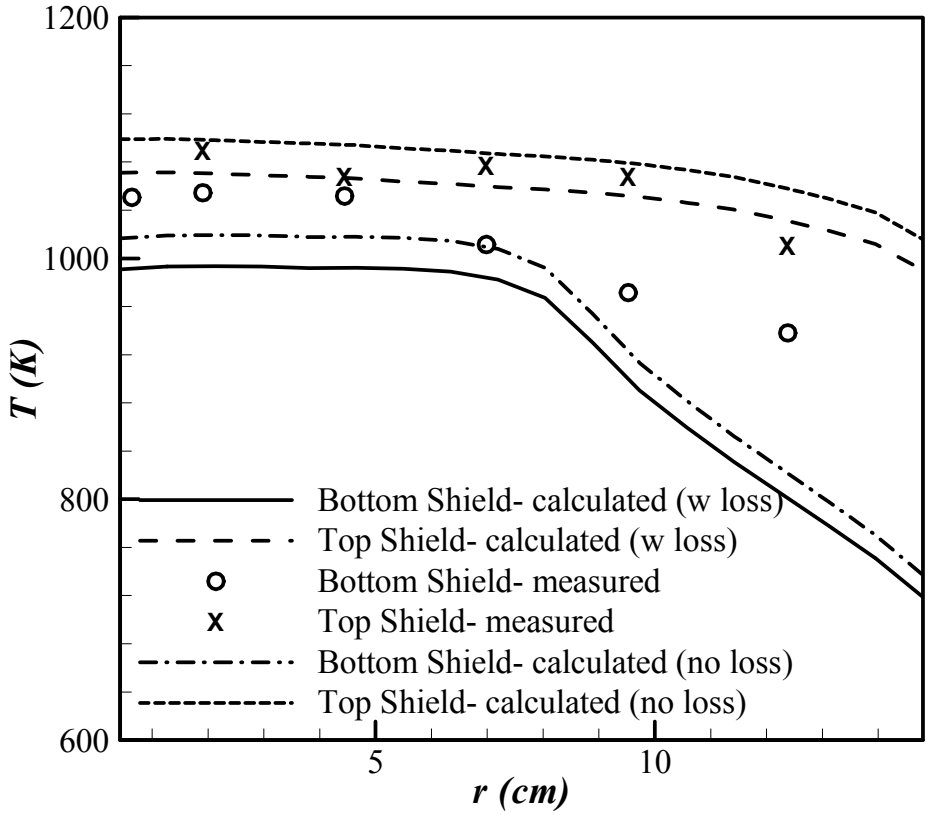

Figure 7.6: Comparison of the predictions of the two forward solutions, one considering heat losses (w loss) and one without considering heat losses (no loss), and the measured values at the top and bottom shields for the case with inner and outer heater powers of 354.6 and 1187.7 W.

and 1.4 percent. The thermocouples are not attached to the shield surfaces by any means such as soldering. Therefore, some of the thermocouples might not have enough contact with the shield surfaces leading to a slight fluctuating trend observed in the measured values.

For the bottom shield there is a significant discrepancy especially for the part of the shield facing the Inconel ring. It must be underlined that the Inconel ring is the item with the most thickness; therefore it is the part with the most thermal inertia in the system. Although, there is no experimental data to validate the conjecture, it appears that neglecting the diffusive heat transfer along the Inconel plate results in some error, and the temperature distribution along the part of the bottom shield facing the Inconel is affected by this poor approximation. For the part of the shield facing the Inconel, the maximum and average temperature differences between the measured and calculated values (considering heat losses) are 140 and 105 K, respectively. The corresponding errors are 14.9 and 11 percent. For the inner part of the shield, the maximum and average differences are 60 and 52 K, and the corresponding maximum and average errors are 5.7 and 5 percent.

Figure 4.7 is the similar plot for the side shields. The maximum and average discrepancy in the side shield is 8 and 2.8 K for the solution that considers the heat losses. These values correspond to maximum and average errors of 0.8 and 0.3 percent.

Although there is significant discrepancy between the measured and calculated bottom shield temperature the agreement in the other shields and the

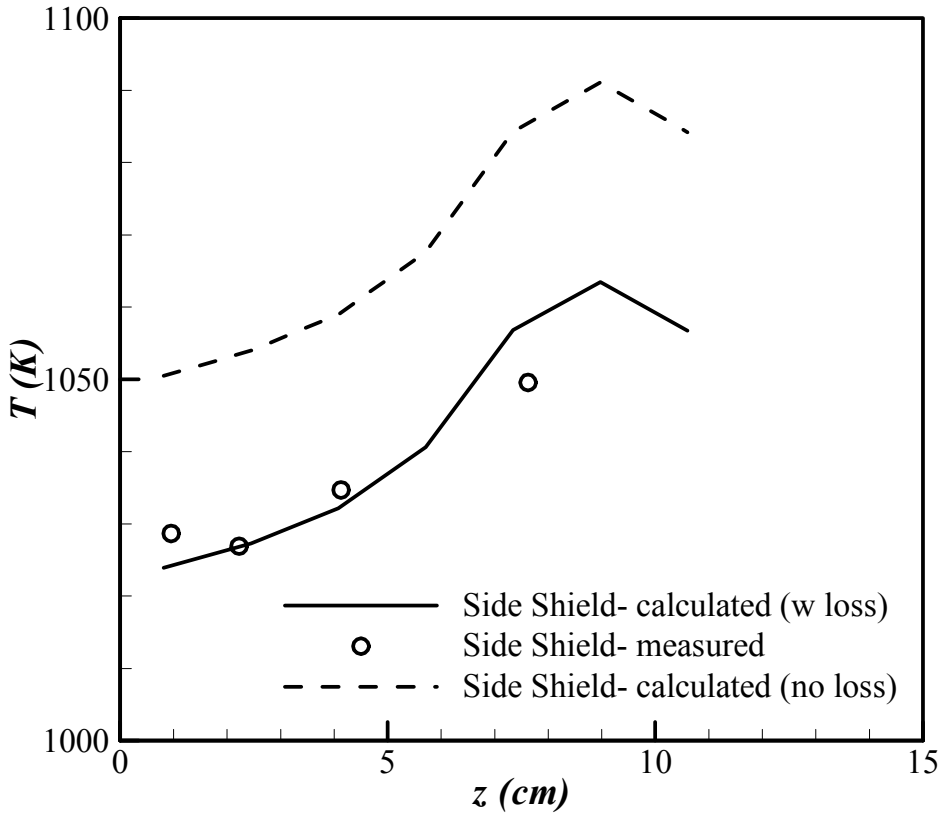

Figure 7.7: Comparison of the predictions of the two forward solutions, one considering heat losses (w loss) and one without considering heat losses (no loss), and the measured values at the side shield for the case with inner and outer heater powers of 354.6 and 1187.7 W.

most important part of the system, the silicon wafer, is acceptable. Therefore, the results validate the model and it can be used as a tool for design of such a system.

7.4.2 Validation of the Inverse Design

Once the numerical model used is validated, the heater powers can be estimated using the inverse design approach and the estimated powers can be

applied to the test rig. Then, the accuracy of the inverse design together with the numerical model used can be demonstrated by comparing the measured wafer temperature distribution with the distribution the heater powers are designed for. Moreover, temperature distributions along the shields are also measured. In addition to the comparison based on desired and achieved wafer temperature distributions, the estimated and measured shield temperatures can also be compared.

As in the previous case, a 24x4x12 grid is used along the r, θ and z coordinates and the MCM is applied using one billion photon samples. The design goal is to keep the wafer at a uniform temperature of 873 K. The boundary conditions for the rest of the system are the same; that is, the outer chamber walls are at 285 K and all other parts are adiabatic as explained before.

Two different heater settings are estimated, one considering the heat losses and one without estimating the heat losses. For the solution of the design problem the inclusion of conductive heat losses is straightforward; the inverse design problem is solved, the heat losses are calculated based on the calculated distributions and the losses are added to calculated heater inputs necessary for radiative transfer. The estimated power for the inner heater is 144.5 watts, while it is 411.3 watts for the outer heater. The CGM is used as a regularized solver and as the constant heat flux constraint is imposed to the heaters all conjugate directions are used on the solution. Considering the heat losses, these settings are modified to 170 and 519.6 watts, respectively.

The estimated settings that do not consider the heat losses are applied with an uncertainty of ?? and ?? percent for the inner and outer heaters and the resulting temperatures are measured. Similarly, the other setting that considers the heat losses are applied with an uncertainty of ?? and ??, for the inner and outer heaters.

The measured temperature over the silicon wafer at locations shown in Fig. 7.4 is presented in Table 7.2. For the case where heat losses are not considered the average temperature measured over the wafer is 839.1 K, 33.8 K below the desired temperature producing average and maximum errors of 3.9 and 4.8 percent, respectively. For the settings where the heat losses are considered, the average temperature measured over the wafer is 881.4 K, 8.4 K above the design goal yielding 1 percent average error and 1.7 percent maximum error. Considering the heat losses in the system through the bolts, supports and the junctions holding it together improves the solution.

Table 7.2: The measured temperature across the wafer for two settings when predictions of inverse design are applied, considering the heat losses (w loss) and not considering heat losses (no loss)

TC #		1	2	3	4	5	6
T (K)	no loss	831.3	837.1	840.8	846.0	842.4	842.4
	w loss	876.2	879.4	883.2	888.3	884.7	884.7
TC #		7	8	9	10	11	12
T (K)	no loss	834.9	834.7	838.6	843.0	839.5	-
	w loss	876.4	876.2	880.1	885.1	881.5	-

The temperature distribution across the wafer is not axisymmetric as the diffuser plate in the system to ensure the axisymmetry in the system, was not rotated for both runs.

Although the design goal is keeping the silicon wafer at a prescribed condition, and the temperature distribution achieved across the wafer is the main concern, it is still useful to investigate the agreement between the predicted and the measured shield temperatures. It is desired to achieve a similar agreement as in the case of the forward problem. The measured and estimated temperatures for the top and the bottom shields are presented in Fig. 7.8. As in the forward problem the agreement in the top shield is better than it is for the bottom shield due to ignoring the conduction along the Inconel ring. The error values are also in the same order of magnitude as that of the forward problem. The equivalent plot for the side shield is presented as Fig. 7.9. Similarly, the agreement for the side shields is similar to that of the forward problem.

Though the achieved accuracy is around one percent, it is not enough for applications of the semiconductor industry. Even so, considering the accuracy of the numerical model, the inverse design proved to be a very promising approach. Although the model used here is very detailed as explained earlier, there are still some simplifications considered such as neglecting conduction across all the elements including the Inconel ring. The results can be improved by further developing the model through including minor effects. This leads to a nonlinear system due to the multimode heat transfer. An iterative solution is required for a

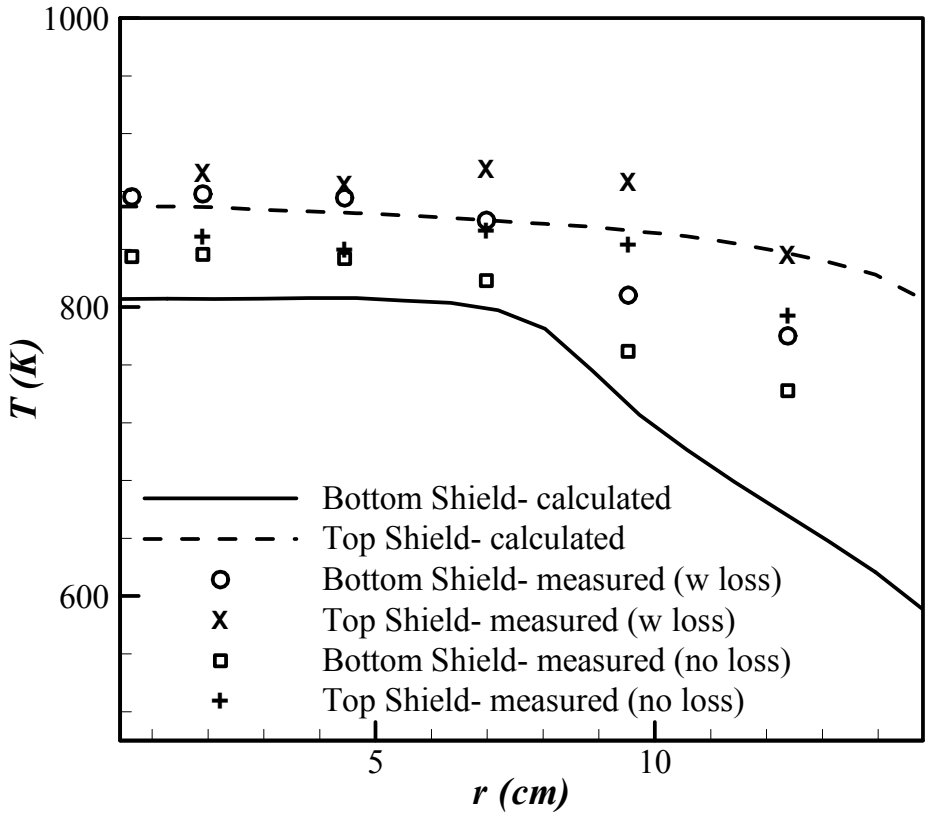

Figure 7.8: Comparison of the predictions of the inverse design and the measured values at the top and bottom shields. For a uniform wafer temperature of 873 K, the inner and outer heater powers are estimated as: 144.5 and 411.3 W without heat losses, 170 and 519.6 with heat losses.

steady boundary condition estimation problem as explained in França et al. (2002).

Another approach is to use the results of the inverse design as an initial guess for a trial-and-error solution based on a more detailed model. When the

achieved accuracy is considered, it is obvious that finding a solution will be an easy task requiring only a few iterations.

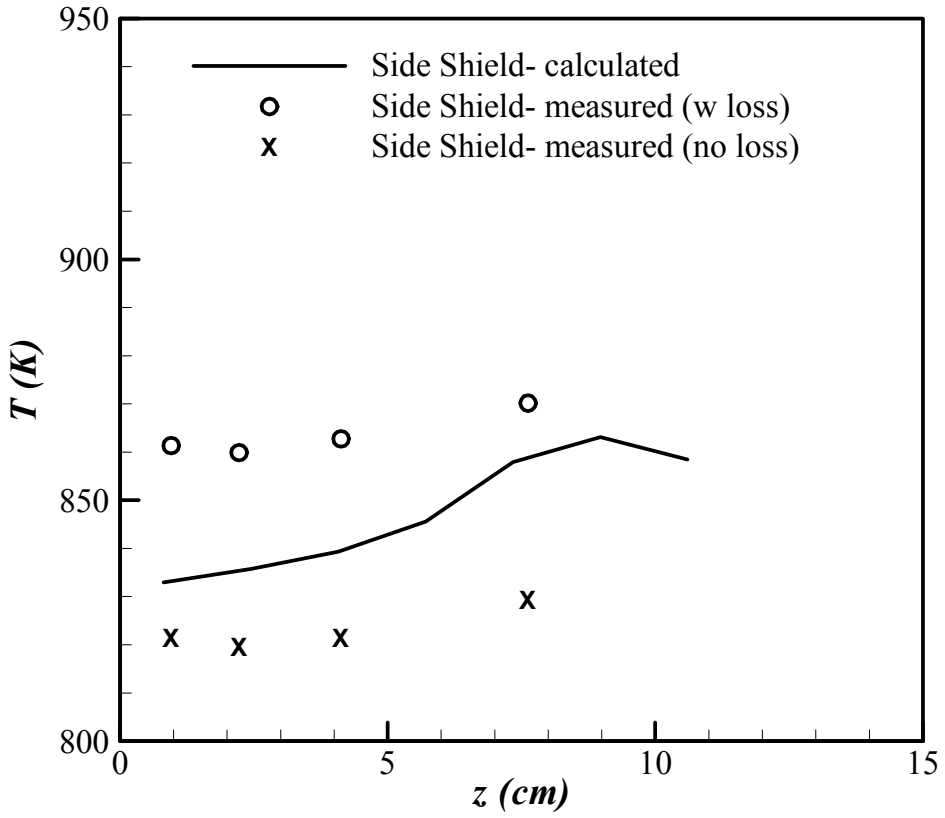

Figure 7.9: Comparison of the predictions of the inverse design and the measured values at two circumferential locations on the side shield. For a uniform wafer temperature of 873 K, the inner and outer heater powers are estimated as: 144.5 and 411.3 W without heat losses, 170 and 519.6 with heat losses.

CHAPTER 8

Conclusions and Recommendations for Future Work

8.1 CONCLUSIONS

This study focuses on design, in particular design of thermal processing systems that contain components with high temperatures. The design of such systems consists of coupled geometry, property, boundary condition and/or load estimation problems. Every one of these sub-problems is challenging by itself due to the governing complex physics of multimode heat transfer and fluid flow. The combined design problem is even more challenging and moreover, highly nonlinear. The solution of the problem involves a number of iterations of prototype building and testing.

The goal of this study is to develop methods to ease the solution of the design problem. To accomplish this goal, the challenges and difficulties of each problem must be investigated separately. For that reason, it is appropriate to isolate the sub-problems and develop the required tools accordingly. Here, only the boundary condition design problem is considered and an extensive investigation of the topic is presented. This problem arises when an existing system is to be used for satisfying certain thermal conditions, based on the needs of the process, in the design environment that is the part of the system where the process of interest takes place. For this type of design problem, the required input for the heaters is to be calculated.

In such a problem, the needs of the process make up two boundary conditions over the design environment, where no information about the conditions in the heater or burner section is available. This is different from a traditional forward problem where a condition is defined for all surfaces and the medium and the effects of a certain cause are estimated from the knowledge of the physical system. Hence, the calculation of unknown inputs for heaters or burners forms an inverse problem as the cause that results in a desired effect is sought. This constitutes an ill-posed problem unlike the well-posed forward problem. The ill-posed system results in unstable solutions, very sensitive to uncertainties in the properties or design requirements. Moreover, the solution is often unphysical.

The traditional solution to the boundary condition design problem is with trial-and-error techniques, which involves the solution of a series of forward problems based on estimates for unknown conditions. The estimates are modified until the conditions in the design surface are satisfied. Using this approach, it is often hard to converge to a reasonable solution. When optimization techniques are used for modifying the estimates, the solution may become computationally very expensive.

Alternatively, an inverse formulation is implemented for the solution of the problem in this study. Although direct solutions are possible with inverse formulation, regularization or filtering must be employed in order to achieve reasonable and stable solutions. Through the use of regularization or filtering techniques, the ill-posed system is modified to a well-posed system with the expense of some error in the solution.

The solution of a wide variety of design and control problems is possible using an inverse formulation. Both steady and transient boundary condition design of radiating enclosures are considered here. In the steady design problems, enclosures with an absorbing-emitting and anisotropically scattering medium, and irregular geometries with blockage effects are considered. The conjugate gradient method, truncated singular value decomposition and Tikhonov regularization are used to achieve smooth and accurate solutions. It is demonstrated that alternative solutions of different accuracy can be produced using different regularization or filtering levels. Unlike the measurement problems, this is preferred for a design problem, as having alternatives can be beneficial at times. The general trend is; as a higher level of regularization is used, the solutions become smoother and less accurate. Therefore, there is an optimal level of regularization based on the process under consideration where the desired solution accuracy together with smoothness or solution shape is achieved. The L-curve, which demonstrates the change in the norm of the residual as a measure of accuracy with the solution norm, is a very useful tool to detect the optimal solution.

Among the three regularization methods investigated in this study, the conjugate gradient method and the truncated singular value decomposition produce very similar results, while Tikhonov regularization slightly differs from the other two. The conjugate gradient method is the most efficient one both in terms of memory requirement and computation time. Another aspect that has strong influence on the efficiency of the solution is the way the problem is formulated. More generic formulations usually result in larger systems requiring

more memory and computation time while problem specific formulations can yield remarkable amounts of savings when they are applicable.

Moreover, the solution accuracy is strongly dependent on how sensitive the design surface is to the changes in heaters or burners. If the sensitivity of the heaters or burner elements over the design surface is not significant, controlling the conditions over the design surface becomes a difficult task. This situation arises when the conditions over a surface is desired to be controlled by using heaters when there is optically thick participating medium or when the design surface and the heaters are so far apart that the geometric shape factors are very small. In such situations, the filtered information can constitute a significant portion of what defines the relation between the heaters or burners and the design object and filtering results in significant errors.

The inverse design approach is also applicable to transient boundary condition estimation problems where the behavior with time is of interest. These problems arise when an object is to be heated following a specified temperature history together with a spatial distribution. Furthermore, in some systems the thermal conditions and the positions of the objects can both be changing with time as in the case with conveyor belt systems used in continuous mass production lines.

In such systems, the thermal capacity of the elements together with the multi-mode heat transfer introduces non-linearity making the problem more interesting and challenging. Although they necessitate using very small time step sizes, explicit time discretization schemes linearize the governing system. As in

the case of the steady problems, the desired solution must be accurate and spatially smooth. Moreover, it must also be smooth along time in the transient problem. This can be accomplished using a constant level of regularization for the consecutive solutions along discrete time steps. As a result, the overall solution accuracy is very much dependent on the regularization level.

It should be kept in mind that the backbone of the inverse design is the numerical model used and the realization of the design is very much dependent on the accuracy of the model. Although, the application of inverse design for steady boundary condition problems is validated using an instrumented test rig using numerical models in some problems, it can be difficult to include all the details about the physics. As a result, some difference between the behavior of the physical system and the predictions of the numerical model can be observed. In the absence the of possibility of adding further details to the numerical model, the use of an alternative model, such as one based on artificial neural networks, can be used to improve the solution accuracy.

Inverse design is a very useful tool for the boundary condition design. Although the boundary condition design is just one of the sub-problems that constitute the complete design problem, it can be used as a tool for the overall design problem. Avoiding the computational expense of the trial-and-error solutions for the boundary condition estimation problem by using inverse design, even trial-and-error type solutions would become feasible for geometry or material estimation within a reasonable computation time.

8.2 RECOMMENDATIONS FOR FUTURE WORK

Considering the information available in the literature and the contents of this study, recommended future work is listed as follows:

Experimental Validation of Transient Boundary Condition Design

Although the experimental validation of a steady boundary condition estimation problem is presented in this study, similar validation for transient systems have not been presented. In order to be able to do that an instrumented physical system that is capable of heating an object is required. Once the system is built, both the inverse design of transient system and control using artificial neural networks can both be applied.

More Complex Problems

This study extended the application of inverse design from steady systems to transient systems and from simple geometries to complex geometries. Although, the problems tackled in this study involve physical phenomena such as anisotropic scattering and specularly reflecting walls, some simplifying assumptions such as all properties being gray and temperature independent are employed. Solutions with wavelength and temperature dependent properties can be produced. Moreover, the thermal systems considered in this study do not involve fluid flow or significant natural convection effects. These could also be implemented together with the complex physics to represent a more realistic system.

Complete Design Problem

Together with the ongoing research about other design sub-problems, geometry and property estimation, solution procedures for the complete design problem can be outlined. Different solution methodologies for each sub-problem can be coupled to develop alternative algorithms and these can then be compared based on accuracy, efficiency and versatility.

Implementing Available Software

The proposed design methods presented in this study are not limited to the particular methods used here. Although the same method is used for modeling thermal radiation and only three methods are used for solving the ill-conditioned system of equations, inverse design can be applied using any tool that is capable of modeling heat transfer and fluid flow and any method for solving ill-conditioned systems. The majority of the software required was developed for this study. However, there are many generic modeling tools available in the market for heat transfer and fluid flow problems. Therefore, the ideas developed here can be implemented using available software.

Application to Measurement Problems

The applications in this study are limited to design problems. The analysis can be extended to measurement problems, where the thermal conditions at a location is to be calculated from the available information in another location. One possible application will be temperature sensing. This problem will be of interest to the semiconductor industry as measuring temperature distribution directly using thermocouples is not applicable during manufacturing

semiconductor wafers. Then the only way to detect the temperature distribution over the wafer is to calculate the distribution using the measurements taken elsewhere.

References

Alifanov, O. M., 1994, *Inverse Heat Transfer Problems*, Springer-Verlag, Berlin.

Alifanov, O. M., Artyukhin, E. A. and Rumyantsev, S. V., 1995, *Extreme Methods for Solving Ill-Posed Problems with Applications to Inverse Heat Transfer Problems*, Begell House, New York.

Ball, K.S., Huston, K.S., Noska,B.L., Simonich, M.A., Geyling, F.T., Sing, D.,Tichy, R.S., and Baharav, Y., 2001, "The UT/NIST/SA/ISMT Thermometry Test Bed – 2001", Proceedings of 9th International Conf. on Advanced Thermal Processing of Semiconductors .

Beck, J. V., Blackwell, B. and St. Clair, Jr., C. R., 1985, *Inverse Heat Conduction*, John Wiley and Sons Inc., New York.

Beckman, F. S., 1960, "The Solution of Linear Equations By the Conjugate Gradient Method", Mathematical Methods For Digital Computers, A. Ralston and H. S. Wilf, eds., John Wiley and Sons, New York,pp.62-72.

Bertsekas, D. P., 1999, *Nonlinear Programming*, Second Edition, Athena Scientific, Belmond, MA.

Bird, G. A., 1976, *Molecular Gas Dynamics*, Clarendon Press, Oxford.

Daun, K, Howell, J.R. and Morton, D.P., 2001, "Geometrical Optimization of Radiating Enclosures through Nonlinear Programming," Proceedings of ASME International Mechanical Engineering Congress and Exhibition**,** New York City, New York.

Daun, K. J., Howell, J. R., and Morton, D. P., 2002, "Design of Radiant Enclosures using Inverse and Non-linear Programming Techniques," Proceedings of the Canadian Society of Mechanical Engineers Forum, Kingston, Ontario, Canada.

Daun, K. J., Ertürk, H. and Howell, J. R., 2002, "Inverse Methods for High Temperature Systems", in press for Arab Journal of Science and Engineering.

Demuth, H. and Beale, M., 2001, *Neural Network Toolbox: For Use with MATLAB®*, The MathWorks, Natick.

Dulikravich, G. S. and Martin, T. J., 1997, "Inverse Shape and Boundary Condition Problems and Optimization in Heat Conduction", Advances in Numerical Heat Transfer, W. J. Minkowycz, and E. M. Sparrow, eds., vol. 1, Taylor and Francis, Washington DC.

Ertürk, H., 1997, "Mathematical Modeling of Radiative Transfer in Participating Media", M.S. Thesis, Middle East Technical University, Ankara, Turkey

Ertürk, H., Arınç, F. and Selçuk, N., 1997, "Accuracy of Monte Carlo Method Re-Examined on a Box-Shaped Furnace Problem", Radiative Heat Transfer II: Proceedings of Second International Symposium on Radiative Heat Transfer, ed. Mengüç, M. P., Begell House, New York, pp. 85-95.

Ertürk, H., Ezekoye, O. A., and Howell, J. R., 2000, "Inverse Solution of Radiative Transfer in Two-Dimensional Irregularly Shaped Enclosures", Proceedings of ASME International Mechanical Engineering Congress and Exhibition, Orlando, Florida.

Ertürk, H., Ezekoye, O. A., and Howell, J. R., 2001a, "Inverse Transient Boundary Condition Estimation Problem in a Radiating Enclosure", Proceedings of ASME National Heat Transfer Conference, Anaheim, California.

Ertürk, H., Ezekoye, O. A., and Howell, J. R., 2001b, "Inverse Design of a Three-Dimensional Furnace with Moving Design Environment", Proceedings of ASME International Mechanical Engineering Congress and Exhibition, New York City, New York.

Ertürk, H., Ezekoye, O. A., and Howell, J. R., 2002a, "Comparison of Three Regularized Solution Techniques in a Three-Dimensional Inverse Radiation Problem", Journal of Quantitative Spectroscopy and Radiative Transfer, vol.73, pp. 307-316.

Ertürk, H., Ezekoye, O. A., and Howell, J. R., 2002b, "Design of A Rapid Thermal Processing Chamber Using an Inverse Formulation", Proceedings of AIAA/ASME Joint Thermophysics and Heat Transfer Conference, St. Louis, Missouri.

Ertürk, H., Ezekoye, O. A., and Howell, J. R., 2002c, "The Use of Inverse Formulation in Design and Control of Transient Radiant Systems", Proceedings of International Heat Transfer Conference, Grenoble, France.

Ertürk, H., Ezekoye, O. A., and Howell, J. R., 2002d, "The Application of An Inverse Formulation In The Design of Boundary Conditions for Transient Radiating Enclosures", in press for ASME Journal of Heat Transfer.

Farmer, J. T. and Howell, J. R., 1998, "Comparison of Monte Carlo Strategies for Radiative Heat Transfer in Participating Media", Advances in Heat Transfer, J. P. Hartnett and T. F. Irvine, eds., vol. 31, pp. 333-429, Academic Press, New York.

França, F. H. R., Ezekoye, O. A. and Howell, J. R., 1999, "Inverse Heat Source Design Combining Radiation and Conduction Heat Transfer", Proceedings of ASME International Mechanical Engineering Congress and Exposition, Nashville, Tennessee

França, F. H. R., 2000, "Inverse Thermal Design Combining Radiation, Convection and Conduction", Ph. D. Dissertation, Department of Mechanical Engineering, The University of Texas at Austin, Austin, Texas.

França, F. H. R., Ezekoye, O. A., and Howell, J. R., 2001, "Inverse Boundary Design Combining Radiation and Convection Heat Transfer", ASME Journal of Heat Transfer, vol. 123, no. 5, pp. 884-891.

França, F. H. R., Howell, J. R., Ezekoye, O. A., and Morales, J. C., 2002, "Inverse Design of Thermal Systems", Advances in Heat Transfer, J. P. Hartnett and T. F. Irvine, eds., vol. 36, pp. 1-110, Academic Press, New York.

Gamba, M., 2002, "Inverse Design of Thermal Systems: An Experimental Validation of the Method", M.S. Thesis, The university of Texas at Austin, Austin, Texas.

Gamba, M., Ertürk, H., Ezekoye, O. A., and Howell, J. R., 2002, "Modeling of a Radiative RTP-type Furnace Through an Inverse Design: Mathematical Model and Experimental Results", Proceedings of ASME International Mechanical Engineering Conference and Exhibitions, New Orleans, Louisiana.

Geyling, F., Van Eck, B., Ball, K.S., Powers, B., Blakeney, J., 2000, "The UT/NIST/SA/ISMT Thermometry Test Bed ," Proceedings of 8th International Conference on Advanced Thermal Processing of Semiconductors – RTP 2000, D.P. DeWitt, J. Kowalski, B. Lojek, and A. Tillman, eds., Colorado Springs, Colorado, pp. 74-82.

Glassner, A. S., 1989, *An Introduction to Ray Tracing*, Academic Press, New York.

Hadamard, J., 1923, *Lectures on Cauchy's Problem in Linear Differential Equation*, Yale University Press, New Haven, Connecticut.

Haji Sheikh, A and Sparrow, E. M., 1967, "The Solution of Heat Conduction Problems by Using Probability Methods", ASME Journal of Heat Transfer, Vol. 89, pp. 121-131.

Hammersley, J. M. and Handscomb, D. C., 1964, *Monte Carlo Methods*, Wiley, New York.

Hansen, P. C., 1992, "Numerical Tools for Analysis and Solution of Fredholm Integral Equations of the First Kind", Inverse Problems, vol. 8, pp.849-872.

Hansen, P. C., 1998, *Rank-Deficient and Discrete Ill-Posed Problems: Numerical Aspects of Linear Inversion*, SIAM Publications, Philadelphia, Pennsylvania.

Harutunian, V., Morales, J. C. and Howell, J. R., 1995, "Radiation Exchange Within an Enclosure of Diffuse-Gray Surfaces: The Inverse Problem", Proceedings of ASME/AIChE National Heat Transfer Conference, Portland, Oregon.

Hokenson, G., 1979, "Inverse Design of Optimal Diffusers with Experimental Corroboration", ASME Journal of Fluids Engineering, vol. 101, pp. 478-482.

Hosseini Sarvari, S.M., Howell, J.R. and Mansouri, S.H., 2002, "Inverse Boundary Design Radiation Problem in Absorbing-Emitting Media with Irregular Geometry," in press, Journal of Numerical Heat Transfer, Part A.

Howell, J. R. and Perlmutter, M., 1964, "Monte Carlo Solution of Thermal Transfer Through Radiant Media Between Gray Walls", Journal of Heat Transfer, vol. 86, pp. 116-122.

Howell, J. R., 1968, "Application of Monte Carlo to Heat Transfer Problems", Advances in Heat Transfer, J. P. Hartnett and T. F. Irvine, eds., vol. 5, pp. 1-54, Academic Press, New York.

Howell, J. R., 1998, "The Monte Carlo Method in Radiative Heat Transfer", ASME Journal of Heat Transfer, vol. 120, pp. 547-560.

Howell, J. R., 1999, "Optimal Design Method for Heat Exhange Equipment Dominated by Radiative Transfer", Technical Report submitted to Research Institute Ishikawajima-Harima Heavy Industries.

Howell, J. R., Ezekoye, O. A. and Morales, J. C., 2000, "Inverse Design Model for Radiative Heat Transfer", ASME Journal of Heat Transfer, vol. 122, pp. 492-502.

Howell, J. R., Daun, K. J. and Ertürk, H, 2001, *An Annotated Bibliography of Thermal Radiation Validation Data for Fire Applications*, Technical Report, Sandia National Laboratories, Albuequerque, New Mexico.

Hsu, P. and Farmer, J. T., 1997, "Benchmark Solutions of Radiative Transfer Within Nonhomogeneous Participating Media Using The Monte Carlo and YIX Methods", ASME Journal of Heat Transfer, vol. 119, pp.185-188.

Incropera, F.P. and DeWitt, D.P., 2002, *Fundamentals of Heat and Mass Transfer*, 5th ed., John Wiley and Sons, New York.

Kennon, S. R. and Dulikravich, G. S., 1985, "The Inverse Design of Internally Cooled Turbine Blades", Journal of Engineering Gas Turbine Power, vol. 107, pp. 123-126.

Kudo, K., Kuroda, A., Eid, A., Saito, T. and Oguma, M., 1995, "Solution of the Inverse Radiative Load Problems by The Singular Value Decomposition" Proceedings of ICHMT First International Conference of Radiative Transfer, Kuşadası, Turkey, M. P. Mengüç, ed., pp.568-578.

Mengüç, M. P. and Manickavasagam, S., 1993, "Inverse Radiation Problem in Axisymmetric Cylindrical Scattering Media", Journal of Thermophysics and Heat Transfer, vol. 7, no 3, pp. 479-486.

Mills, A. F., 1995, *Heat and Mass Transfer*, Irwin, Boston, Massachusetts.

Modest, M. F., 1993, *Radiative Heat Transfer*, Mc Graw-Hill Book Co, Singapore.

Nelson, M. M. and Illingworth, W.T., 1993, *A Practical Guide to Neural Nets*, Addison-Wesley, Reading.

Özışık, M. N. and Orlande, H. R. B., 2000, *Inverse Heat Transfer*, Taylor and Francis, New York.

Park, H. M. and Jung, W. S., 2001, "Recursive Solution of an Inverse Heat Transfer Problem in Rapid Thermal Processing Systems", International Journal of Heat and Mass Transfer, vol. 44, pp. 2053-2065.

Press, W. H., Teukolsky, S. A., Vetterling, W. T. and Flannery, B. P., 1992, *Numerical Recipes*, Cambridge University Press, New York.

Selçuk, N., 1985, "Exact Solutions for Radiative Heat Transfer in Box-Shaped Furnaces", ASME Journal of Heat Transfer, vol. 107, pp.648-655.

Siegel, R., and Howell, J. R., 2002, *Thermal Radiation Heat Transfer*, 4th Ed., Taylor and Francis, Washington DC.

Silva Neto, A. J. and Özışık, M. N, 1994, "An Inverse Heat Conduction Problem of Unknown Initial Condition", Proceedings of International Heat Transfer Conference, 14-18 August 1994, Brighton, UK, ed. Hewitt, G. F., pp.421-426.

Sun, B.K., Zhang, X., and Grigoropoulos, C.P., 1997, "Spectral Optical Functions of Silicon in the range of 1.13-4.96 eV at Elevated Temperatures", International Journal of Heat and Mass Transfer, vol. 40, pp. 1591-1600.

Taussky, O. and Todd, J., 1956, "Generating and Testing of Pseudo Random Numbers", Symposium on Monte Carlo Methods, Meyer, H. A. ed., pp.15-28, Wiley, New York.

Tikhonov, A. N., Goncharsky, A. V., Stepanov, V. V., and Yagola, A. G., 1995, *Numerical Methods for Solving Ill-Posed Problems*, Kluwer Academic Publishers, Boston, Massachusetts.

Touloukian, Y.S., DeWitt, D.P., 1970, *Thermophysical Properties of Matter*, vol. 7, IFI/PLENUM, New York-Washington.

Vogel, C., 2002, *Computational Methods for Inverse Problems*, SIAM Publications, Philadelphia, Pennsylvania.

Volpe, G. and Melnik, R.E, 1984, "Role of Constraints in Inverse Design for Transonic Airfoils", AIAA Journal, Vol. 22, pp. 1770-1778.

Walters, D. V. and Buckius, R. O., 1992, "Rigorous Development For Radiation Heat Transfer in Nonhomogeneous Absorbing, Emitting and Scattering Media", International Journal of Heat and Mass Transfer, Vol. 35, pp. 3323-3333.

Werbos, 1992, "Neurocontrol and Supervised Learning: An Overview and Evaluation", Handbook of Intelligent Control: Neural, Fuzzy and Adaptive Approaches, D. A. White and D. A. Sofge, eds., Van Nostrand Reinhold, New York, pp. 65-90.

Wu, C. -Y. and Wu, S. –H., 1999, "A New Application of Successive Approximation to Radiative Exchange Among Surfaces: Direct and Inverse Problems", International Journal of Heat and Mass Transfer, Vol. 42, pp. 2255-2267.

Yang, T. and Nishi, M., 1980, "Inverse Design of Optimal Diffusers with Experimental Corroboration", ASME Journal of Fluids Engineering, vol. 102, pp. 121-124.

Yang, W. J. Y., Taniguchi, H. and Kudo, K., 1995, "Radiative Heat Transfer by the Monte Carlo Method", Advances in Heat Transfer, J. P. Hartnett and T. F. Irvine, eds., vol. 27, Academic Press, New York.

Vita

Hakan Ertürk was born in Ankara, Turkey, in March 16, 1973, the son of Altan and Sevgi Ertürk. He graduated from TED Ankara Koleji Private High School in 1990, and upon his graduation started his studies in Department of Mechanical Engineering of Middle East Technical University, Ankara, Turkey. He received his Bachelor of Science in Mechanical Engineering in July 1994. He continued his studies in the Middle East Technical University, where he also worked as a teaching assistant for the Department of Mechanical Engineering, and received his Master of Science in Mechanical Engineering in September 1997. In August 1998, he moved to Austin, Texas, to pursue a doctoral degree in the Department of Mechanical Engineering of the University of Texas at Austin, where he was appointed as a research assistant.

Permanent address: Gama Sitesi, Yuvacık Sokak No. 18
Çayyolu, 06530, Ankara, Turkey

This dissertation was typed by the author.